



Norwegian University of
Science and Technology

Compact Separation - Concept Study

Experimental and Simulation Study of
Oil-Water Multiphase Flow in Helically Coiled
Pipe

Erik Hjertholm
Henrik Nikolai Kulseth

Subsea Technology

Submission date: June 2016

Supervisor: Sigbjørn Sangesland, IPT

Co-supervisor: Tor Berge Gjersvik, IPT
Milan Stanko, IPT

Norwegian University of Science and Technology
Department of Petroleum Engineering and Applied Geophysics

Preface

This is the master thesis of Erik Hjertholm and Henrik N. G. Kulseth written at the Department of Petroleum Engineering and Applied Geophysics at the Norwegian University of Science and Technology.

In our work, we have received both theoretical and practical assistance in different parts of the project and for this we are grateful. Our supervisors Professor Sigbjørn Sangesland and Professor II Tor Berge Gjersvik have been available to us throughout the whole project, and their inputs have been of great value. Associate Professor Milan Stanko has given us good advice and has been our go-to person on a number of different challenges. PhD-candidate Gilberto Nunez and fellow student Jon Arne Karstad Opstvedt have helped us with the simulations and in building the experimental rig we have received assistance from Senior Engineer Georg Voss, Senior Engineer Steffen Wærnes Moen, Engineer Håkon Myhren, Engineer Terje Bjerkan, Staff Engineer Roger Overå and Senior Engineer Noralf Vedvik.

Trondheim, June 2016

Henrik N. G. Kulseth

Erik Hjertholm

Summary

This master thesis is written as part of a SUBPRO project whose long term goal is to identify multiphase flow separation performance of a helically coiled pipe and determine if it's viable for further industrial development. SUBPRO is an applied research center consisting of relevant contributors from the industry and the Norwegian University of Science and Technology. One of their stated goals is to «*develop new knowledge and technology to meet future challenges in subsea production and processing*». This thesis is a continuation of the work previously done in the specialization project «*Compact Separation; Concept Study of Helically Coiled Pipe and Preparation for Experimental Setup*» and will later be continued as a PhD study.

The objective of this thesis is to develop an experimental setup and conduct experiments to qualitatively determine the potential of using a helically coiled pipe as a compact separator or flow conditioner and its potential for further industrial development. In the end, recommendations based on the results is to be made. In addition, CFD simulations will be performed to support the data from the experiments.

Main work done in this project consists of:

- Development of experimental setup. This includes completion of design, ordering of parts, construction, instrumentation and system testing and calibration.
- Generation of CAD drawings and CFD meshing for simulations.
- Simulations in Computational Fluid Dynamics.
- Execution of experiments with oil-water multiphase flow with varying oil ratio and flow rates.

Simulations in Ansys CFX were performed so that numerical results that was difficult to obtain visually could be extracted. This includes separation performance, secondary flow and turbulence. The geometry used in the simulations was limited to the loop and one meter of straight section before and after the loop. Simulations were primarily done with *mixture model* but results from *particle model* simulations are also evaluated. The simulations indicated relatively low separation performance but showed a significant reduction in turbulence caused by the loop compared to a straight pipe section with the same length.

The experiments conducted featured an oil-water phase in a helically coiled pipe. Photographs were taken of the flow at the inlet and outlet of the loop for a range of oil ratios and flow rates and were used to visually identify if any phase segregation occurred. None of the photos showed any indication of phase segregation in the experimental range. The flow regime at both the inlet and outlet was identified as various degrees of emulsion were a low oil ratio gave a pink emulsion with low degree of translucency and a high oil ratio gave a reddish emulsion with some translucency. The experiments were affected by problems with emulsion buildup in the separator, especially at low oil ratios, and turbidity in the water which gave the water a white color, hence reduced contrast to the oil. Due to limited time, only one coil geometry was tested. Less comprehensive tests with air-oil flow showed segregation of these two phases as stratified flow.

The experimental study and results from the simulations gave no indications that the helical coil could be applicable as a compact separator for oil-water flows. However, due to the limited experimental range and sources of error this experimental study can't completely disprove the concept studied concept for oil-water flow. Improvements of the experimental setup including the ones mentioned in "*Recommendations for further work*" could yield other results. The results from the simulations did show a significant reduction in turbulence from the loop compared to a straight pipe which may give it applicability as a flow conditioner.

Sammendrag

Denne masteroppgaven er skrevet som en del av et SUBPRO prosjekt hvis langsiktige mål er å identifisere separasjonsegenskapene til et heliksformet rør for flerfasestrømning og avgjøre om dette konseptet er levedyktig for videre industriell utvikling. SUBPRO er et senter for anvendt forskning som består av medvirkende bedrifter fra industrien og Norges teknisk-naturvitenskapelige universitet. En av de uttalte målene deres er å «*utvikle ny kunnskap og teknologi for å møte fremtidige utfordringer innen undervannsproduksjon og –prosessering*». Denne oppgaven er en fortsettelse av arbeidet som er gjort i spesialiseringsprosjektet «*Compact Separation; Concept Study of Helically Coiled Pipe and Preparation for Experimental Setup*» og vil bli videreført som en PhD studie.

Målet med denne oppgaven er å utvikle et eksperimentelt oppsett og utføre eksperimenter for å kvalitativt avgjøre om et heliksformet rør har potensiale til å kunne brukes som en kompakt separator eller *flow conditioner* og dens potensiale for videre industriell utvikling. Anbefalinger basert på resultatene vil bli gjort i slutten av oppgaven. I tillegg vil CFD simuleringer bli utført for å støtte dataene fra eksperimentene.

Hovedarbeidet som er blitt gjort i dette prosjektet består av:

- Utvikling av eksperimentelt oppsett. Dette inkluderer ferdigstilling av design, bestilling av deler, konstruksjon, instrumentering og systemtesting og-kalibrering.
- Generering av CAD tegning og CFD meshing for simuleringene.
- Simuleringer i Computational Fluid Dynamics.
- Utføring av eksperimenter med olje-vann flerfasestrømning med et spekter av blandingsforhold og strømningsrater.

Simuleringene gjort i Ansys CFX ble utført for å få numeriske resultater som var vanskelig å innhente visuelt. Dette inkluderer separasjonsytelse, sekundærstrømning og turbulens. Geometrien som ble brukt i simuleringene var begrenset til selve loopen og en meter rett seksjon før og etter loopen. Simuleringene var primært gjort med *mixture model* men resultater fra *particle model* simuleringer er også evaluert. Simuleringene indikerte relativt lav separasjonsytelse men viste at

loopen førte til en vesentlig reduksjon i turbulens ved slutten av loopen sammenlignet med en rett rørseksjon av tilsvarende lengde.

De utføre eksperimentene bestod av å pumpe en olje-vann strømning gjennom et heliksformet rør. Bilder ble tatt av strømmingen ved innløpet og utløpet av loopen for et bestemt utvalg av oljeforhold og strømningsrater, disse ble brukt til å visuelt avgjøre om noen form for fasesegregering oppstod. Ingen av bildene indikerte noen form for segregering innen den eksperimentelle rekkevidden. Strømningsregime ved både innløp og utløp av loopen ble identifisert som emulsjon av varierende grad, hvor et lavt oljeforhold gav en rosa emulsjon med lav grad av gjennomsiktighet, mens et høyt oljeforhold gav en rødlig emulsjon med noe gjennomsiktighet. Eksperimentene ble påvirket av problemer med emulsjonsoppbygging i separatoren, spesielt ved lavt oljeforhold, og turbiditet i vannet som gav vannet en hvit farge og dermed redusert kontrast i forhold til oljen. Tidsbegrensning gjorde at eksperimentene kun ble utført med én geometri for loopen. Mindre omfattende tester med luft-olje strømning viste segregering av disse to fasene som stratifisert strømning.

Den eksperimentelle studien og resultatene fra simuleringene gav ingen indikasjon på at et heliksformet rør kan anvendes som en kompakt separator for olje-vann strømninger. Men, på grunn av den begrensede eksperimentelle rekkevidden og feilkilder, kan ikke dette studiet avkrefte det studerte konseptet for olje-vann strømning. Forbedringer av det eksperimentelle oppsettet, inkludert det som er nevnt som anbefalinger for videre arbeid, kan gi andre resultater. Resultatene fra simuleringene viste at loopen førte til en vesentlig reduksjon i turbulens, noe som kan gi den anvendelighet som en flow conditioner.

Table of Contents

- 1 Introduction..... 1
- 2 Specialization Project Summary 3
- 3 Experimental Study 4
 - 3.1 Experimental Setup 4
 - 3.1.1 Overview..... 4
 - 3.1.2 Pipes 6
 - 3.1.3 Valves..... 6
 - 3.1.4 Helical Coil 6
 - 3.1.5 Supporting Structure 8
 - 3.1.6 Pumps..... 9
 - 3.1.7 Frequency Converters 11
 - 3.1.8 Separator 11
 - 3.1.9 Data Acquisition and Control 13
 - 3.1.10 Camera Setup 22
 - 3.2 Experimental Fluids 24
 - 3.2.1 Exxsol D60..... 24
 - 3.2.2 Water..... 25
 - 3.2.3 Bacterial Inhibitor 25
 - 3.2.4 Coloring of Liquid..... 25
 - 3.2.5 Measured Properties of Fluids 27
 - 3.3 Experimental Execution..... 28
- 4 Simulations in Ansys CFX 33
 - 4.1 Geometry..... 33
 - 4.2 Meshing..... 34
 - 4.3 Settings in CFX 35
 - 4.4 Steady-state vs transient flow 36
 - 4.5 Method of measuring efficiency 36

4.6	Parametric study	37
4.7	Secondary flow	38
4.8	Turbulence.....	39
5	Results	41
5.1	Experimental results.....	41
5.1.1	Water and Oil	41
5.1.2	Oil and Air	44
5.2	Simulation results.....	46
6	Discussion	52
6.1	Experimental Results.....	52
6.2	Simulations	52
6.3	Potential of helical coil principle	53
6.4	Limitations and uncertainties.....	54
6.4.1	Experimental Setup	54
6.4.2	Simulations	55
6.5	Recommendations for Further Work	56
7	Conclusion	59
	References.....	60
	Appendix A Part list and Budget.....	62
	Appendix B System Procedures.....	63
	Appendix C Calibration Sheet.....	70
	Appendix D LabVIEW Block Diagram.....	71
	Appendix E Experimental Matrix.....	72
	Appendix F CFX Settings	73
	Appendix G Raw data from Mixture model simulations	89
	Appendix H Raw data from particle model simulations.....	90
	Appendix I Graphs from Particle Model.....	91
	Appendix J Risk Assessment	93
	Appendix K Exxsol D60 datasheet	104

List of figures

Figure 3-1 P&ID of experimental setup with numerical indicators for components later referred to.	4
Figure 3-2 3D illustration of experimental setup. The numbers indicates key components referred to later in this thesis.....	5
Figure 3-3 A particle moving in a circular motion with a constant radius and tangential velocity. (Vidnes, Engvik et al. 2015)	7
Figure 3-4 Illustration describing the helical coil properties where R is curvature radius, d is inner diameter of pipe and p is the helical pitch.....	8
Figure 3-5 3D illustration of the supporting structure.	9
Figure 3-6 Combining the Pump characteristics H and system characteristics H_A gives the operation point.....	10
Figure 3-7 Illustration of separator used.....	11
Figure 3-8 Illustration of the oil outlet nozzle.	12
Figure 3-9 Parts of a DAQ system. (Instruments N.A)	13
Figure 3-10 The components of the turbine meters. (Cameron 2012)	14
Figure 3-11 Wheatstone bridge for the temperature sensor.....	16
Figure 3-12 Illustration of a typical Strain Gauge pressure sensor. (Instruments N.A)	17
Figure 3-13 LabVIEW block diagram used for this setup. Full A4 sized picture can be found in Appendix D.	20
Figure 3-14 LabVIEW front panel interface.....	21
Figure 3-15 Camera control and live view on the computer	23
Figure 3-16 How shutter speed affect an image. Brown (2014).....	24

Figure 3-17 Screenshots from the color sample test. Timestamp indicates the time each sample used to separate. 26

Figure 3-18 Example from the experimental matrix at 0.9 oil ratio. Wanted Conditions in the left segment and Measured Conditions in the right..... 28

Figure 3-19 Water phase section at start and after 2 minutes when running 300 l/min water and 300 l/min oil. 31

Figure 3-20 Oil phase section at start and after 3,5 minutes when running 300 l/min water and 300 l/min oil. 31

Figure 3-21 When running experiments with low oil ratio and relatively high flow rate the water, oil and mixed phases started to look alike..... 32

Figure 4-1 Loop geometry used in simulations..... 34

Figure 4-2 Representative view of the flow after T-pipe..... 34

Figure 4-3 Screenshot of meshing with inflation..... 35

Figure 4-4 Half-circle plane on inlet and outlet of loop. 36

Figure 4-5 Illustration of a secondary flow pattern. (S A Berger, L Talbot et al. 1983)..... 39

Figure 4-6 Planes distributed in 4 m long pipe. 40

Figure 5-1 Illustration of what a perfect oil-water segregation would look like at oil ratio 0.5..... 41

Figure 5-2 0.7 oil ratio at 20g..... 42

Figure 5-3 0.9 oil ratio at 40g..... 42

Figure 5-4 0.5 oil ratio at 50g..... 43

Figure 5-5 Flow regime resembling intermittent flow when running below 10g. 43

Figure 5-6 Best conditions according to simulations. Oil ratio 0.1 at 70g..... 44

Figure 5-7 Oil and air flow with clear segregation at loop outlet. 45

Figure 5-8 Half-circle plane on inlet and outlet of loop. 46

Figure 5-9 3D graph of Relative efficiency given Oil ratio and g's. Upper cross section. 47

Figure 5-10 Different Oil ratios plotted against Relative efficiency and g's. Upper cross section..... 47

Figure 5-11 Number of g's plotted against Relative efficiency and Oil ratio. Upper cross section. 47

Figure 5-12 3D graph of Relative efficiency given Oil ratio and g's. Lower cross section. 48

Figure 5-13 Different Oil ratios plotted against Relative efficiency and g's. Lower cross section. 48

Figure 5-14 Number of g's plotted against Relative efficiency and Oil ratio. Lower cross section..... 48

Figure 5-15 The measure of secondary flow given Oil ratio and number of g's. 49

Figure 5-16 Vector plot of secondary flow at loop outlet for different oil ratios at 30 g's. 50

Figure 5-17 Reduction in turbulence caused by loop compared to a straight pipe of equal length.... 51

Figure 6-1 Cross Flow Media..... 56

Figure 6-2 Strains of coalescence fiber. 57

Nomenclature

Symbol	Description	Unit
a_c	Centrifugal acceleration	m/s^2
v	Velocity	m/s
R	Curvature radius	m
g	Gravitational acceleration (9,81 m/s^2)	m/s^2
Q	Flow rate	m^3/s
Q_{low}	Minimum set flow rate (LabVIEW)	m^3/s
Q_{high}	Maximum set flow rate (LabVIEW)	m^3/s
Q_{tot}	Total flow rate	m^3/s
Q_{oil}	Flow rate oil	m^3/s
Q_{water}	Flow rate water	m^3/s
$I_{measured}$	Current measured by DAQ device	mA
I_{low}	Minimum output current	mA
I_{high}	Maximum output current	mA
R_x	Resistance across PT100 element	Ohm
R_0	Resistance at 0°C	Ohm
R_1	Resistance across resistor 1	Ohm

R_2	Resistance across resistor 2	Ohm
R_3	Resistance across resistor 3	Ohm
V_R	Measured voltage across Wheatstone	V
V_{exc}	Excitation voltage	V
t	Temperature	°C
A	Constant A	-
B	Constant B	-
C	Constant C	-
P	Pressure	bar
P_{high}	Maximum sensor pressure	bar
P_{low}	Minimum sensor pressure	bar
d	Pipe/hose diameter	m

1 Introduction

This master thesis is written as part of a SUBPRO project where the long term goal is to identify multiphase flow separation performance of a helically coiled pipe and determine if it's viable for further industrial development. SUBPRO is an applied research center consisting of relevant contributors from the industry and the Norwegian University College of Science and Technology. One of their stated goals is «*develop new knowledge and technology to meet future challenges in subsea production and processing*». This thesis is a continuation of the work previously done in the specialization project «*Compact Separation; Concept Study of Helically Coiled Pipe and Preparation for Experimental Setup*» and will later be continued as a PhD study.

The objective of this project is to develop an experimental setup and conduct experiments to qualitatively determine the potential of using a helically coiled pipe as a compact separator or flow conditioner and its potential for further industrial development. In the end, recommendations based on the results is to be made. In addition, CFD simulations will be performed to support the data from the experiments.

Since most of the relevant theory has been covered in the specialization project, a general theory chapter has not been added in this report. Rather, a short presentation of relevant theory has been introduced in the respective subchapters. If the reader is in need of a more detailed explanation, she or he is referred to the specialization project. The fluids used in the experimental study were limited to tap water and Exxsol D60. A test with air and Exxsol D60 was also conducted to get proof of concept. The loop was kept at a single bend radius and inner diameter. Even though methods for quantitative measuring are investigated in this report, the results and conclusion are based on a qualitative assessment.

The structure of the report after introduction is as follows:

- Chapter 2 presents a short summary of the specialization project written previous semester.
- Chapter 3 presents the experimental study with the helical coil. This includes a description of the experimental setup in terms of function and components. It also describes the fluids used and the experimental procedures.

- Chapter 4 describes the simulations conducted in terms of geometry, meshing, settings and which parameters were studied.
- Chapter 5 presents the results from the experiments and simulations.
- Chapter 6 features a discussion of the results and the applicability of the helical coil concept. Limitations and uncertainties and recommendations for further work are also discussed here.
- Chapter 7 lists the main conclusions.

2 Specialization Project Summary

A specialization project was written the semester prior to this project and served as a preparation for this master thesis. This chapter will summarize what was done in the specialization project and the results of the study.

The objective of the pre-study was to perform a literature study and investigate the potential of using a helical coil as a compact separator or for flow conditioning for an oil-water flow in addition to planning the experimental setup for this master thesis.

Main work done in the specialization project included:

- Literature study of fluid dynamics and multiphase flow fundamentals, separation principles and existing separation technologies.
- Study of previous publications regarding multi-phase flow in helical coils.
- Preparations for the experimental setup in the form of practical planning regarding existing equipment, hydraulic and physical design, budgeting, identifying relevant equipment suppliers and placement of purchase orders.
- Familiarization with Computational Fluid Dynamics.

Results of the literature study implied that centrifugal based separation is extensively used and has proven benefits both in efficiency and in size and that a helical coil has many characteristics that could make it a suitable compact separator.

Previous publications found in the specialization project showed that the concept of using a helical coil for separation or flow conditioning has been studied, but not extensively. These publications were mostly focused on gas-liquid flow and showed promising results in terms of gas-liquid phase segregation.

The most significant parameters that affected segregation seemed to be pipe diameter, curvature radius and flow rate. Experiments done by Vidnes, Engvik et al. (2015) also indicated that using one loop gave better results for gas-liquid flow compared to several loops.

3 Experimental Study

This chapter describes the experimental study conducted in this thesis. The chapter includes description of the experimental setup and its components in addition to the procedures that were followed when conducting the experiments. The complete list of parts can be found in Appendix A.

3.1 Experimental Setup

3.1.1 Overview

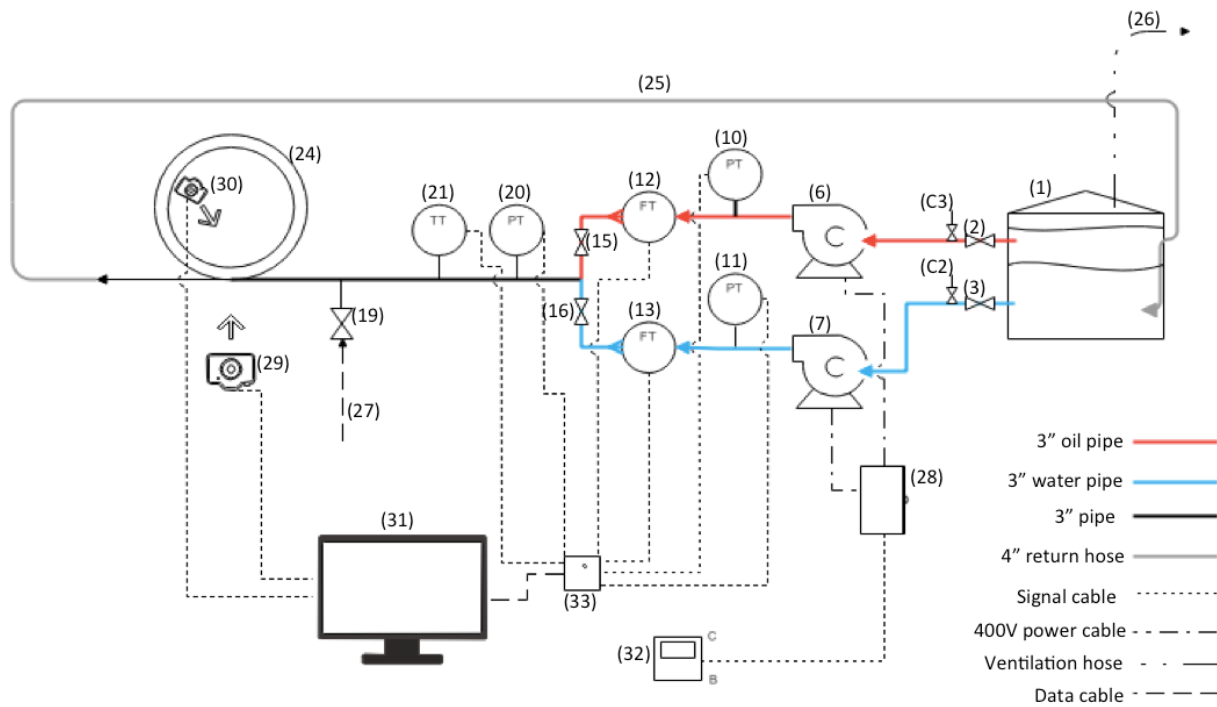


Figure 3-1 P&ID of experimental setup with numerical indicators for components later referred to.

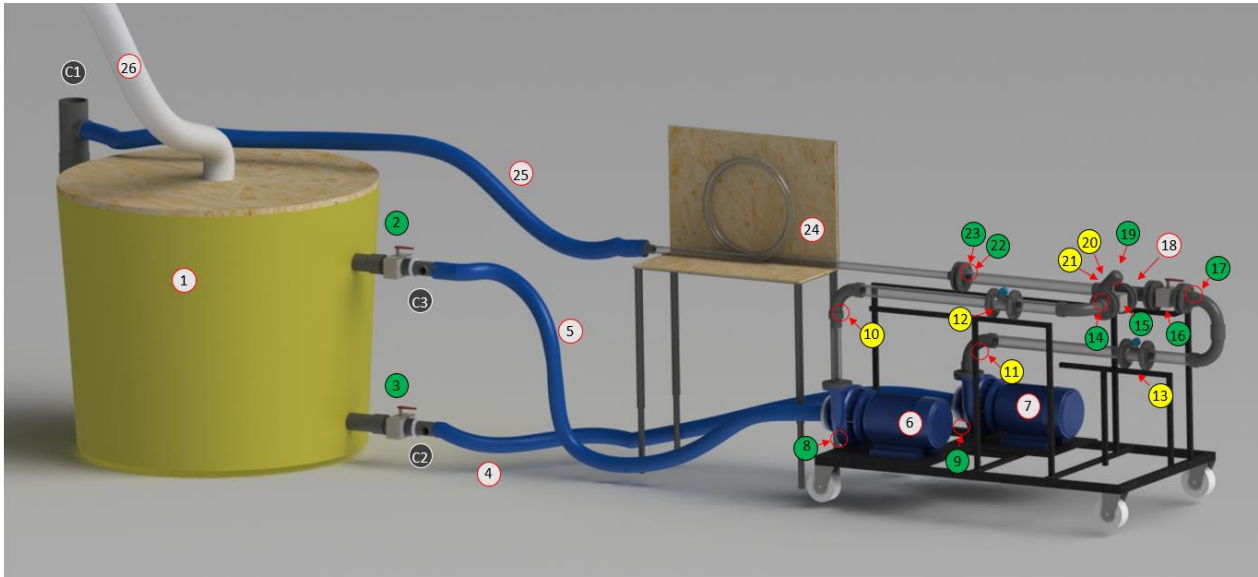


Figure 3-2 3D illustration of experimental setup. The numbers indicates key components referred to later in this thesis.

Indicated components from the P&ID in Figure 3-1 and 3D illustration in Figure 3-2:

- | | | |
|-----------------------------------|---------------------------------|---|
| 1) Separator | 12) Flow meter/oil | 24) Helical coil |
| 2) Master valve/oil | 13) Flow meter/water | 25) Return hose |
| 3) Master valve/water | 14) Venting valve | 26) Ventilation hose |
| 4) Suction hose/water | 15) Control valve/oil | 27) Air supply |
| 5) Suction hose/oil | 16) Control valve/water | 28) Frequency converters |
| 6) Pump/oil | 17) Venting valve | 29) Side-view camera |
| 7) Pump/water | 18) T-pipe (oil/water junction) | 30) Top-view camera |
| 8) Drainage valve/oil | 19) Air inlet/venting valve | |
| 9) Drainage valve/water | 20) Pressure sensor | C1-3) Connection point for external system. |
| 10) Pressure sensor at oil pump | 21) Temperature sensor | |
| 11) Pressure sensor at water pump | 22) Sample valve/bottom | |
| | 23) Sample valve/side | |

In this system, oil and water is pumped from the separator (1) by pumps (6, 7) to the T-pipe (18) through separate 3" pipe sections. Here the two phases mix and goes through an observation section, before it enters the loop (24). After the loop, the flow enters the return hose (25), and is routed back to the separator.

For monitoring of the system, both the oil and water section are equipped with its own pressure sensor (10, 11) and flow meter (12, 13). In addition a pressure sensor (20) and temperature sensor (21) are placed after the T-pipe. Ball valves (15, 16) are used to isolate the oil and water sections to enable single phase flow.

Several small ball valves are installed in the system for drainage (8, 9), venting (14, 17), sampling (22, 23) and air inlet (19) respectively.

As a general safety measure and in the case of leakage each separator outlet is equipped with a gate master valve (2, 3) so that the separator can be isolated. This also enables drainage of the system.

The system also has three connection points (C1, C2, C3) to an external experimental system. The connection point are closed and opened by ball valves.

The procedures for start-up, shutdown and drainage of system can be found in Appendix B.

3.1.2 Pipes

The straight pipes used in this experimental setup are transparent PVC pipes with an outer diameter of 75 mm and wall thickness of 3.6 mm. These pipes have the pressure classification PN 10, meaning they have a maximum allowable operating pressure of 10 bar (polypipe n.d). The piping components used (bends, T-pipe etc.) are also PVC, with an inner diameter of 75 mm and pressure classification PN 16, i.e. maximum allowable operating pressure of 16 bar. The straight piping are connected to the piping components by internal gluing with PVC glue.

3.1.3 Valves

For closing and opening of oil and water outlets two 4 inch gate valves (2, 3) are installed at the separator. Two 3 inch PVC ball valves (15, 16) are placed before the T-pipe (18) for closing and opening of water and oil section of the system. A total of 7 small ball valves (8, 9, 14, 17, 19, 22, 23) are installed in the system for drainage, venting and fluid sampling.

3.1.4 Helical Coil

The helical coil (24) is the component which applies centrifugal force to the multiphase flow. The amount of centrifugal acceleration induced is governed by the tangential flow velocity v and the curvature radius R of the coil. As seen in equation 3-1 higher velocity and smaller curvature radius

results in higher centrifugal acceleration. The centrifugal acceleration a_c is presented as a multiple of the gravitational acceleration g .

$$a_c = \frac{v^2}{Rg} \quad (3-1)$$

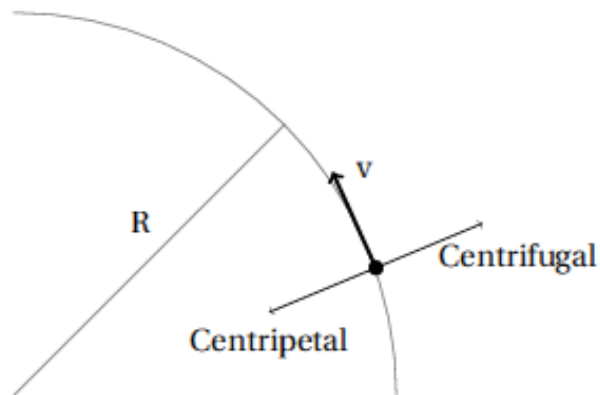


Figure 3-3 A particle moving in a circular motion with a constant radius and tangential velocity. (Vidnes, Engvik et al. 2015)

When deciding the geometry of the helical coil, the aim was to achieve a centrifugal acceleration of around 100 g's. With the relatively high capacity of the pumps used in this setup, it was deemed adequate to use a hose with a diameter of 2 inches. Since the studies conducted by da Mota and Pagano (2014) and Vidnes, Engvik et al. (2015) indicated that an increased number of loops in the coil did not have a positive impact on water-air phase separation, it was decided to use only one loop in the coil. The study by da Mota and Pagano (2014) also showed that pitch variation had no noticeable effect on the phase separation. The pitch was therefore the same as the outer diameter of the hose.

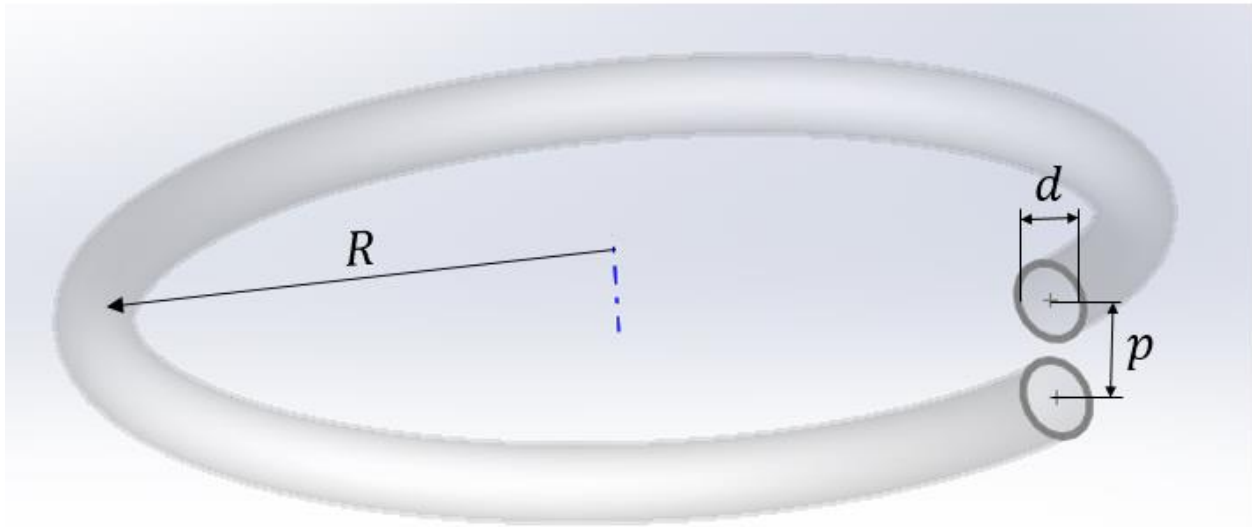


Figure 3-4 Illustration describing the helical coil properties where R is curvature radius, d is inner diameter of pipe and p is the helical pitch.

The hose used was a 2 inch, clear, reinforced PVC hose called “MiljøTESS” with an operating pressure of 4 bar and a bursting pressure of 12 bar at 20°C.

The coil shape is achieved by clamping the hose to a vertical board at four different positions as seen in Figure 3-15. The clamps are adjustable so that the distance between them, i.e. the size of the loop, can be adjusted.

3.1.5 Supporting Structure

For practical purposes it was a desired feature to have a movable experimental rig. To achieve this the two pumps and all piping before the helical coil were mounted on a supporting structure with wheels. The supporting structure is made out of 50x50 mm and 30x30 mm square steel tubing with a wall thickness of 3 mm and two steel plates for the pumps to be bolted on.

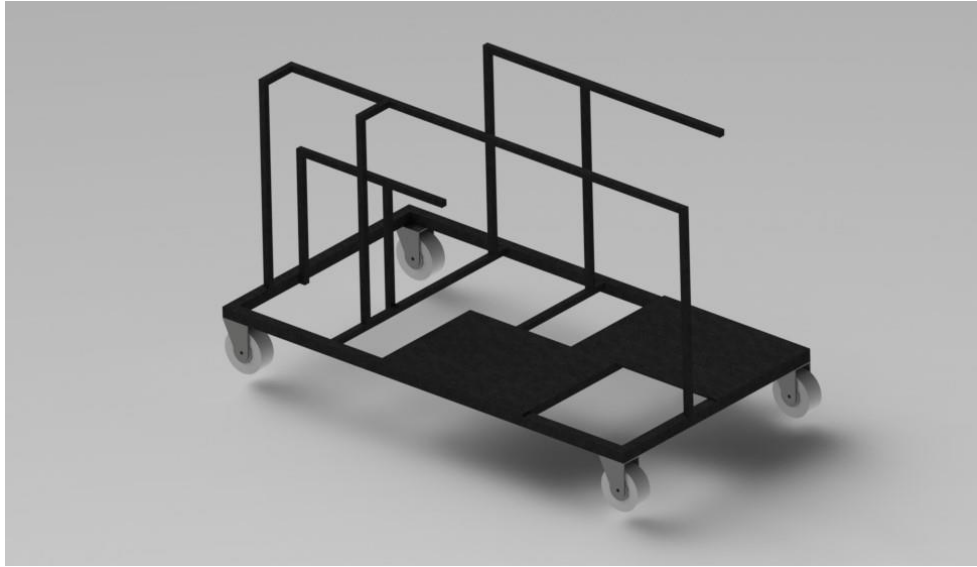


Figure 3-5 3D illustration of the supporting structure.

3.1.6 Pumps

To achieve the desired amount of centrifugal force, a high flow rate was required. It was therefore decided to use centrifugal pumps for this setup, which are typically characterized with the ability to provide high flow rates and relatively smooth flow. (Chemacinc 2012)

The performance of the centrifugal pumps is determined by its *Pump characteristics*. When the flow rate varies, so does the power consumption, efficiency and head of the pump, i.e. the outlet pressure. Plotting these values against the flow rate gives the pump characteristics. The intersection between the pump characteristics and system characteristics is called the operation point. This is where the head generated by the pump is equal to the head required by the system. $H=H_A$. (Gulich 2010)

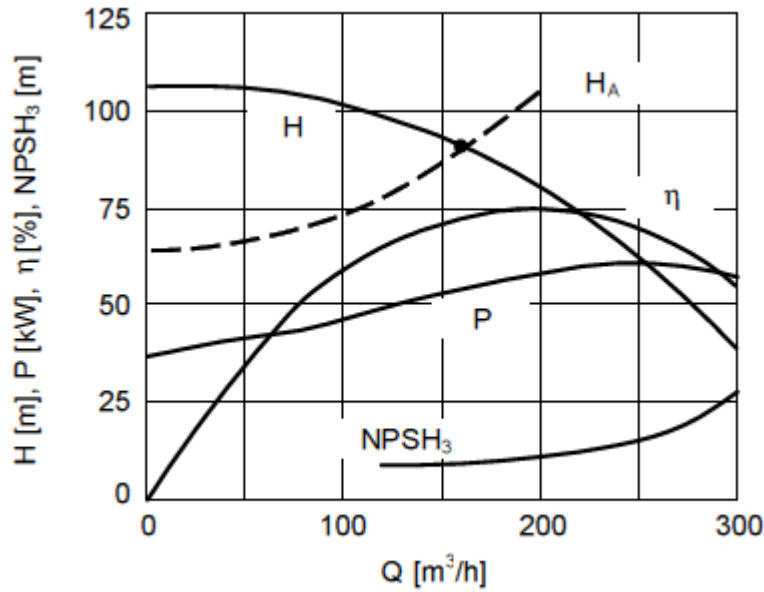


Figure 3-6 Combining the Pump characteristics H and system characteristics H_A gives the operation point.

One high capacity pump (Pedrollo F65/200AR) is used for the water, and one lesser capacity pump (Pedrollo F50/200B) is used for the oil. The main specifications of the pumps and the amount of flow they can supply at different heads are given in Table 1.

Model	Power		Voltage (three phase)	Q (l/min)	400	600	800	1000	1200	1400	1600	1800	2000	2100
	kW	HP			Head (m)									
Pedrollo F50/200B	15	20	400 V	Head (m)	52	52	52	50	47	44	40			
Pedrollo F65/200AR	22	30	400 V		57	57	57	57	56	55	53	50,5	47,5	46

Table 1 Flow rate at different head for the two pumps.

A fan was mounted on each pump for cooling of the motor driving the pumps. Each motor is controlled by a detachable control panel that came with the frequency converters mentioned in the following chapter.

3.1.7 Frequency Converters

Using a frequency converter enables regulation of the rotational speed of the electrical motors, hence the speed of the pumps. Most commonly, the frequency converters produce a variable frequency by pulse-width modulating (PWM) the voltage source. In its simplest form, it develops a voltage directly proportional to the frequency and the voltage determines the speed of the motor. Modern frequency converters have Programmable Logic controllers, which enables the pumps to be controlled by a computer with a suitable software. (Technology 2004)

The frequency converters used in this experimental setup are of the type Vacon 100 HVAC (15kW) for the small pump and Vacon 100 HVAC (22kW) for the larger pump. Each frequency converter is equipped with a detachable control panel. For safety measures, the frequency converters are equipped with an emergency shutdown switch.

3.1.8 Separator

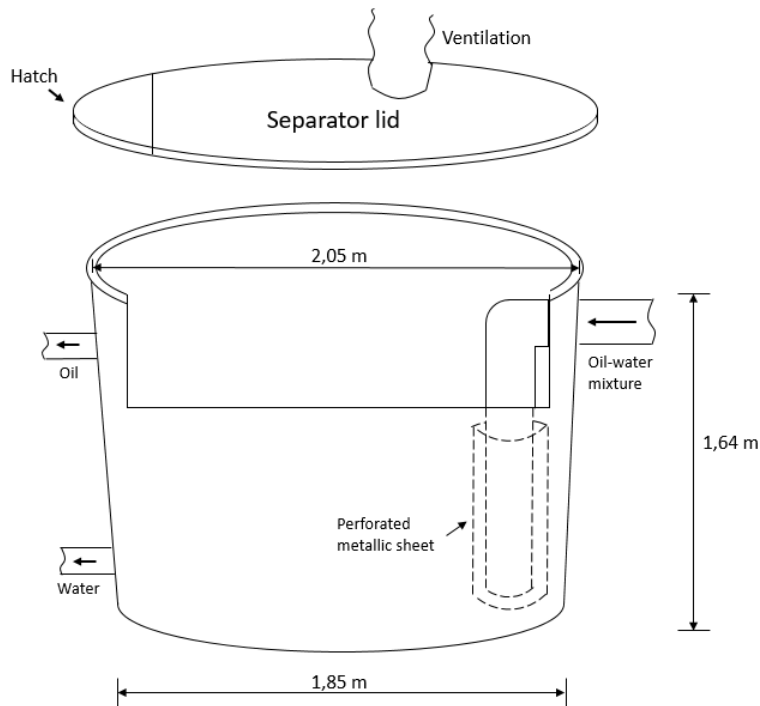


Figure 3-7 Illustration of separator used.

To separate the oil-water mixture coming from the helical coil, a gravity-based separator is used. The separator also functions as a reserve from which the water and oil is pumped. The material used for the separator is fiberglass and the total volume is five cubic meters. Oil-water mixture enters the separator inlet and is led to the bottom to decrease mixing. The density difference between oil and water separates the mixture, making the oil float to the top and water to the bottom. The two liquids are then extracted through two different outlets; oil outlet at the top and water outlet at the bottom. A plywood lid sits on top of the separator with a hole connected to a ventilation hose for evacuation of fumes from the oil.

The efficiency of the separator is difficult to realistically calculate, but the separator has been used successfully in previous experiments with similar flowrates. There are also special internals called *cross flow media* that could be added in the separator and are said to decrease turbulence and improve the separation process. Due to shortage of time, no internals were used in these experiments but are mentioned under recommendations for further work.

In order to reduce the likeliness of getting emulsion or air in the oil outlet of the separator, a nozzle was designed and installed. The end of the nozzle is wide and rectangular shape to get more suction in the horizontal plane and less in the vertical plane. It was constructed in aluminum and has floating elements attached to it to ensure that it floats in the oil level of the separator. Additionally a perforated metallic sheet was attached around the internal inlet to reduce turbulence.

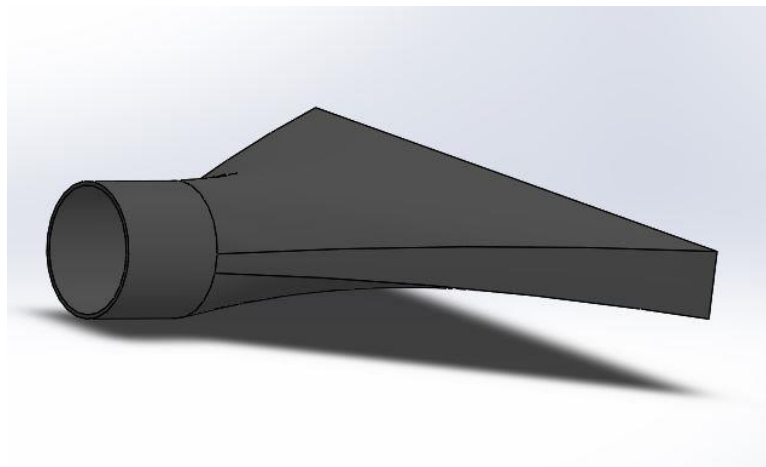


Figure 3-8 Illustration of the oil outlet nozzle.

3.1.9 Data Acquisition and Control

A Data Acquisition System (DAQ) was used in this experiment to monitor the experimental setup and retrieving experimental data. “Data acquisition is the process of measuring an electrical or physical phenomenon such as voltage, current, temperature, pressure, or sound with a computer”.

Instruments (N.A)



Figure 3-9 Parts of a DAQ system. (Instruments N.A)

A DAQ system consists of sensors, a DAQ device and a computer with a software with the ability to interact with the DAQ device. Below is a description of the DAQ components used in this experimental setup.

3.1.9.1 Sensors

Measuring a physical phenomenon such as the flow rate of a liquid, the temperature or pressure in a system, requires some form of sensor. A sensor converts a physical phenomenon into an electrical signal, which can either be voltage, current, resistance or another electrical output that varies over time. The sensors used in this setup required external power supply and a sealed box was used to contain all necessary wiring for the sensors and the DAQ device.

3.1.9.1.1 Flow meter

To get a measurement of the flow rate for both water and oil two flow meters was installed, one downstream of the water pump and one downstream of the oil pump. The flow meters are of the type Halliburton EZ-IN Liquid Turbine Meter sized at 3 inches. These are turbine flow meters which contain a spinning turbine that turns at a speed that is proportional to the flow velocity and can be

used for both oil and water, unlike an electromagnetic flow meter, which only works with conducting liquids. The spinning turbine produces electric pulses for each turn which is read and converted to a flow measurement like m³/s or l/min (Cameron 2012).

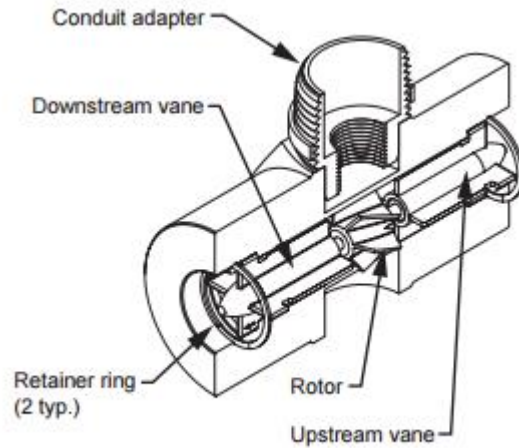


Figure 3-10 The components of the turbine meters. (Cameron 2012)

Each flow meter was connected to a Fluidwell F110 programmable flow rate indicator, which displayed the current flow rate as l/min or m³/s and the accumulated flow. These displays also outputs a current of 4-20 mA according to what the user have set to represent minimum and maximum flow rates. These currents were used to transfer the flow values to the application software LabVIEW with the following equation:

$$Q = \frac{Q_{high} - Q_{low}}{I_{high} - I_{low}} * (I_{measured} - I_{low}) \quad (3-2)$$

$$Q = \frac{Q_{high} - Q_{low}}{20mA - 16mA} * (I_{measured} - 4mA)$$

The measured flow rate was also used to determine the oil-water ratio of the liquid and for calculating the centrifugal force induced in the loop.

3.1.9.1.2 Temperature Sensor

It is generally desired to have control over the temperature in an experimental system as for instance viscosity varies with temperature. It also provides a safety measure in the sense that the system can be shut down if the temperature reaches a certain threshold.

The temperature sensor that was used for this setup is a platinum resistance thermometer of the type PT100. The principle of this thermometer is to measure the resistance of a platinum element which has a relationship with the temperature it is exposed to. This relationship is linear over a temperature range, but it may be necessary to linearize the resistance for precision measurement. The characteristics of the PT100 element is that it has a resistance of 100 ohms at 0 °C.

The most recent definition of the resistance-temperature relationship by International Temperature Standard 90 (ITS 90), is:

$$R_x = R_0 * (1 + A * t + B * t^2 + C(t - 100) * t^3) \quad (3-3)$$

Which can be deduced to find the temperature:

$$t = \frac{-R_0 * A + \sqrt{R_0^2 * A^2 - 4 * R_0 * B * (R_0 - R_x)}}{2 * R_0 * B} \quad (3-4)$$

Where R_t is the resistance at temperature t , R_0 is the resistance at 0 °C and the constants A, B and C are respectively:

$$A = 3,9083 * 10^{-3} \quad B = -5,775 * 10^{-7} \quad C = -4,183 * 10^{-12} < 0 \text{ °C} < 0$$

(Technology N.A)

For this setup the temperature sensor was connected in a Wheatstone bridge by a 3-wire connection seen in Figure 3-11 where the excitation voltage V_{exc} is 10 V, R_1 and R_3 is 1 k Ω , R_2 is 200 Ω and the variable resistance R_x is the PT100 element. The voltage V_R measured across the bridge by the DAQ device is used to calculate R_x with the following equation:

$$R_x = (R_2 * R_3 + R_3 * (R_1 + R_2) * \frac{V_R}{V_{exc}}) / (R_1 - (R_1 + R_2) * \frac{V_R}{V_{exc}}) \quad (3-5)$$

(daycounter.com 2016)

Resistance R_x is then used to calculate the temperature in equation 3-4.

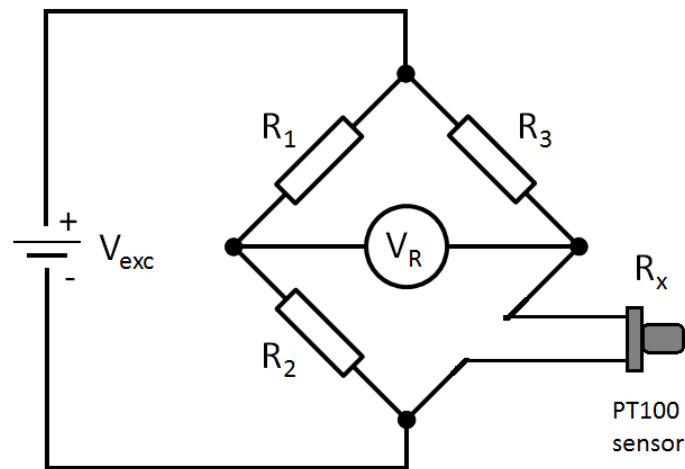


Figure 3-11 Wheatstone bridge for the temperature sensor.

3.1.9.1.3 Pressure sensors

In order to have control over the pressure in the system, three pressure sensors were installed and set to output the gauge pressure. One was installed after each pump and one before the helical coil. Components such as the PVC piping, hoses and fittings that was used in the setup are certified for a certain amount of pressure and the pumps have a limited amount of pressure they can supply. Like the temperature, measurement of the maximum pressure provides a safety measure and can give additional information to the experimental results.

The pressure sensors that was used are Strain Gauge Pressure Sensors of the type UNIK 5000 manufactured by GE. The principle behind the strain gauge sensor is that a change in pressure causes a diaphragm to deflect and a corresponding change in resistance is induced in a strain gauge. The pressure sensors outputs a current that is linear to the change in resistance, which can be converted into a pressure measurement such as bar. (Instruments N.A)

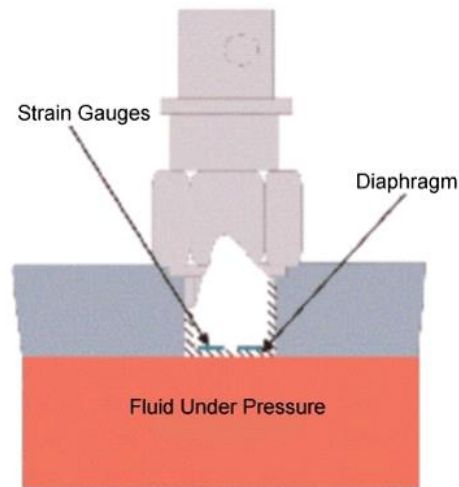


Figure 3-12 Illustration of a typical Strain Gauge pressure sensor. (Instruments N.A)

The UNIK 5000 pressure sensor outputs a current of 4-20 mA which is linear to its pressure range of 0-16 bars. A DAQ was used to measure the current output which was converted to bar by the following equation:

$$\begin{aligned}
 P &= \frac{P_{high} - P_{low}}{I_{high} - I_{low}} * (I_{measured} - I_{low}) \\
 P &= \frac{16bar - 0bar}{20ma - 4ma} * (I_{measured} - 4ma) \\
 &= \frac{16bar}{16ma} * (I_{measured} - 4ma)
 \end{aligned}
 \tag{3-6}$$

3.1.9.2 Calibration

To ensure that the values received from each sensor was correct, each sensor was calibrated. The calibration technique was different for each type of sensor. See Appendix C for the full calibration sheet.

3.1.9.2.1 Calibrating Turbine Flow Meters

A *Nominal Calibration Factor* or *k-factor* was used to calibrate the flow meters. This is the approximate number of pulses the meters should produce for each given amount of volume that has passed. The *k-factor* is read from the data sheet for a 3 inch Halliburton Liquid Turbine Flow Meters as 15200 pulses per m³ for water, but can be adjusted on the Fluidwell flow rate indicators.

To see if the given *k-factor* was accurate for this setup, water was pumped to a 1000 liter tank with level indicators. The volume accumulated in the tank was then compared to the accumulated value displayed on the Fluidwell indicators. This was repeated three times for each flow meter and the average error was used to tune the k-factor. Equation 3-7 was used to calculate the standard deviation of the k-factor where \bar{x} is the sample mean average and n is the sample size. The standard deviations were 0.43% and 0.16% for the oil and water flow meter respectively. Since the sample size was small and the experiments was validated qualitatively the standard deviation was not used further. Even though the k-factor was calibrated using water, the indicators showed accurate readings when it later was tested with oil.

$$\sqrt{\frac{\sum(x - \bar{x})^2}{(n - 1)}} \quad (3-7)$$

3.1.9.2.2 Calibrating Temperature sensor

Even though the temperature sensor should show an accurate value with the formula used, a minor electrical disturbance could cause inaccuracy. In this case the sensor showed a few degrees too high compared to a thermometer and a calibration was necessary. The temperature value shown by the sensor was compared to a thermometer at different temperatures varying from boiled water to cold

tap water. The errors were used to create a graph in excel and a correction formula was created using regression. This formula was then used in the software LabVIEW to correct the sensor error limiting it to about 1 degree Celsius.

3.1.9.2.3 Calibrating Pressure sensors

To ensure the pressure sensors were transmitting the correct value, pressure gauges were installed in the proximity of the sensors. Since the sensors showed approximately the same value as the gauges, it was determined that calibration was not necessary.

3.1.9.3 DAQ Device

The DAQ device acts as the interface between the computer and signals acquired from the sensors. Its primary function is to digitize incoming analog signals which enables a computer to interpret them.

The processed signal is transferred to the computer over a computer bus, in this case USB, which serves as the interface between the DAQ device and computer for passing instructions and measured data. DAQ devices exist for the most common buses like USB, PCI and Ethernet.

For this experimental setup a USB-6009 Multifunction DAQ by National Instruments was used. The USB-6009 provides basic DAQ functionality for simple data logging and portable measurement applications. It features eight analog inputs with a resolution of 14-bits and a voltage range -10 V to 10 V. It has two analog outputs with a resolution of 12 bits and a voltage range of 0 V to 5 V.

3.1.9.4 LabVIEW

The software that used for this setup was LabVIEW which is a software developed by National instruments. LabVIEW is a programming environment commonly used for measuring and control applications. Since LabVIEW is developed by the same company as the DAQ device being used, it ensured a highly compatible DAQ system.

LabVIEW consists of two parts, a front panel and a block diagram. The front panel acts as the user interface with buttons and visual indicators for data acquired from the measuring devices. The block diagram is where the programming code is built and is based on the data flow rather than text lines. Data flow is represented by icons or boxes with various functions which is dropped in the

diagram and connected by wires. Figure 3-13 shows the block diagram for this setup. A larger version is found in Appendix D.

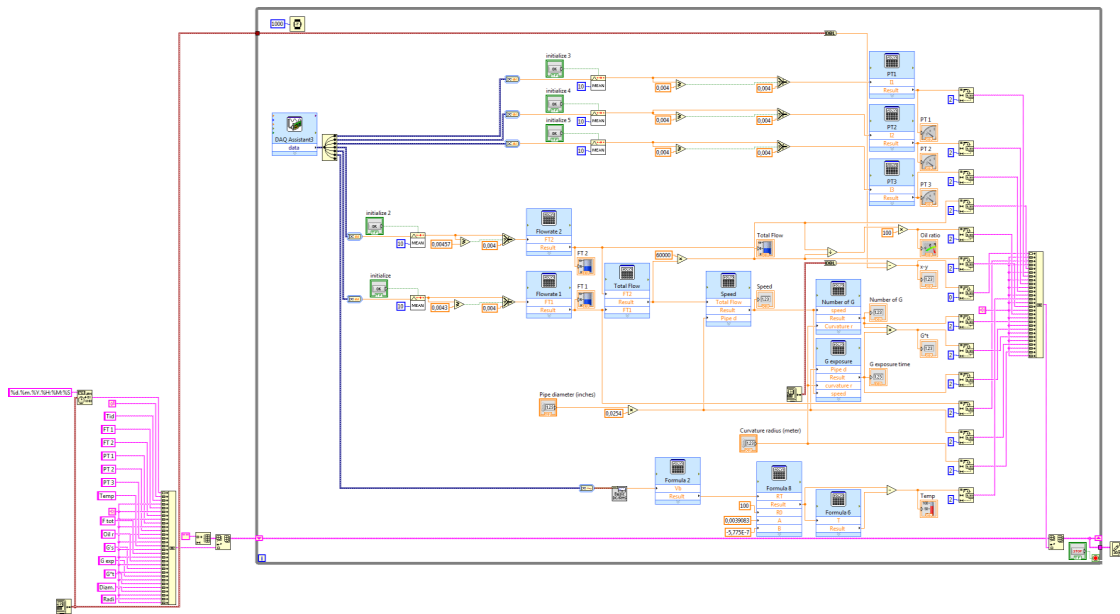


Figure 3-13 LabVIEW block diagram used for this setup. Full A4 sized picture can be found in Appendix D.

Figure 3-14 shows the LabVIEW front panel interface created for logging and monitoring of the experimental system and a description of its functions.

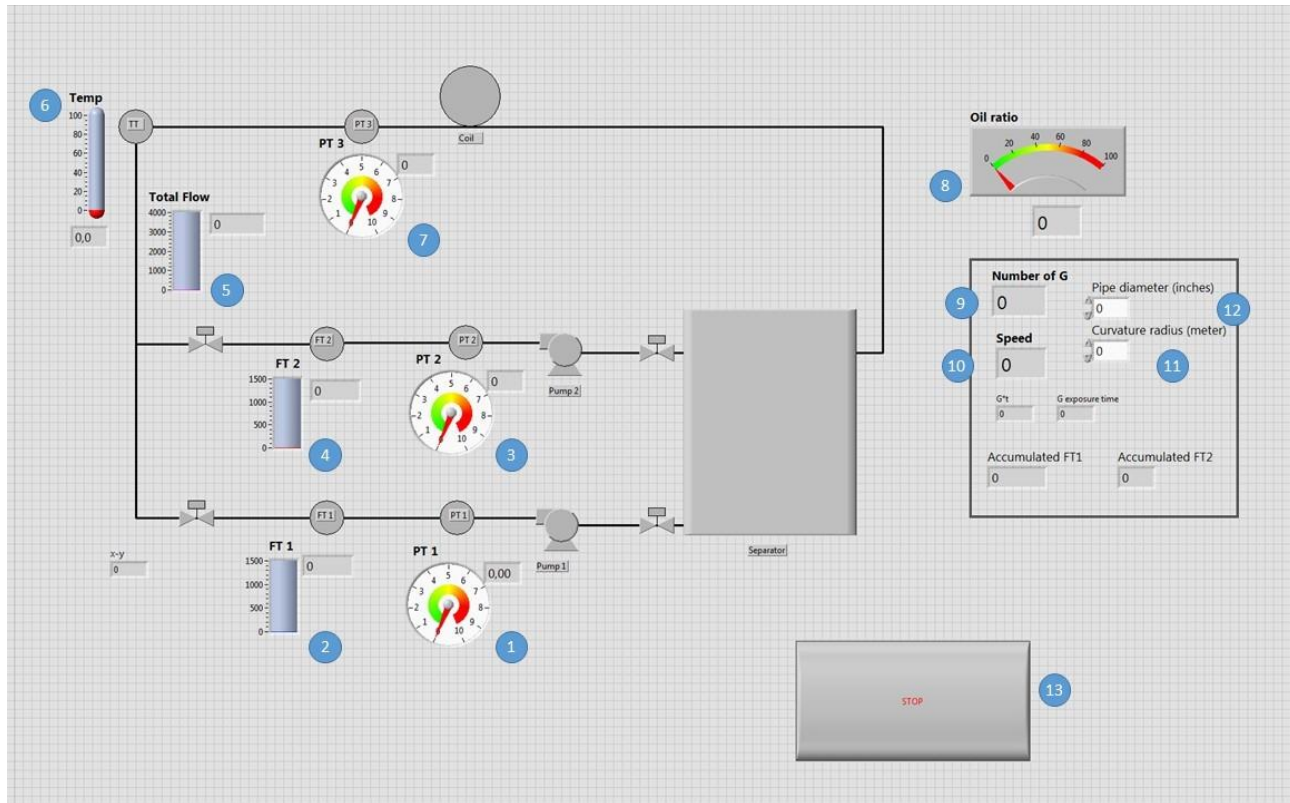


Figure 3-14 LabVIEW front panel interface.

3.1.9.4.1.1 Indicators

- | | |
|---------------------------|------------------------------|
| 1) Pressure at water pump | 2) Flow rate from water pump |
| 3) Pressure at oil pump | 4) Flow rate from oil pump |
| 5) Total flow rate | 6) Flow temperature |
| 7) Pressure at loop inlet | 8) Oil ratio |
| 9) Number of g | 10) Flow velocity |

3.1.9.4.1.2 Data input

The pipe diameter d (12) and curvature radius R (11) could easily be adjusted as an input for the calculation of number of g's a_c and flow velocity v .

3.1.9.4.1.3 Logging

For each experiment, measurements from the pressure sensors, flow meters and temperature sensor was stored in a spreadsheet from the moment the LabVIEW program was started until the stop button (13) was pressed. In addition these measurements worked as a continuous input for calculations of number of g's, velocity, oil ratio and total flow which also was logged.

The equations used for the mentioned calculations are:

$$a_c = \frac{v^2}{Rg} \tag{3-8}$$

$$v = \frac{Q_{tot}}{\frac{\pi}{4} * d}$$

$$Q_{tot} = Q_{oil} + Q_{water}$$

3.1.10 Camera Setup

To visually document and analyze the multiphase flow at the start and end of the helical coil, a Canon EOS 70D DSLR camera with an 18-55mm lens and a Samsung NX2000 with an 18-55mm lens was used to photograph the multiphase flow. The Canon camera was positioned to take side-view photos of the loop, capturing the start and the end while the Samsung camera was positioned in the middle of the loop to take top-view photos of the start and end. The Canon camera was remotely controlled by a computer via *tethering*. Tethering enables a live view from the camera on the computer screen and allows remote adjustment of camera settings like focus and shutter speed and remote control of the shutter itself. This is illustrated in Figure 3-15. Tethering also saves the captured pictures directly on the computer which enables direct analysis of the pictures without having to manually transfer them from the camera. The Samsung camera was controlled via a smartphone app. This is similar to computer tethering but lack adjustments of camera settings.

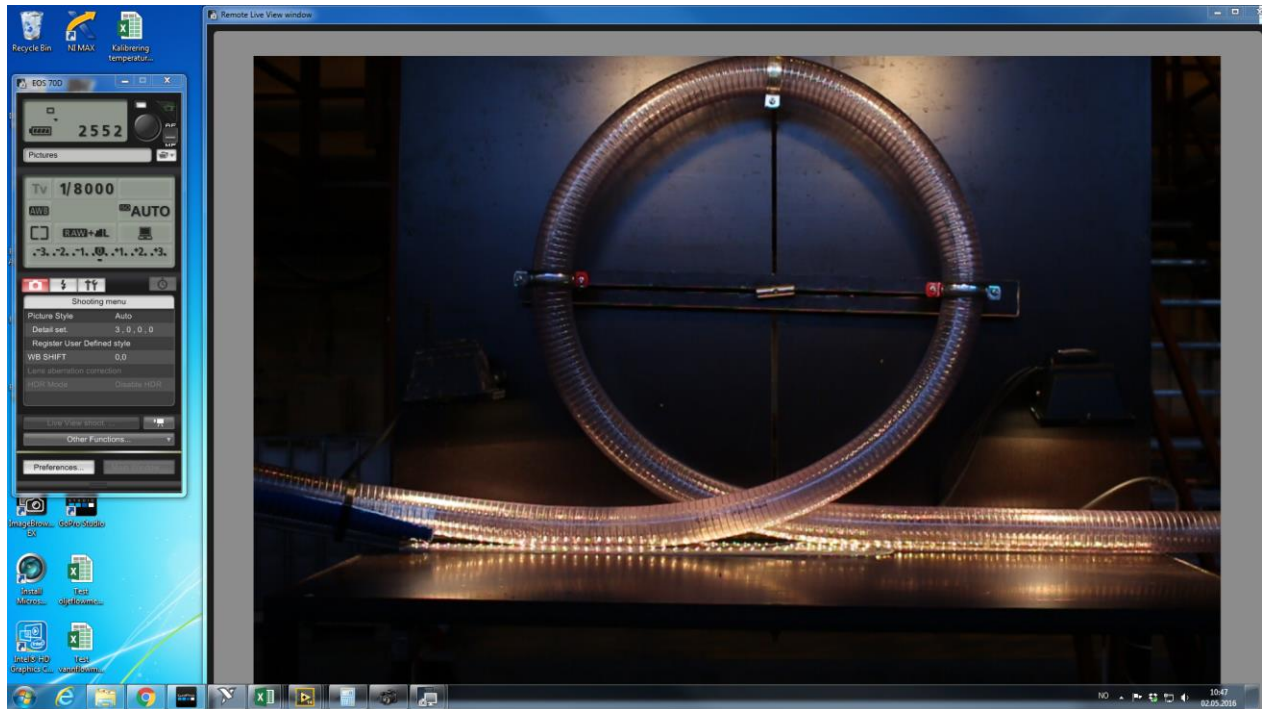


Figure 3-15 Camera control and live view on the computer

Photos from the Canon camera was captured with a shutter speed of $1/2000$ s, ISO 3200, aperture of $f/5,6$ and a resolution of 20,2 megapixels. The high shutter speed means that it can take pictures of fast moving objects without too much motion distortion or blur. As an example a fluid velocity of 10 m/s will result in a motion distortion of around 5 mm. A downside of using a high shutter speed is that the pictures requires a large amount of lighting. The Samsung camera only allowed auto setting when remotely shooting with a smartphone, so the settings may have changed for the different photos for that camera.

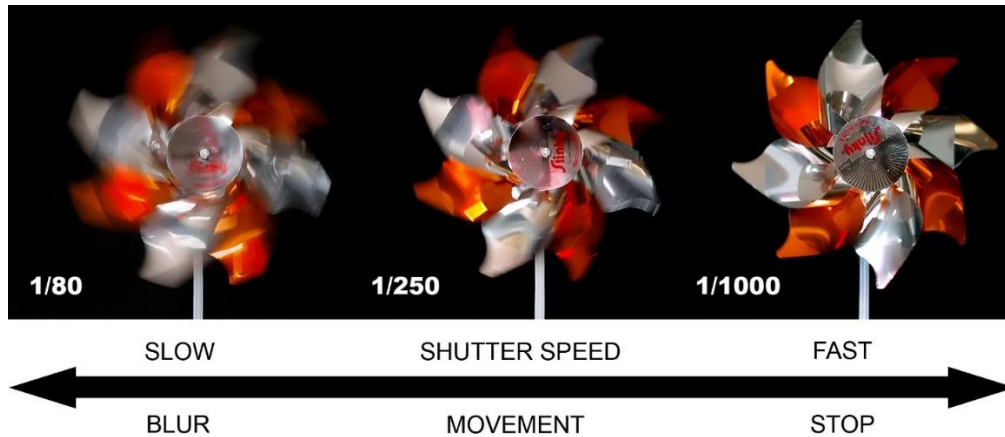


Figure 3-16 How shutter speed affect an image. Brown (2014)

To achieve similar lighting for each photo a tent was made of tarp which shielded the loop and cameras from external light such as sunlight. One LED strip was attached behind the inlet and outlet of the loop for background lighting. A light rig consisting of four halogen lamps was also built, but the halogen lights gave a fair amount of reflection in the reinforced hose and was therefore not used for the result photos.

3.2 Experimental Fluids

In the specialization project, it was decided to conduct the experiments with two liquids instead of air-water. This was due to the work already done in (da Mota and Pagano 2014) and (Vidnes, Engvik et al. 2015) regarding liquid-gas phase segregation in a helical coil. The two liquids used were Exxsol D60 and tap water.

3.2.1 Exxsol D60

Exxsol D60 was chosen as the oil representative because it is a widely used hydrocarbon solvent with a stated density of 793 kg/m^3 at $15 \text{ }^\circ\text{C}$ and viscosity of $1,64 \text{ cP}$ at $25 \text{ }^\circ\text{C}$ (measured values: 787 kg/m^3 and $1,53 \text{ cP}$ at $26 \text{ }^\circ\text{C}$). These properties are very similar to the average properties of North African crude oil which has a density of 801 kg/m^3 at $15 \text{ }^\circ\text{C}$ and a viscosity of $1,4 \text{ cP}$ at $38 \text{ }^\circ\text{C}$ (Lundberg 2009). In addition it has a low odor and generally low hazardous properties. See Appendix K for Exxsol D60 datasheet.

3.2.2 Water

In (Ghajari 2005) it was experienced that water from different sources resulted in different degrees of separation in the inclined separator system used in that study. Despite of this, for the present study only tap water was employed and no study was performed on the effects of the water source in the overall properties of the oil water multiphase mixture. The density of the tap water was measured to be 998 kg/m^3 at $24 \text{ }^\circ\text{C}$ with a viscosity of 1.09 cP at $22.7 \text{ }^\circ\text{C}$ and surface tension of 61.02 mN/m at $22.5 \text{ }^\circ\text{C}$.

3.2.3 Bacterial Inhibitor

To reduce the amount of bacterial growth in the separator a bacterial inhibitor was mixed in the oil and water. The inhibitor was of the type IKM CC-33 and a total of 1.8 liters was mixed in the separator with approximately 5 m^3 of liquid. Viscosity and surface tension tests showed that the inhibitor had no noticeable effect on the properties of Exxsol D60 and water.

3.2.4 Coloring of Liquid

Since Exxsol D60 and water are both transparent liquids, some form of colorization was necessary to distinguish the two phases. This could either be done by colorization of the oil, water or both. Three colorization methods were tested to establish which color seemed to bring the best distinction between the water and oil and what effect the coloring had on the separation properties. The tests were conducted by shaking a frame with four samples mounted; 1) Clear oil and water as reference, 2) Oil colored red with *OIL RED O* color powder and clear water, 3) Water colored green with *Merck* color powder and clear oil and 4) Water colored blue with *Ulefos* color powder and clear oil.

The tests were filmed with a camera attached to the same frame. These test were conducted with and without a bacterial inhibitor and the inhibitor showed no effect on the separation properties.

All six tests conducted showed that the sample with the red colored oil and clear water was the fastest to separate with a separation time of approximately 30 seconds. Followed by blue colored water with clear oil (38 seconds), clear oil and water (42 seconds) and lastly green colored water with clear oil (64 seconds). The red color also seemed to give the best visual distinction between oil and water. See Figure 3-17.

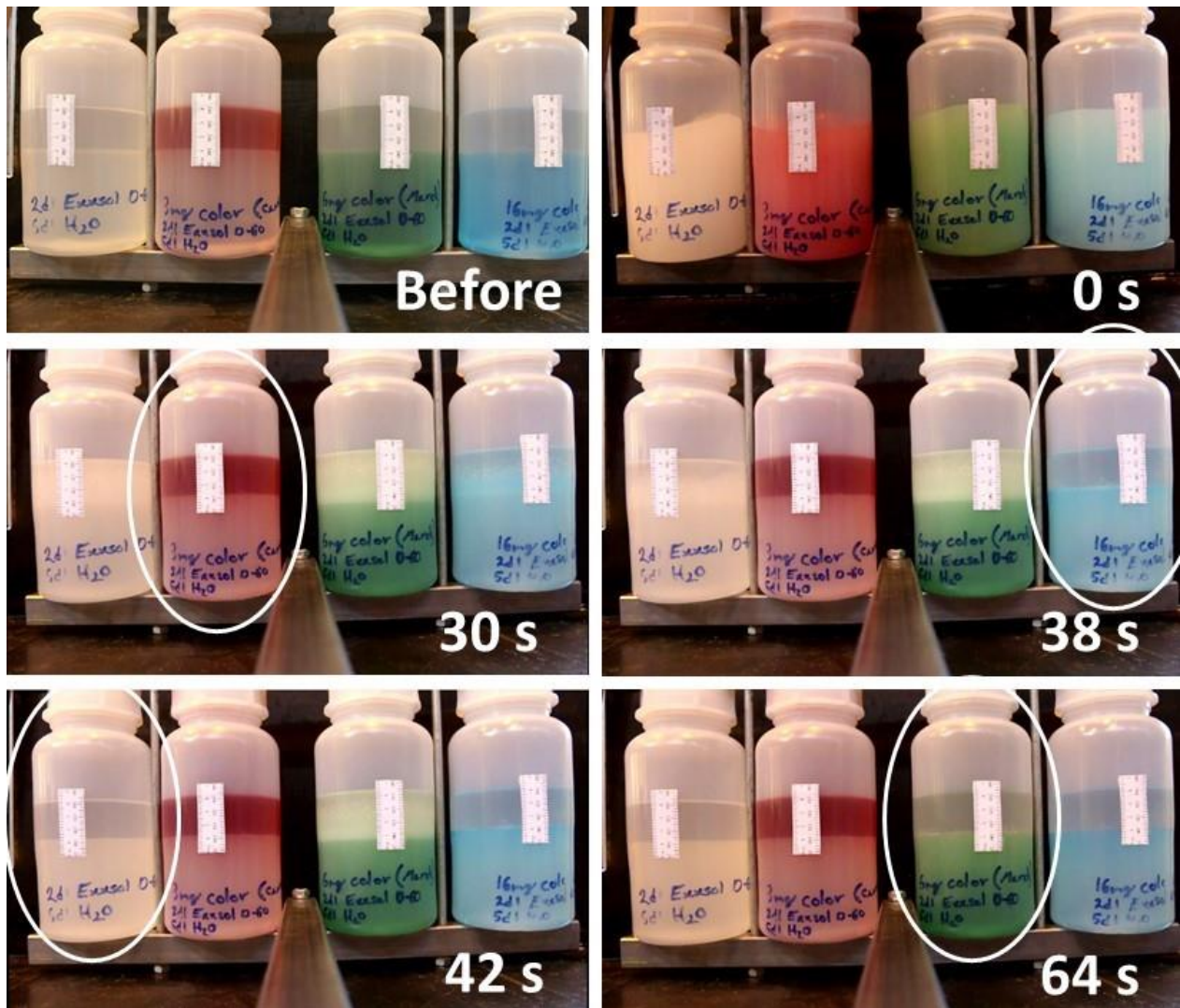


Figure 3-17 Screenshots from the color sample test. Timestamp indicates the time each sample used to separate.

Based on what was observed through the shake tests, the red color for oil was chosen for colorization. Measurements showed that both viscosity and density of the Exxsol D60 increased slightly when colored with OIL RED O color powder. See Table 2. It is uncertain if this increase had an actual impact on the segregation properties of the flow.

Coloring of both water and oil was also tested, but was quickly discarded as the two colors seemed to rub off on each other.

3.2.5 Measured Properties of Fluids

The water and oil density, viscosity, surface tension and interfacial tension was measured at the start and end of the experimental period to see if the properties of the fluids had changed due to factors such as bacterial growth or precipitation of minerals. A tensiometer was used to measure the surface tension and interfacial tension, a viscometer was used for the viscosity measurements and a pycnometer in combination with a scale (+/- 0.01 g) was used for density measurements. All the equipment was available at one of the institute's laboratories.

Before experimental period (26°C)	Density (kg/m³)	Viscosity (cP)	Surface tension (mN/m)	Interfacial tension (mN/m)
<i>Spring water</i>	998	1.09	61.02	
<i>Exxsol D60 without coloring</i>	787	1.53		
<i>Exxsol D60 w/antibac</i>	789	1.54		
<i>Exxsol D60 w/antibac & OILRED color</i>	784	1.65		25.4
Beginning of experimental period (from separator) (23°C)				
Water	998	1.14	44.40	30.89
Exxsol D60	786	1.59	24.67	
End of experimental period (from separator) (22°C)				
Water	997	1.15	54.87	26.55
Exxsol D60	787	1.51	24.6	

Table 2 Measurement of water and Exxsol D60 properties before, at the beginning and at the end of experimental period.

As seen in Table 2 the viscosity and density of water and Exxsol D60 taken from the separator did not change significantly during the period experiments were conducted. However, our measurements showed that surface tension of water increased 23% and that there was a decrease in interfacial tension between the water and Exxsol D60. The 23% increase in surface tension of water seems high but no visual change in flow behavior was observed.

3.3 Experimental Execution

It was desired to investigate a broad range of both oil ratio and number of g's. The maximum number of g's was limited by the capacities of the pumps. A matrix was made for the experiments with oil ratio ranging from 0.1 to 0.9 with increments of 0.1 and number of g's ranging from 10-70 with increments of 10. Even though the frequency converters could be adjusted with increments of 0.01 Hz, achieving specific flow rates proved to be difficult. In addition challenges with emulsion, explained in more detail later in this chapter, resulted in not having pure phases in the two outlets. Because of this the matrix contains two sections. The first section describes the wanted conditions, i.e. what the oil and water flow rates should be to achieve a given number of g's at different oil ratios. The second section is where the measured ratios and actual total flow rates were entered.

Wanted ratio						Measured Conditions						
ID	Oil flow [l/min]	Water flow [l/min]	Total flow [l/min]	Velocity [m/s]	g	Total volume [ml]	Water volume [ml]	Ratio Sample	Ratio LabVIEW	Total Flow [l/min]	Oil flow [l/min]	Water flow [l/min]
0,9_10	604	67	671	5,5	10,0	480,0	55,0	0,89	0,89	695,0	615,4	79,6
0,9_20	854	95	948	7,8	20,0	500,0	50,0	0,90	0,89	948,0	853,2	94,8
0,9_30	1045	116	1162	9,6	30,0	485,0	55,0	0,89	0,90	1166,0	1033,8	132,2
0,9_40	1207	134	1341	11,0	40,0	510,0	50,0	0,90	0,90	1337,0	1205,9	131,1
0,9_50	1350	150	1500	12,3	50,0	485,0	45,0	0,91	0,89	1555,0	1410,7	144,3

Figure 3-18 Example from the experimental matrix at 0.9 oil ratio. Wanted Conditions in the left segment and Measured Conditions in the right.

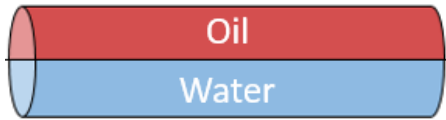
- | | |
|---|---|
| 1) Oil ratio | 8) Total sample volume. |
| 2) Identification of each test | 9) Water volume in sample. |
| 3) Oil flow needed to achieve wanted ratio and number of g's. | 10) Calculated oil ratio in sample. |
| 4) Water flow needed to achieve wanted ratio and number of g's. | 11) Ratio indicated in LabVIEW. |
| 5) Total flow needed to achieve wanted number of g's. | 12) Total flow rate indicated in LabVIEW. |
| 6) Fluid velocity | 13) Calculated oil flow rate from measured ratio. |
| 7) Wanted number g's. | 14) Calculated water flow rate from measured ratio. |

The experimental procedures for each test is as follows:

1. Start LabVIEW program.
2. Adjust oil and water pumps to approximately match the flow rates in the matrix.
3. Enter the achieved total flow rate indicated by LabVIEW in *Total Flow* under *Measured Conditions* in the experimental matrix.
4. Capture photo with Canon and Samsung camera.
5. Take sample from one of the sample valves (22, 23).
6. Adjust pumps to match next step in the matrix, and repeat until all steps at a certain ratio are completed.
7. Stop LabVIEW program and save the LabVIEW log.
8. Pour each sample in a measuring glass and enter the *Total Volume* and *Water Volume* of each sample in the experimental matrix under *Measured Conditions* to get the actual ratio.

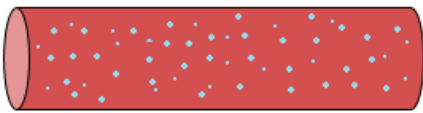
The photos was analyzed and the flow regimes at the inlet and outlet of the loop were compared. According to Rodriguez and Castro (2014) the flow regime of an oil-water flow can be identified as *stratified, dispersed, intermittent* or *emulsion* shown in Table 3.

Stratified



A stratified flow is characterized as a flow of parallel immiscible phases divided by an interface that can be smooth, wavy or with droplets of one phase entrained in the other phase.

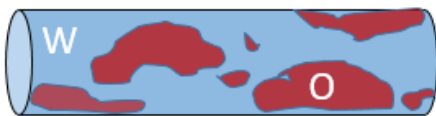
Dispersed



Water dispersed in oil

Dispersed flow is characterized as a multiphase flow where one of the phases is dispersed in the other continuous phase as droplets.

Intermittent



Intermittent flow is characterized by its irregular alternation of phases and is commonly observed in fluids that are turbulent or near the transition to turbulence.

Emulsion



An emulsion is characterized as a uniform mixture of two immiscible fluids and can form when there is sufficient mixing.

Table 3 Different flow regimes of liquid-liquid flow

During testing of the setup it was quickly discovered that there was going to be some problems with formation of emulsion. The purity of the oil and water phases coming from the separator outlets began to diminish when running the experiments, where particularly the water phase quickly became contaminated with oil. This was especially apparent when conducting tests with an oil ratio around 0.5 and below, where the emulsion started to appear from both oil and water outlets at low flow rates. The problem was less apparent when conducting tests with high oil ratios. It was therefore decided to start the experimental matrix at an oil ratio of 0.9 and move downwards in terms of ratio until the ratio measured from the sample began to deviate significantly from the ratio goal. This started to happen when reaching a ratio of 0.6. The experimental matrix was then followed at oil ratio 0.1 and 0.2 where the problem quickly became evident again. Because of the deviating sample ratio it was decided not to follow the experimental matrix for oil ratios of 0.3, 0.4, and 0.5 but some test were conducted. The experimental matrix was therefore followed for oil ratio 0.9, 0.8, 0.7, 0.6 and 0.1 and 0.2. The full experimental matrix can be found in Appendix E.

The problem with emulsion is illustrated by the Figure 3-19, 3-20 and 3-21.

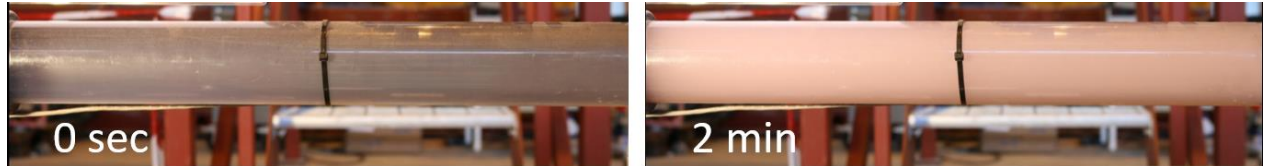


Figure 3-19 Water phase section at start and after 2 minutes when running 300 l/min water and 300 l/min oil.

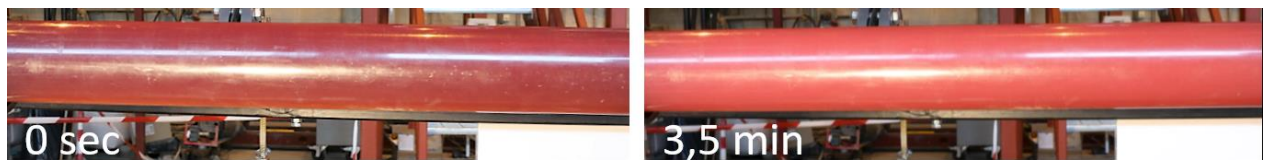


Figure 3-20 Oil phase section at start and after 3,5 minutes when running 300 l/min water and 300 l/min oil.

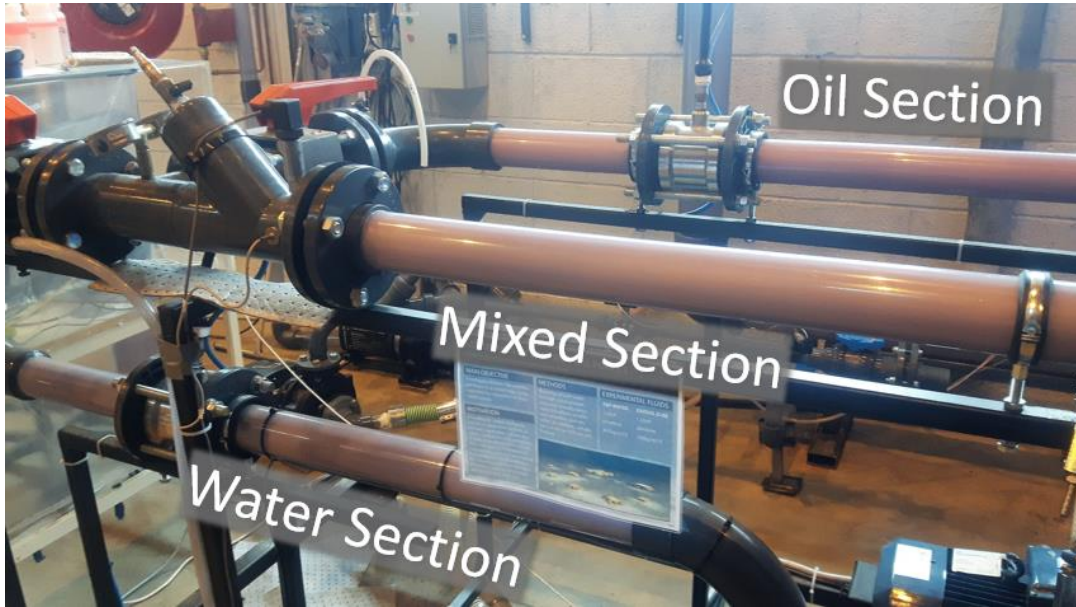


Figure 3-21 When running experiments with low oil ratio and relatively high flow rate the water, oil and mixed phases started to look alike.

Due to limited amount of time left to conduct the experiments, the experimental matrix was only completed using one coil configuration consisting of a 2 inch pipe diameter and a 0.31 m curvature radius.

4 Simulations in Ansys CFX

In the beginning of the project it was decided to do CFD simulations in addition to the experimental work. This was done so that numerical results could be extracted in addition to visual ones from the experiments.

4.1 Geometry

For modeling the geometry that was going to be used in the simulations, Design Modeler in Ansys Workbench was used. A decision on how much of the system that was to be modeled had to be made, and it was advised to only add components that had a direct effect on the flow. Early experiments had shown a very homogeneous flow after the T-pipe as Figure 4.2 shows, and it was therefore decided to only model the loop itself and 1 meter of hose before and after the loop as seen in Figure 4.1. The flow would be defined in CFX as homogeneous flow with the respective velocity and mix ratio. The alternative would be to add the T-pipe with a pure oil and water phase from their respective openings to also see what effect the T-shape would have on the mixing. This is added as a point in the chapter with recommendations for further work. Dimensions of the loop are written in Table 4.

Parameter	Dimension
Pipe diameter	50 mm
Loop radius	0.31 m
Loop pitch	50 mm
Pre loop length	1 m
Post loop length	1 m

Table 4 Geometry dimensions

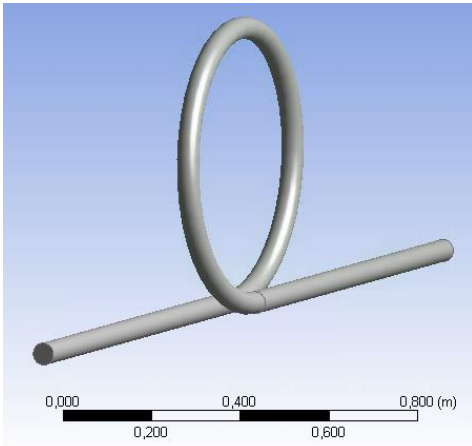


Figure 4-1 Loop geometry used in simulations.



Figure 4-2 Representative view of the flow after T-pipe.

4.2 Meshing

CFX uses *finite volume technique* to solve the simulations. This means that the main volume is divided into small sub volumes. The Navier-Stokes equations are solved for each of the volumes simultaneously, and the results are then combined for the total volume. These small volumes are called a mesh, and how they are divided has to be defined. After unsuccessful simulations using a mesh made in ICEM, it was decided to make a simpler mesh using the built-in meshing tool in Ansys Workbench. Two different meshes were made, one with 112.487 nodes and one with 135.357 nodes, both having 10 layers close to the wall with the layer height increasing by a factor of 1.2 for each layer. This was done so that a mesh independence test could be performed. The mesh independence test is performed to ensure that the simulation results do not depend on the mesh resolution. With an inlet velocity of 5 m/s and an oil ratio of 0.9, simulations were performed and the results were compared. Two planes were set 0.5 meter from the inlet and outlet respectively, and the difference in average pressure over the two planes was calculated. This difference was approximately 1% from the first to the second mesh, and it was decided that the mesh was accurate enough. As the simulation time was not too long, the mesh with the highest amount of nodes was selected for further simulations, as more nodes will likely give a more accurate representation of reality.

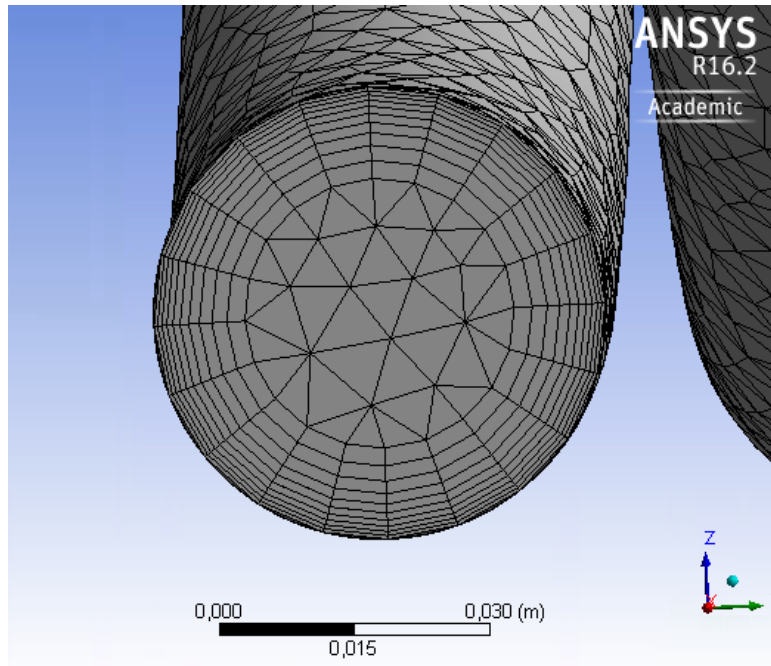


Figure 4-3 Screenshot of meshing with inflation.

4.3 Settings in CFX

The settings used in CFX are exported and attached in Appendix F, but the most important ones are mentioned here. Water and turpentine was chosen as *materials* for the simulations, as Exxsol D60 is often used as a replacement for turpentine. The values for density, and viscosity were edited to match the measured values of the Exxsol D60. Both liquids were defined as continuous as the flow in early experiments seemed homogeneous. Both Mixture model and Particle model was used, with an interface length scale of 1 mm and mean droplet diameter of 1 mm respectively. Particle model is suitable for dispersed multiphase flow such as gas bubbles in liquid, solid particles in liquid and liquid droplets in another immiscible liquid. Mixture model is suitable for non-dispersed liquid-liquid flows. The reason for doing the simulations with both models is that the flow may be described as dispersed before a potential segregation and non-dispersed after. Convergence criterion was set to $1e-4$ (RMS). (NZ-Chemical-Suppliers 2016)

4.4 Steady-state vs transient flow

As some of the practical experiments showed small, periodic flow variations at the end of the loop, it was decided to run a transient analysis to see if it was correct to assume that a steady-state flow was present. The simulation was conducted with a time step of 0.01 s, and a total time of four seconds. No transient behavior was observed after one second. It was therefore decided that the steady state assumption was justified and the rest of the simulations were conducted as steady-state simulations.

4.5 Method of measuring efficiency

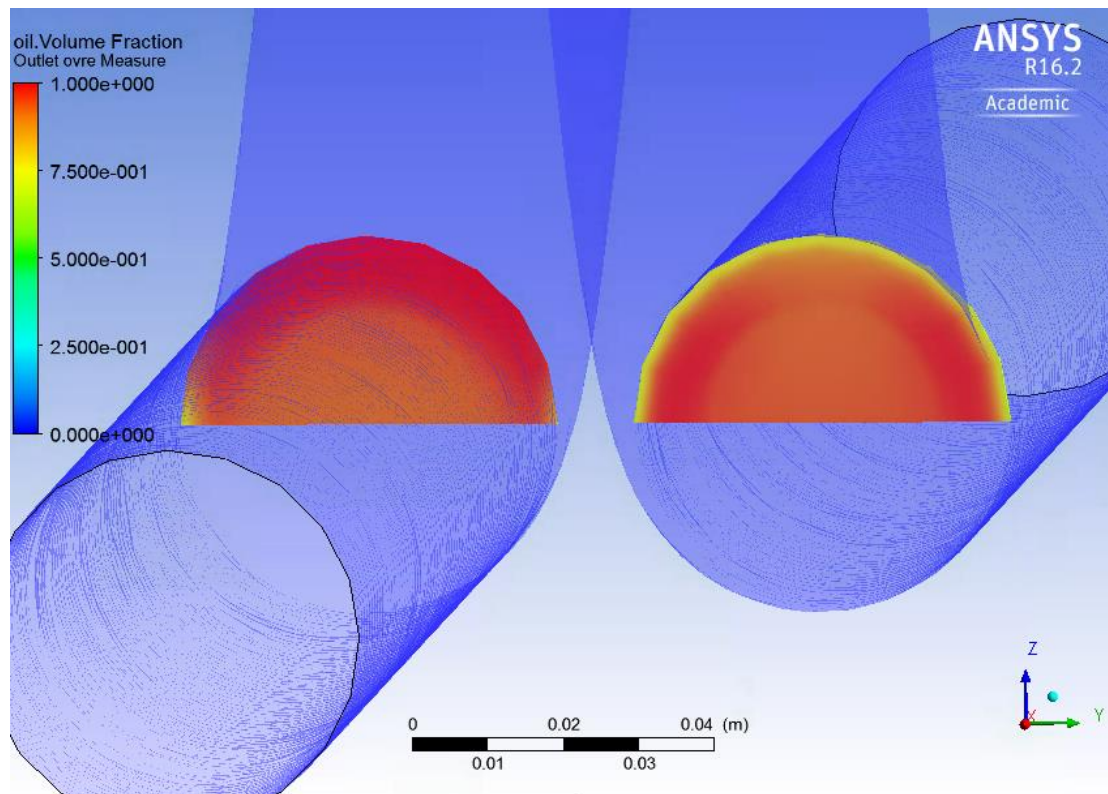


Figure 4-4 Half-circle plane on inlet and outlet of loop.

There are a number of ways to visualize the separation in the software used, but as it was desired to do a parametric study with 63 different simulations, having a numerical value would ease the comparison. As a way to get a numerical value for the separation, two planes were placed in the upper half of the cross section of the beginning and end of the loop respectively as seen in Figure 4-

4. An expression for the absolute difference in average volume fraction of oil between the two planes was made and became the measure of separation. The reason for measuring the difference between the outlet and inlet instead of just measuring it directly on the outlet is that it was desired to isolate the separation effect caused by the loop. This measure was later adjusted to be a percentage of the theoretical maximum separation for the different ratios used in the simulations. The reason for this is that the theoretical maximum difference with an oil ratio of 0.9 is 0.1 while the same value is 0.5 for a ratio of 0.5. Because of this, one would naturally expect different values with different ratios. Dividing by the theoretical maximum yields a more correct comparison between the different simulations. This parameter was called *relative efficiency* and was calculated using the functions in CFD-post shown in equation 4-1 and then divided by the given theoretical maximum difference, in excel.

$$\begin{aligned} & (\text{areaAve}(\text{oil. Volume Fraction})@\text{upperOutlet} \\ & - \text{areaAve}(\text{oli. Volume Fraction})@\text{upperInlet}) \end{aligned} \quad (4-1)$$

4.6 Parametric study

In Ansys Workbench, one can perform a parametric study by adding input and output parameters within the different applications in the project. In this case an expression for the velocity given the input number of g's was made as seen in equation 4-2.

$$v = \sqrt{a_c * R * g} \quad (4-2)$$

The velocity together with oil ratio, was used as input parameters. The area average oil fractions over the planes in Figure 4-4 and the kinetic energy turbulence over the whole cross sections in the beginning and end of the loop was used as output parameters. Table 5 shows the different inputs that were entered into the study.

Number of g's/ Oil ratio	10%	20%	30%	40%	50%	60%	70%	80%	90%
10g	-	-	-	-	-	-	-	-	-
20g	-	-	-	-	-	-	-	-	-
30g	-	-	-	-	-	-	-	-	-
40g	-	-	-	-	-	-	-	-	-
50g	-	-	-	-	-	-	-	-	-
60g	-	-	-	-	-	-	-	-	-
70g	-	-	-	-	-	-	-	-	-

Table 5 Parameter study inputs in terms of number of g's and oil ratio in percent.

4.7 Secondary flow

As the centrifugal acceleration is given by velocity and curvature radius, the flow at the inner wall of the pipe experiences a larger centrifugal force compared to the flow at the outer wall where the radius is effectively larger. This difference induces something called *secondary flow*, and variations of the flow pattern seen in figure 4-5, will occur. In simple terms, it is flow that is tangential to the main flow direction, and from a segregation standpoint it is unwanted. It was therefore decided to measure the magnitude of secondary flow to see how it is related to velocity and oil ratio. To get a numerical value of the secondary flow, the area average values of equation 4-3 over the outlet of the loop was calculated and called *measure of secondary flow* (mosf).

$$\sqrt{velocity_v^2 + velocity_w^2} \quad (4-3)$$

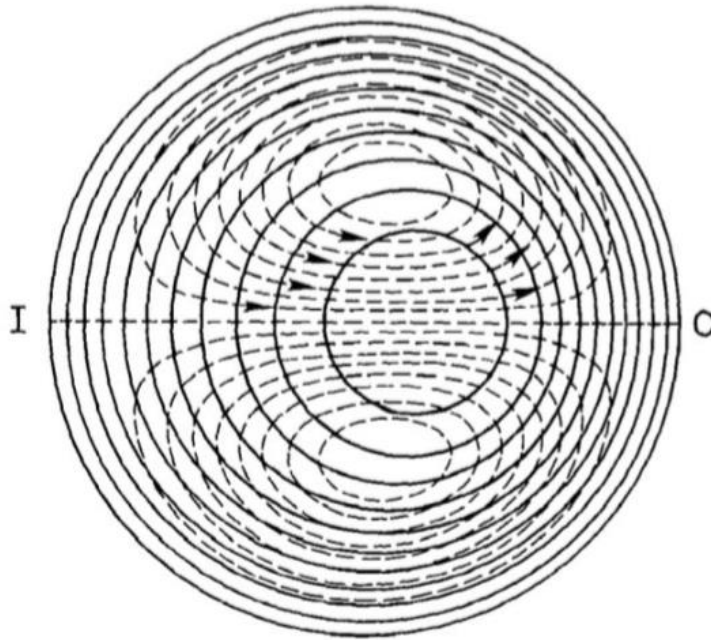


Figure 4-5 Illustration of a secondary flow pattern. (S A Berger, L Talbot et al. 1983)

4.8 Turbulence

To see if the helical coil has properties that could make it suitable as a flow conditioner, behavior regarding turbulence was also investigated in the simulations.

A straight pipe geometry with a length equal the total length of the loop including the straight section before and after was modeled. This was used as a reference to see if the turbulence behavior was caused by the loop geometry or just the length of the pipe itself. Planes were distributed at 0.3 m intervals over the pipe to be able to monitor the turbulence development.

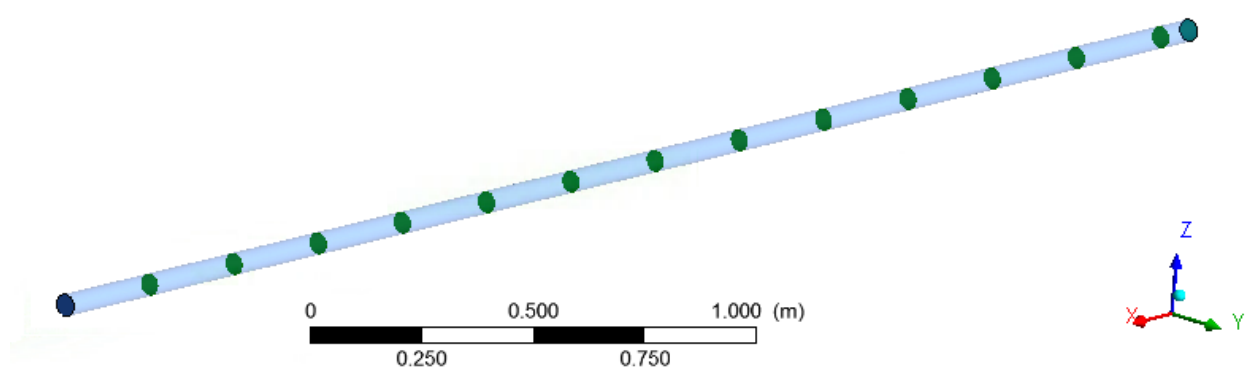


Figure 4-6 Planes distributed in 4 m long pipe.

5 Results

This chapter presents the results from the experiments and simulations. Only a selected handful of photos taken during the experiments are presented because they showed similar result.

5.1 Experimental results

5.1.1 Water and Oil

To get an indication of what a perfect segregation would look like a test with pure oil and pure water respectively, was performed and photographed. These pictures were then merged with a photo editing software shown in Figure 5-1. It is worth mentioning that the light strip was placed under the hose in this picture as opposed to behind the hose in the other figures.



Figure 5-1 Illustration of what a perfect oil-water segregation would look like at oil ratio 0.5.

Figure 5-2 to 5-4 are samples from the photos taken when conducting the experimental matrix, and as they show there is no visible segregation of oil and water. This was representative for all the flow rates and ratios tested in the experimental matrix. The flow regime present in the pictures both at inlet and outlet of the loop resembles *emulsion* of various degrees. The emulsion varied from being more reddish and translucent at higher oil ratios, to a pink emulsion with very little translucency at lower oil ratios.

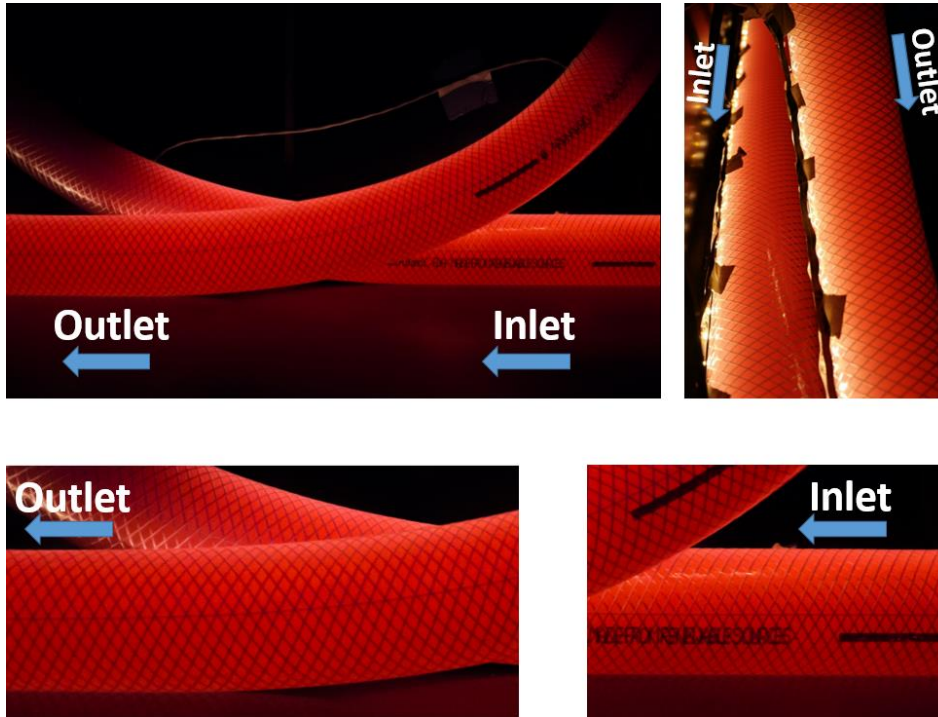


Figure 5-2 0.7 oil ratio at 20g.

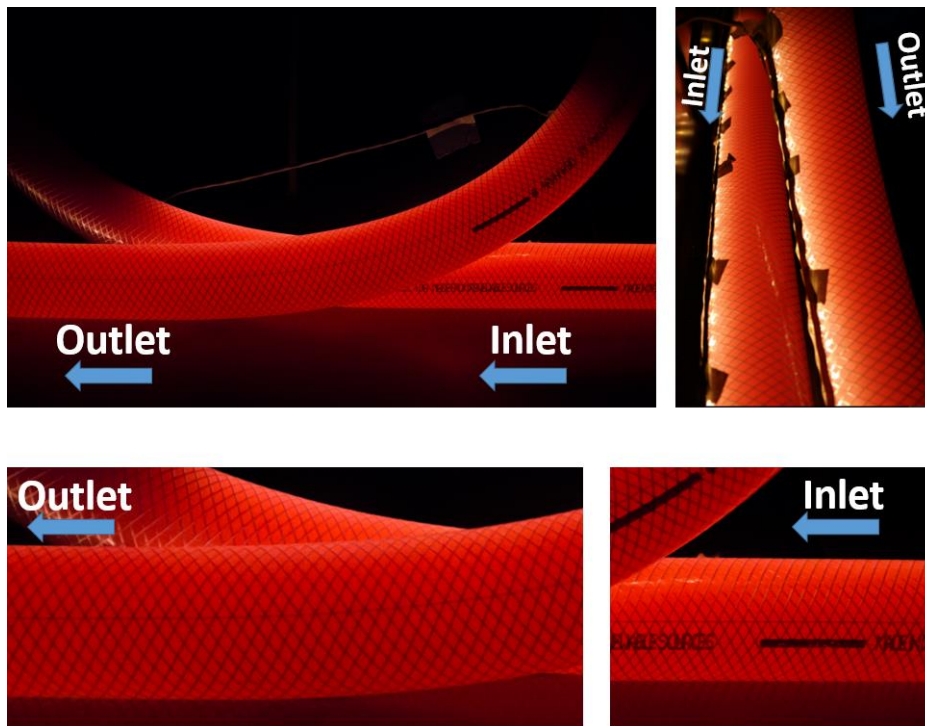


Figure 5-3 0.9 oil ratio at 40g.

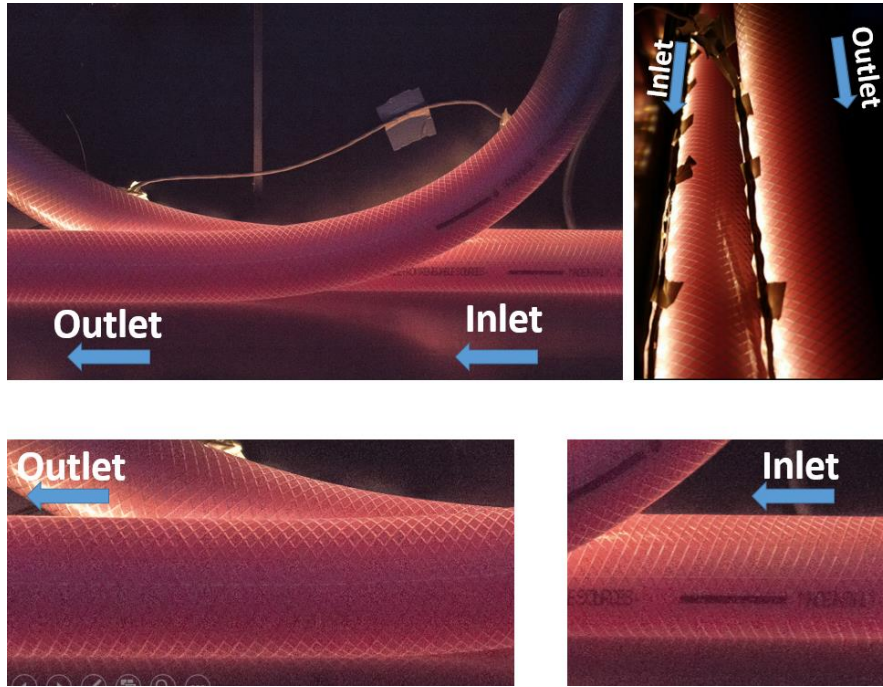


Figure 5-4 0.5 oil ratio at 50g.

When conducting some experiments below the g-range of the experimental matrix the flow regime resembled more an *intermittent* flow at both inlet and outlet. This can be seen in Figure 5-5.

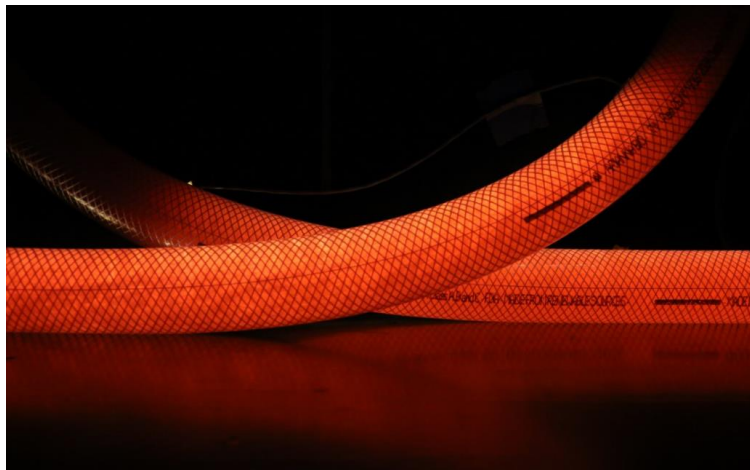


Figure 5-5 Flow regime resembling intermittent flow when running below 10g.

As mentioned in chapter 3.3, not all the ratios were completed due to the buildup of emulsion in the tank. Even if emulsion quickly became apparent at oil ratio 0.1 some experiments were conducted

with this oil ratio at approximately 70g since these were the parameters that seemed most promising in the simulations. As Figure 5-6 shows, these parameters did not show much difference compared to the samples in figure 5-2 to 5-4.

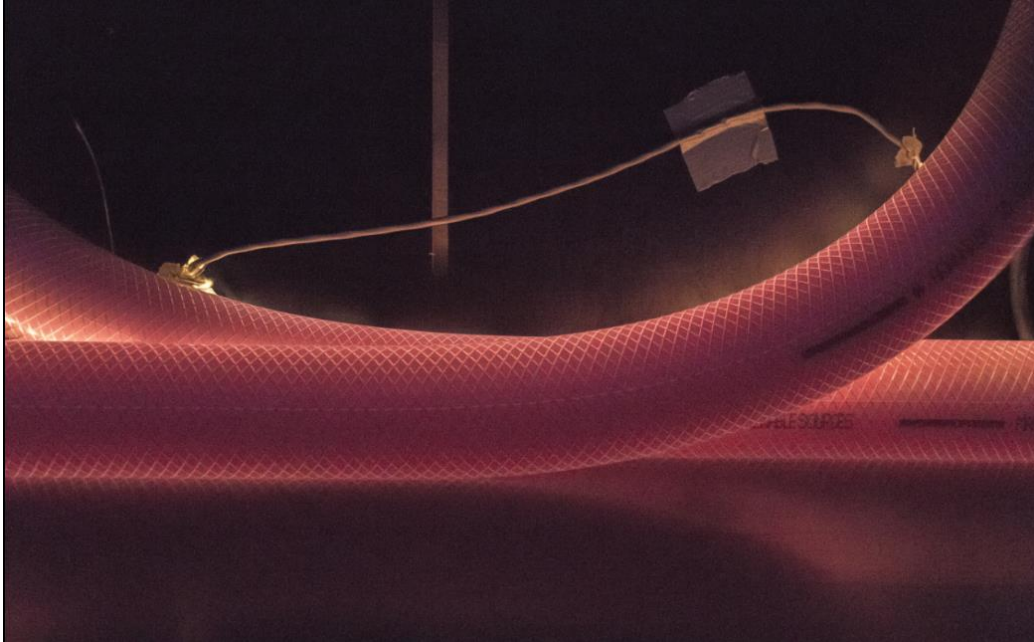


Figure 5-6 Best conditions according to simulations. Oil ratio 0.1 at 70g.

5.1.2 Oil and Air

As no visible evidence of segregation could be seen with oil and water, it was decided to do a simple test with air and oil to get proof of concept with gas-liquid flow. Oil and air were chosen instead of water and air, as the density difference is smaller and successful segregation would then be proven for what was considered more difficult conditions for segregation.



Figure 5-7 Oil and air flow with clear segregation at loop outlet.

As Figure 5-7 shows, there is a clear segregation of the air phase at the top of the flow. This was also the case when the airflow was varied by sending rapid bursts of air into the oil flow relatively low flow rates, though this was not recorded. This indicates that the helical coil principle may be applicable for gas-liquid flows as the work done by Vidnes, Engvik et al. (2015) and da Mota and Pagano (2014) also suggests.

5.2 Simulation results

As mentioned in the simulations chapter, two half-circle planes were made in the upper part of the inlet and outlet of the loop section. See Figure 5-8.

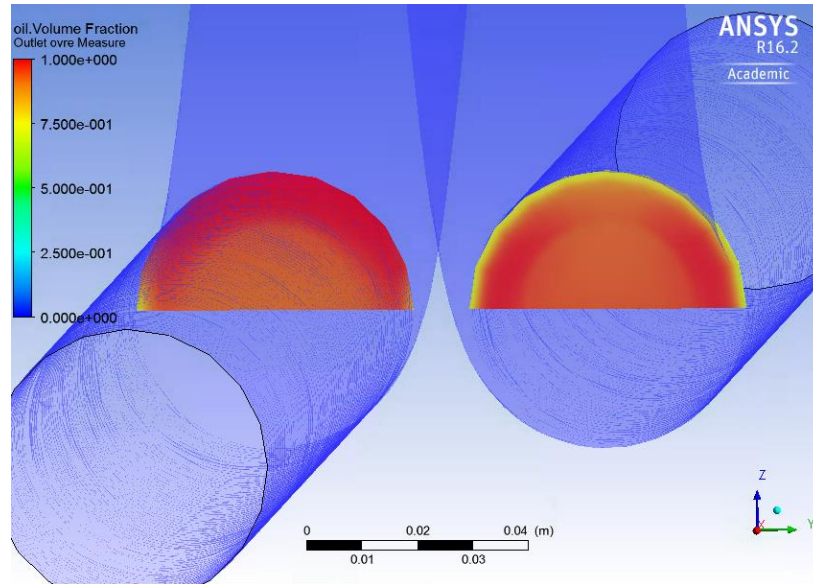


Figure 5-8 Half-circle plane on inlet and outlet of loop.

To get a measure of the segregation effect, the difference in the area average oil fraction between the two planes was used as an output parameter in the parametric study. This was then divided by the theoretical maximum difference mentioned in chapter 4.5, to obtain the *relative efficiency* for each scenario.

As mentioned in chapter 4, 63 simulations were done varying the oil ratio and number of g's according to Table 5. In Figure 5-9, the results from these simulations in terms of relative efficiency given the oil ratio and number of g's is presented as a 3D-surface, and in Figure 5-10 and Figure 5-11, as 2D-graphs. It was decided to also monitor the relative efficiency for the lower cross section as well and the results from this is presented in Figure 5-12, 5-13 and 5-14. The figures mentioned above are from mixture model simulations. The results from the simulations done with particle model show the same patterns, but with lower values and these are presented in Appendix I.

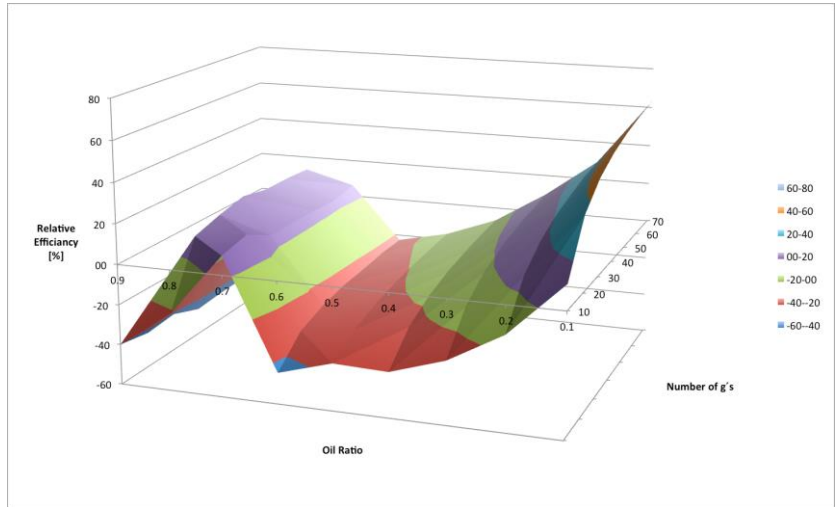


Figure 5-9 3D graph of Relative efficiency given Oil ratio and g's. Upper cross section.

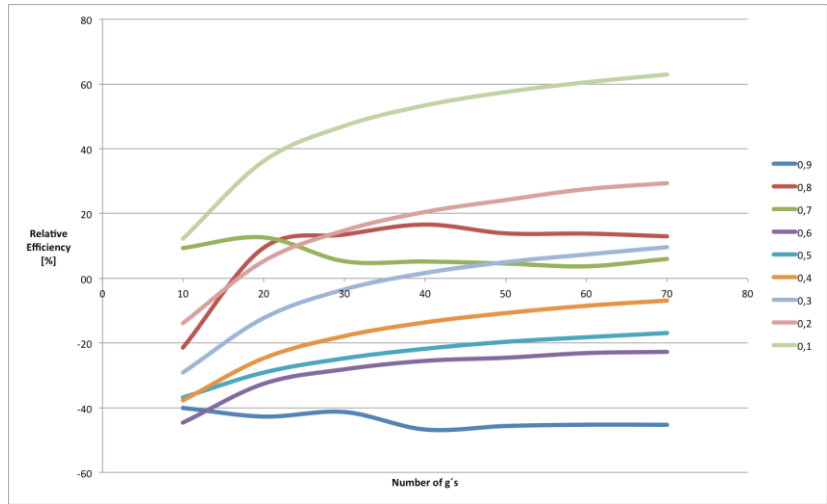


Figure 5-10 Different Oil ratios plotted against Relative efficiency and g's. Upper cross section.

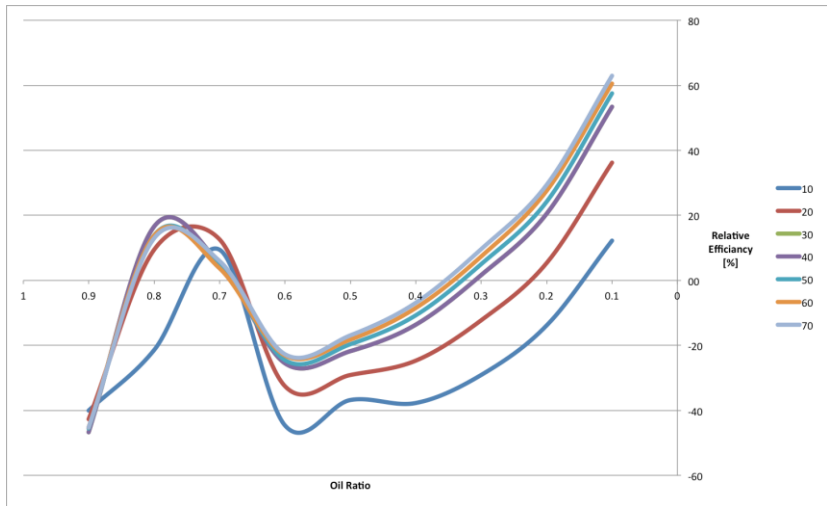


Figure 5-11 Number of g's plotted against Relative efficiency and Oil ratio. Upper cross section.

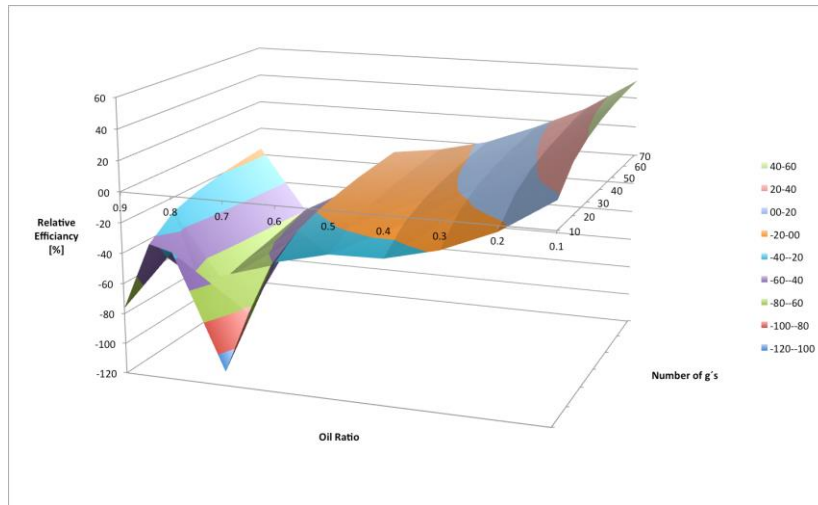


Figure 5-12 3D graph of Relative efficiency given Oil ratio and g's. Lower cross section.

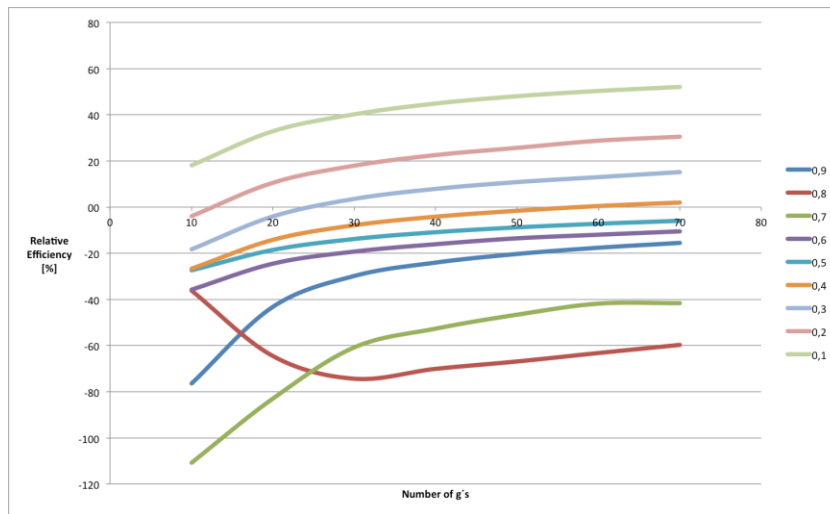


Figure 5-13 Different Oil ratios plotted against Relative efficiency and g's. Lower cross section.

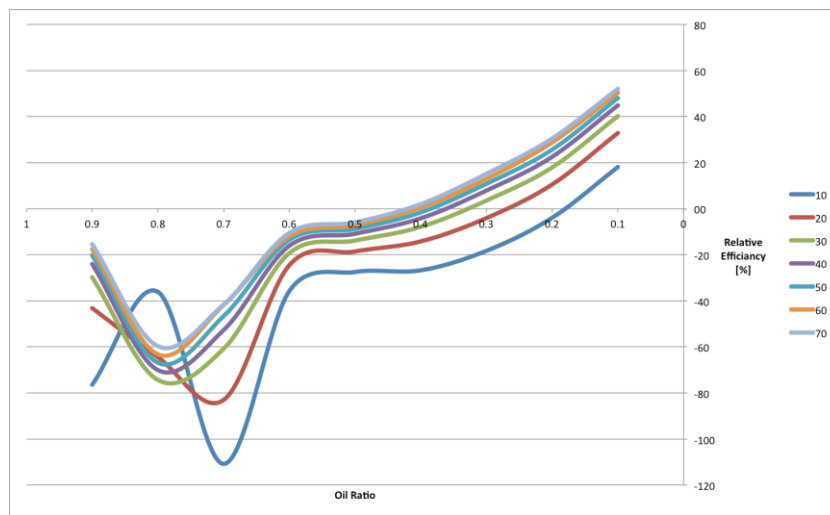


Figure 5-14 Number of g's plotted against Relative efficiency and Oil ratio. Lower cross section.

The 3D graphs from the upper cross section and lower cross section, Figure 5-9 and 5-12 respectively, show different patterns but as seen in figures 5-10, 5-11, 5-13 and 5-14 the varying oil ratio seem to have a larger impact on the relative efficiency compared to varying the number of g's. In terms of oil ratio both upper and lower cross section shows a general minimum in relative efficiency at around 0.8 and 0.6 respectively. Both upper and lower section show a maximum in relative efficiency at the oil ratio of 0.1 and 70 g's. From Figure 5-11 and 5-14 it is observed that the relative efficiency increases as the oil ratio decreases from the minimum points.

The measure of secondary flow (mosf) are presented in Figure 5-15 in relation to the oil ratio and number of g's, and also as vector plots for water and oil with varying oil ratios and a velocity equivalent to 30 g's in Figure 5-16. Figure 5-15 indicates that the measure of secondary flow increases with increased number of g's and decreases with decreased oil ratio.

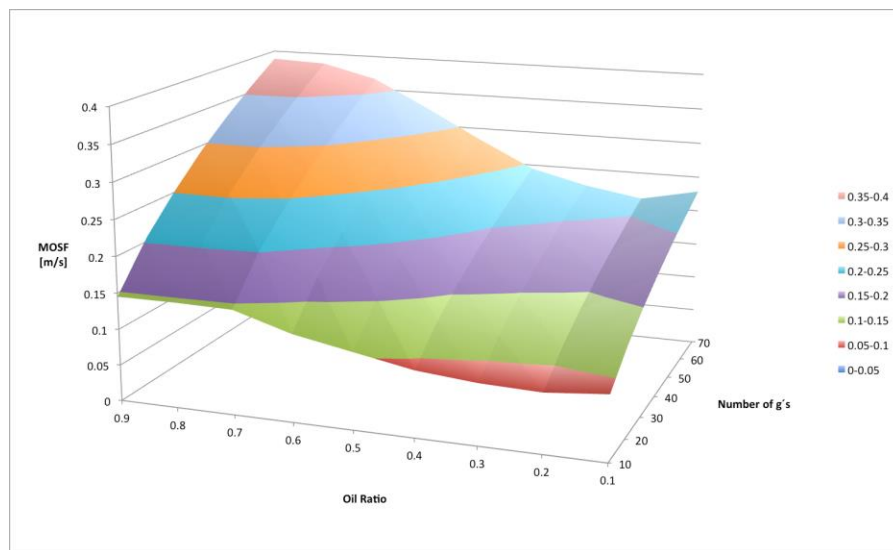


Figure 5-15 The measure of secondary flow given Oil ratio and number of g's.

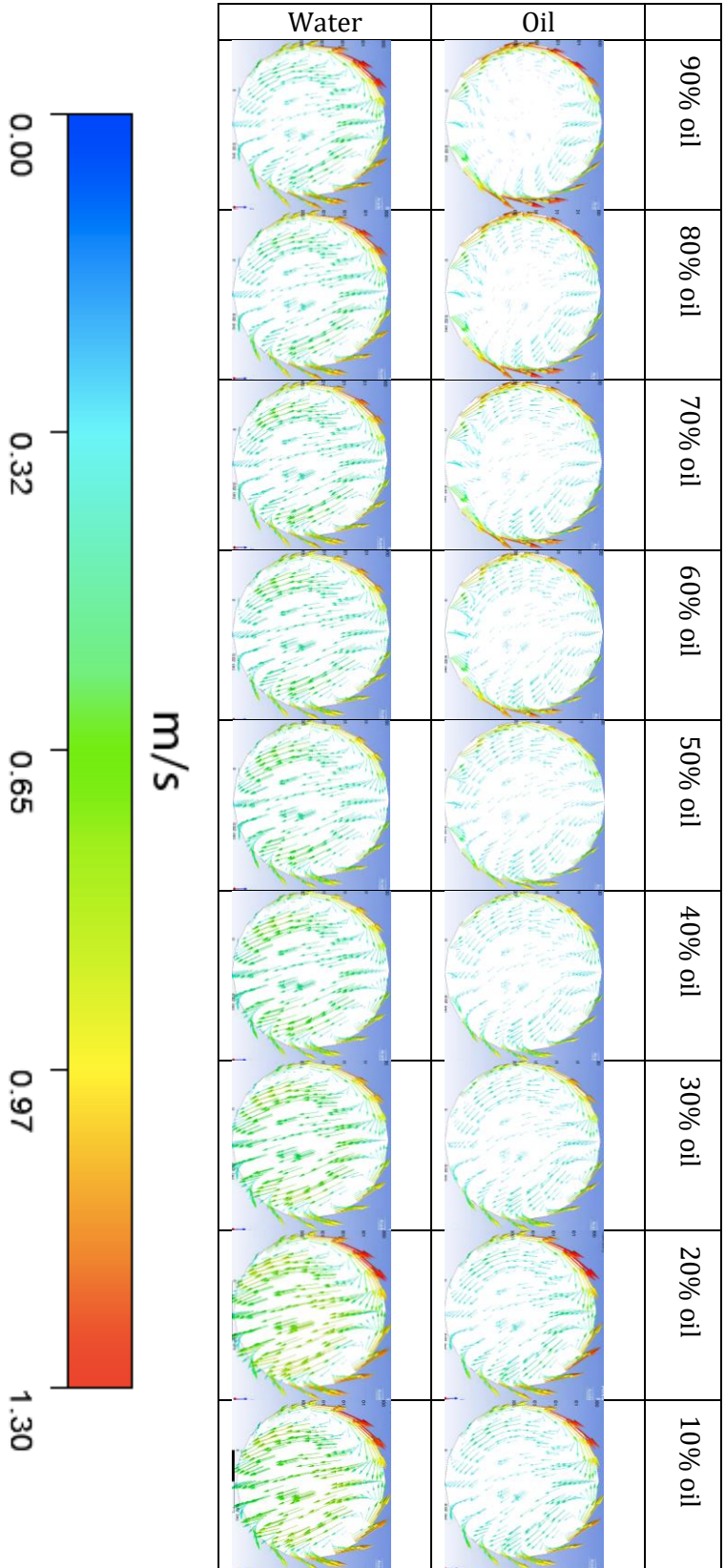


Figure 5-16 Vector plot of secondary flow at loop outlet for different oil ratios at 30 g's.

In terms of turbulence, the simulations shows that there is approximately a 70% reduction in turbulence (kinetic energy) in the outlet of the loop, compared to the corresponding length in a straight pipe. This was consistent over the whole parametric study (10-70g and oil ratio 0.1-0.9) as seen in Figure 5-17. The numbers on the x-axis corresponds to the design points in the parametric study. See the first column in Appendix G for design point parameters.

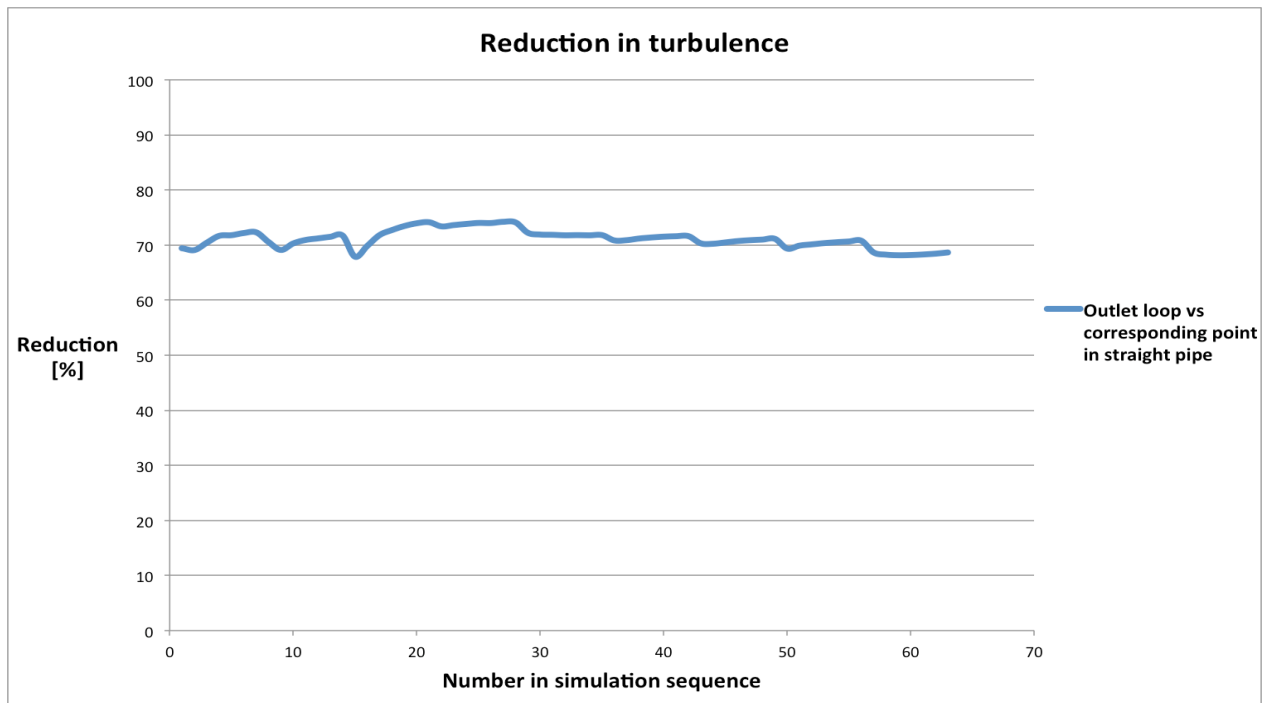


Figure 5-17 Reduction in turbulence caused by loop compared to a straight pipe of equal length.

6 Discussion

6.1 Experimental Results

The experimental study in this thesis was conducted to study the potential of using a helically coiled pipe as a compact separator or flow conditioner. For the helical coil principle to be an adequate phase separator a distinct and layered phase distribution had to be visually identifiable.

As mentioned in the chapter 5, at least by measuring visually, there is not much evidence of segregation of the oil and water phase. Both the oil ratio and velocity were varied throughout the experiments, but none of them seemed to have any influence on the flow regime at the outlet compared to the inlet. The experiment was also tested with oil and air to see if segregation would occur with a higher density difference between the fluids. The result of this test was quite unequivocally and this was used as a confirmation that the loop did at least stimulate segregation in the flow adequate to induce a stratified regime for air-oil flow. This indicates that there might actually be a degree of segregation of oil-water flow in the loop even though it was not possible to see by the naked eye or in pictures. As it was decided that the result was to be analyzed qualitatively by visual inspection, numerical results that could reveal the actual effect on an oil-water flow has not been pursued in this study. Different methods for doing this are mentioned in recommendations for further work.

6.2 Simulations

When comparing the results from the experiments with the simulations there was similarity in terms of not achieving a stratified flow. The patterns seen in Figure 5-9 and 5-12 were not observed in the experimental study. But because of the challenges with visibility mentioned in chapter 6.4 these patterns may not be possible to observe visually. The scenario that showed the highest relative separation efficiency in the simulations, namely 0.1 oil ratio with a velocity equal to 70g did not visually stand out from the other scenarios in the experiments.

The reduction in flow turbulence caused by the loop compared to a straight pipe of equal length seems substantial. The fact that the reduction is consistent over a broad range of scenarios also seem positive from a practical application standpoint.

Initially, a high number of g's was thought to be the key to achieve phase segregation. However, as seen in Figure 5-10 and 5-13 the response in relative efficiency when the number of g's increased was rather small and was even negative in some cases. As turbulence and secondary flow increase with velocity and therefore the number of g's, the limited increase in efficiency may be caused by the negative separation effect of turbulence and secondary flow.

The relation between oil ratio and relative efficiency seen in Figure 5-11 and 5-14 was very un-linear. This behavior seems unintuitive and a correlation between this and turbulence or secondary flow has not been found. What physical phenomenon is causing this is uncertain and if the indicated behavior is correct it may be interesting to study further as it may have implications on similar systems.

The simulations were performed with both the *particle model* and *mixture model*. As seen in Appendix I the patterns in the relation between oil ratio, number of g's and relative efficiency from the two models are similar even though the values differ. The similarities in the patterns were considered more important than the values, as the patterns may appear in other flows with similar properties while the values most likely will differ.

6.3 Potential of helical coil principle

Because of its size and simplicity a helically coiled pipe has geometric characteristics that makes it suitable as a subsea compact separator. However, the results from the experimental study conducted in this thesis shows no indication that the helical coil principle has applicability as an oil-water phase separator. Even if some segregation occurred, it was not observable and a criteria was that it needed to be something resembling a stratified flow for the helical coil to be used for separation. However, the tests with air-oil flow indicated that it could have applicability as a gas-liquid phase separator as was also suggested in the work of da Mota and Pagano (2014) and Vidnes, Engvik et al. (2015).

The reduction in turbulence seen in the simulations indicates that a helical coil may have potential to be used as a flow conditioner and can reduce retention time if placed before a gravity-based separator (Xiaodong, Jianhua et al. 2003).

6.4 Limitations and uncertainties

6.4.1 Experimental Setup

Even though there was not any visual indications of phase segregation with the methods used, there is a possibility that some segregation did occur which could have been detected using other methods like gamma rays, capacitance measurements or comparing samples from the bottom and top of the hose.

The sample valves were positioned on the bottom and side of the pipe before the helical coil. Although multiple tests showed that the samples from these valves had the same oil ratio, the two phase flow could be unevenly distributed in the pipe cross section which could have led to inaccurate ratio measurements in the experimental matrix.

The T-pipe used as intersection point for the oil and water phase could have created an unnatural amount of turbulence and mixing which may have had a greater negative impact on the separation than the positive impact of the centrifugal force when increasing the flow rate. It may be better to have a smoother transition when mixing the two phases e.g. using a Y-pipe instead of a T-pipe as intersection point.

Bacterial growth quickly became apparent in the separator as a slimy flocculation of bacterial particles. The measurements of interfacial tension between the water and oil showed that it had decreased some during the experimental period, which may have been caused by bacteria. The bacteria may also have had other effects on the properties that didn't show on the measurements.

Tap water used is treated with chemicals which may have caused more turbidity than untreated water. This caused the water to get a white color and less contrast against the oil phase.

The hose used for the helical coil was reinforced with braided polyester which led to reduced transparency. In addition, the cross section of the hose was not perfectly circular which led to a bigger diameter in the horizontal plane than the vertical plane of the hose. In theory, this should lead to less secondary flow as secondary flow is dependent on the diameter in the direction which the centrifugal forces act. This is explained in more detail in the specialization project. Although the flattened cross section could have led to less secondary flow, it could make it more difficult to see any phase segregation. Also, when running the experiments at higher flow rates the geometry of the

coil expanded as a result of the increased pressure which caused some irregularities in the curvature radius.

LED strips attached to the backside of the hose may have caused some uneven lighting. Choosing backlight also led to a variation in light caused by the varying flow mix running through the hose. As the flow rate was increased the mixture became less transparent and less light came through. Because of this, the pictures taken at higher flow rates became darker than the ones taken at lower flow rates. Therefore the brightness on some of the darker photos had to be increased on the computer.

6.4.2 Simulations

6.4.2.1 Mesh

As a convergence was not reached with the mesh generated in the software ICEM, it was resorted to a simpler mesh made in another software. Even though a mesh independence test was performed, there was not enough time to tweak the mesh as it was done in ICEM. A simulation will always be an approximation of the reality, but because of the simpler meshing, the results might be less accurate.

6.4.2.2 Experimental Validation

In general, all simulations have to be validated experimentally to ensure that the data is reliable. In this case the simulations were validated to some degree as both the simulations and experiments showed little evidence of segregation, but due to the optical difficulties there isn't any experimental data that is comparable to the simulation data.

6.4.2.3 Settings

In CFX there are very many options to be able to model a range of different scenarios and physical systems. Some of these might have been missed, and some may be crucial to get accurate data. To distinguish between which are important and which are not, one would have to have more experience than what was gained through this project. Even though it was consulted people with knowledge of CFD, it is likely that the settings can be optimized for a higher degree of accuracy.

6.5 Recommendations for Further Work

During this thesis there were several elements that could have been investigated further but wasn't due to limited time. The following are recommendations for improvements and further work specifically for the setup used and in the subject of helical coil experimentation in general.

- Capacitance measurement. As seen in (Huang, Zhang et al. 2007) capacitance might be used to measure water holdup and this might be exploited to get a numerical measure of the difference in phase distribution before and after a loop.
- Using a *Cross Flow Media* in the separator. Cross Flow Media are modules fabricated from rigid PVC sheets formed with alternating corrugations and are said to reduce the amount of bacteria and enhance the separation process through added horizontal surface area and reduction of turbulence (Ghajari 2005). The problem with emulsion buildup in the separator could be reduced by placing this in the separator.

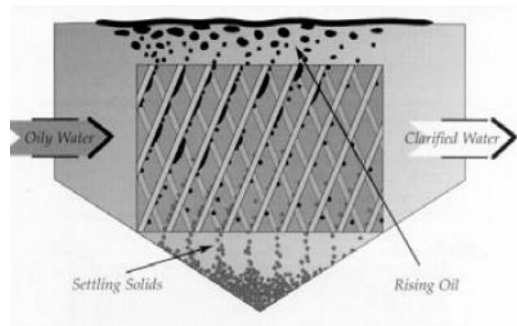


Figure 6-1 Cross Flow Media

- Using gamma ray densitometer. Phase distribution might be measured with gamma rays which could help give a more discrete measure of the segregation than with visual inspection.
- Improve lighting setup. Finding a solution that gives powerful lighting evenly across the inlet and outlet of the helical coil or the entire coil without causing too much reflection could improve the quality of the analyzing photos.

- Try a different type of oil. An oil with different properties than Exxsol D60 could have different effect and reduce the formation of emulsions and improve separation.
- Measure ratio at inlet and outlet of loop. Finding a way of getting a sample from the bottom and top of the loop and comparing the oil ratio could give a numerical indication of phase segregation.
- Investigate the use of *Coalescence fiber* strains. The fibers can be installed in piping upstream of the separator and are supposed to catch pure drops of oil, water foam and drops of water/oil emulsion. This results in a buildup of oil drop size which improves the following separation. Strains of Coalescence fibers expands to something resembling a mesh which gives the fiber an enormous surface compared to its dimension.



Figure 6-2 Strains of coalescence fiber.

- Trying a different hose for loop. Using a completely clear hose for the loop might improve the visual observation of the flow.
- Varying coil geometry. One of the parameters that might affect the degree of segregation is the geometry of the loop. Varying the bend radius and inner diameter of the hose will add another dimension to the results.
- Using Emulsion breaker. As mentioned previously in the thesis, emulsion was a challenge. This might hide or hinder segregation and one should consider trying chemical emulsion breakers to avoid this.

- Using untreated water. The tap water used in the experiments is treated to remove bacteria and reduce corrosion in pipes. These additives might be the reason that the water phase turned white after some time and reduced the contrast to the oil phase. Using untreated water might reduce this problem.
- Adding more components from the experimental system to the simulation geometry. This might give more realistic results from the simulations.

7 Conclusion

The main goal of the experimental study was to qualitatively identify the oil-water phase separation capabilities of a helical coil.

Results from the conducted experiments shows that there was no visible phase segregation of the oil-water flow at the end of the loop. This was the case for all oil ratios and flow rates tested. The flow regime was identified as different degrees of emulsion for the experimental range at both inlet and outlet. When doing tests with flow rates below the experimental range of 10 g's the flow resembled intermittent flow with no noticeable difference between loop inlet and outlet. All the experiments were conducted using a single coil geometry.

The results from the simulations does not seem promising in terms of separation capabilities because the relative efficiency was considered low. In addition the variations in efficiency given oil ratio seem disadvantageous in a practical application.

The experimental study and simulations gave no indications that the helical coil could be applicable as a compact separator for oil-water flows. However, due to the limited experimental range and sources of error this experimental study can't completely disprove the concept. Improvements of the experimental setup mentioned in recommendations for further work could yield other results. The results from the simulations did show a significant reduction in turbulence from the loop compared to a straight pipe which may give the helically coiled pipe applicability as a flow conditioner.

References

- Brown, D. (2014). "Shutter Speed and Motion Blur." Retrieved 01.apr, 2016, from <http://azphotojournal.com/?p=1895>.
- Cameron (2012). "EZ-IN Series Turbine Flow meter Installation Manual." Retrieved 18.feb, 2016, from http://www.ogesc.com/pdfs/Cameron/NuFlo%20EZ-IN%20User%20Manual_Standard.pdf.
- Chemacinc (2012). "Centrifugal vs. Plunger Pumps." Retrieved 02. December, 2015, from <http://chemacinc.com/?p=2623>.
- da Mota, F. R. M. and D. J. Pagano (2014). "Simulation and experimental study of phase segregation in helical pipes: A new method for flow conditioning." Flow Measurement and Instrumentation **35**: 99-108.
- daycounter.com (2016). "Wheatstone Bridge Calculator." Retrieved 04. May, 2016, from <http://www.daycounter.com/Calculators/WheatStone-Bridge/WheatStone-Bridge-Calculator.phtml>.
- Ghajari, A. (2005). "An experimental study of Oil-Water flow in upwards inclined pipes."
- Gulich, J. F. (2010). Centrifugal Pumps. Dordrecht, Springer.
- Huang, S. F., et al. (2007). "Water holdup measurement in kerosene–water two-phase flows." Measurement Science and Technology **18**(12): 3784.
- Instruments, N. (N.A). "How To Measure Pressure with Pressure Sensors." Retrieved 18.feb, 2016, from <http://www.ni.com/white-paper/3639/en/>.
- Instruments, N. (N.A). "What is Data Acquisition?". Retrieved 17.feb, 2016, from <http://www.ni.com/data-acquisition/what-is/>.
- Lundberg, N. H. (2009). "Råolje." Retrieved 15. Feb, 2009, from <https://snl.no/r%C3%A5olje>.
- NZ-Chemical-Suppliers (2016). "Mineral Turpentine." from <http://www.nzchemicalsuppliers.co.nz/content/page/mineral-turpentine>.
- polypipe (n.d). "Pressure Pipe System Ratings." Retrieved 19. May, 2016, from http://www.polypipe.com/cms/toolbox/Terrain_Pressure_HPPE_Pipe_System_Ratings.pdf.

Rodriguez, O. M. H. and M. S. Castro (2014). "Interfacial-tension-force model for the wavy-stratified liquid-liquid flow pattern transition." International Journal of Multiphase Flow **58**: 114-126.

S A Berger, et al. (1983). "Flow in Curved Pipes." Annual Review of Fluid Mechanics **15**(1): 461-512.

Technology, E. S. (2004). Variable Speed Pumping : A Guide to Successful Applications. Burlington, Elsevier Science.

Technology, P. (N.A). "PT100 Platinum Resistance Thermometer." Retrieved 18.feb, 2016, from <https://www.picotech.com/library/application-note/pt100-platinum-resistance-thermometers>.

Vidnes, J., et al. (2015). Analysis of Compact Separation Systems and Experimental Study of Centrifugal Separation in Helically Coiled Pipes, NTNU.

Xiaodong, L., et al. (2003). "Numerical simulation of the effects of turbulence intensity and boundary layer on separation efficiency in a cyclone separator." Chemical Engineering Journal **95**(1-3): 235-240.

Appendix A Part list and Budget

	Description	Art.nr	Range/effect/main dimensions	Vendor	quantity	Unit	Unit price	Sum
Plumbing	Pipe	P23503	75mm	Ahtsell	5	m	NOK 477,00	NOK 2 385,00
	Bend	2433769	90° 75mm	Ahtsell	5	piece	NOK 510,70	NOK 2 553,52
	Collar	2434559	75mm	Ahtsell	7	piece	NOK 142,28	NOK 995,98
	Flange	2434059	75mm	Ahtsell	7	piece	NOK 160,14	NOK 1 120,95
	T-junction	TJ0075	75mm	GPA.no	1	piece	NOK 0,00	NOK 0,00
	T-junction	TRV 075-050	75mm/50mm	GPA.no	2	piece	NOK 120,80	NOK 241,60
	T-junction	TRV 160-110	160mm/110mm	GPA.no	1	piece	NOK 2 160,00	NOK 2 160,00
	Reduction	2436205	50mm/63mm	Ahtsell	3	piece	NOK 45,44	NOK 136,33
	Reduction	2436409	63mm/75mm	Ahtsell	1	piece	NOK 120,64	NOK 120,64
	Muff	MV075	75mm	GPA.no	1	piece	NOK 73,20	NOK 73,20
	Valve	EE	75mm	EE	1	piece	EE	EE
	Valve	EE	75mm	EE	1	piece	EE	EE
	Valve	EE	110mm	EE	1	piece	EE	EE
	Valve	EE	50mm	EE	1	piece	EE	EE
	Collar w/threads	KRFV 110-R100	110mm/4"	GPA.no	2	piece	NOK 233,17	NOK 466,34
	Nipple w/threads	NFV R050	50mm	GPA.no	2	piece	NOK 52,68	NOK 105,36
	Supply hose	11412_48	3"	Tess.no	4	m	NOK 268,00	NOK 1 072,00
Return hose	10415-64	4"	Tess.no	6	m	NOK 150,40	NOK 902,40	
Bend sep.jnl.	GJV160	2434009	GPA.no	1	piece	NOK 882,00	NOK 882,00	
Air valve	30-7105	R15 in/out D:2m H:1,64m	Clas Ohlson	3	piece	NOK 99,00	NOK 297,00	
Separator	EE	EE	EE	1	piece	EE	EE	
Instrumentation	Pressure transmitter	Unik-5000	-	GE	2	piece	EE	EE
	Temperature sensor	-	-	-	1	piece	EE	EE
Pumps	Flowmeter	-	-	-	2	piece	EE	EE
	DAQ	USB-6009	Analog Int:8 Analog out:2 Digital In/dt:12	National Instruments	1	piece	EE	EE
Pumps	Pump w/freq.conv.	F 65/200R	2500 l/min 44m 22kW	Pumpeleknikk	1	Bundle	NOK 106 760,00	NOK 106 760,00
	Pump w/freq.conv.	F50/200B	1300 l/min 46m 15kW	Pumpeleknikk	1	Bundle	NOK 106 760,00	NOK 106 760,00
Miscellaneous	Freq	-	-	-	10	Meter	134,23	NOK 1 342,30
	Cable	Øflex classic 110-CV 4610mm2	10mm*2	Ahtsell	10	Meter	211,08	NOK 2 110,80
	Cable	Øflex classic 110-CV 4616mm2	16mm*2	Ahtsell	1	piece	25000	NOK 25 000,00
	Cabinet	24452344	12x1220x2440mm	byggemakker.no	1	piece	488,99	NOK 488,99
	Plywood	20003142	62x440x1220mm	byggemakker.no	2	piece	303,2	NOK 606,40
	Plank	11302676	48x48mm	byggemakker.no	8	m	9 316,25	NOK 74,53
	Plank (2 by 4)	43259818	48x98mm	byggemakker.no	2,5	m	19 652	NOK 49,13
	Wood screws	30082457	4,5x50mm	byggemakker.no	1	piece	101,4	NOK 101,40
	Drill bit	29744497	TX20	byggemakker.no	1	piece	31,94	NOK 31,94
	Ventilation hose	EE	4"	EE	6	m	EE	EE
	Extractor fan	EE	EE	EE	1	piece	EE	EE
	Exosol D-60	-	-	Kjempex Products AS	1620	kg	24,06	NOK 38 977,20
	Antibacterial agent	IKM CC-33	-	mliteco.no	5	piece	298	NOK 1 490,00
	Lighting	36-6144	3m, white	clas ohlson	1	piece	NOK 149,25	NOK 149,25
	Camera/lense	-	ECOS D-70/18-55mm f/3.5-5.6 IS STM	Ekiopro.no	1	Bundle	NOK 9 940,00	NOK 9 940,00

Sum NOK 51 908,84
 NOK 200 634,27
 Inc. tax NOK 250 792,83

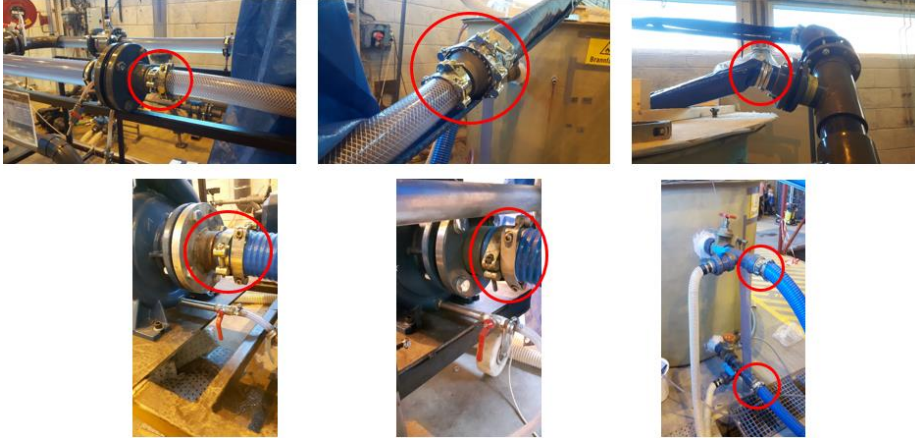
NOK 135 213,10

NOK 13 512,33

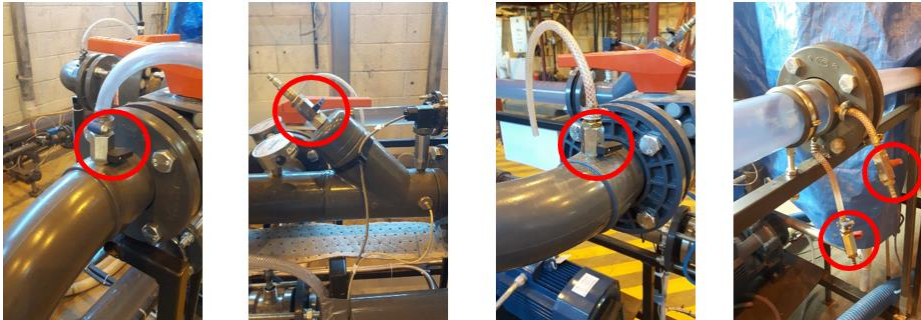
Appendix B System Procedures

Start-up procedures

1. Make sure hose connections aren't loose



2. Make sure venting, drainage and sampling valves are closed



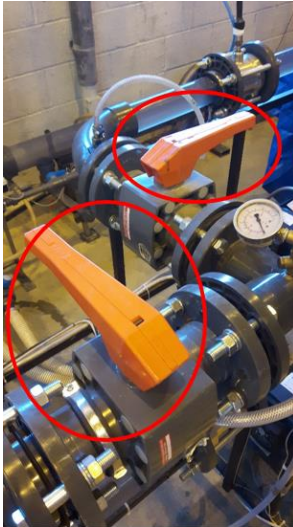
3. Make sure valves to external system are closed



4. Open separator outlet valve(s) according to which liquid(s) you are using



5. Open section valve(s) according to which liquid(s) you are using



6. Turn on the main power and fan switch on the power cabinet



7. Use arrow keys to navigate and adjust the pump frequency/speed. Start pump(s) with pump control(s) at a low frequency (<15 Hz).



8. Slowly adjust pump speed to desired flow rate (max pump speed at 50 Hz).

Shutdown procedures

1. Adjust pump speed to <20 Hz and stop pump(s) with pump control.
2. Close oil section valve.

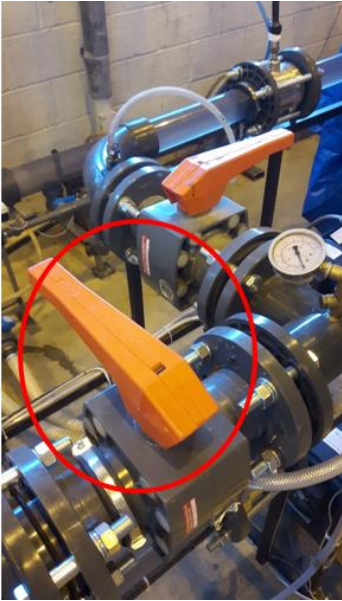


3. Close separator oil outlet valve.



4. To reduce discoloring of loop, a flushing of the loop is necessary; Start pump for water liquid with pump control at low frequency (<15 Hz)
5. Adjust speed to approximately 20 Hz and let it run for about 10 sec.
6. Stop water pump with pump control.

7. Close water section valve.



8. Close separator water outlet valve.

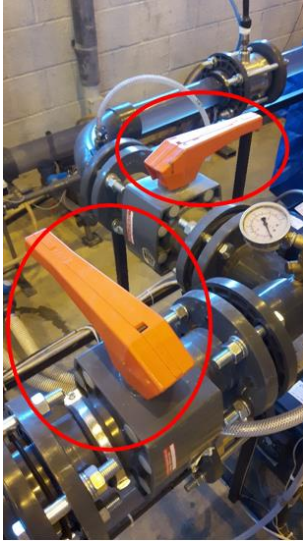


9. Turn off fan switch and main power switch on power cabinet.

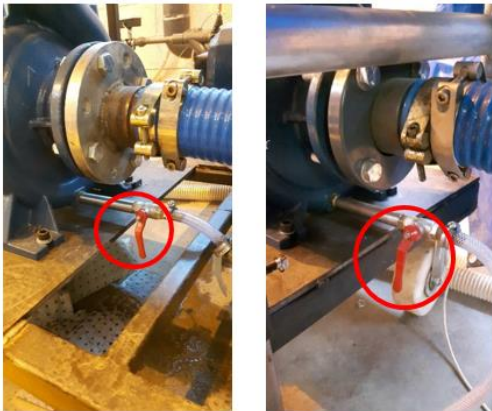
10. Close cabinet.

System drainage procedures

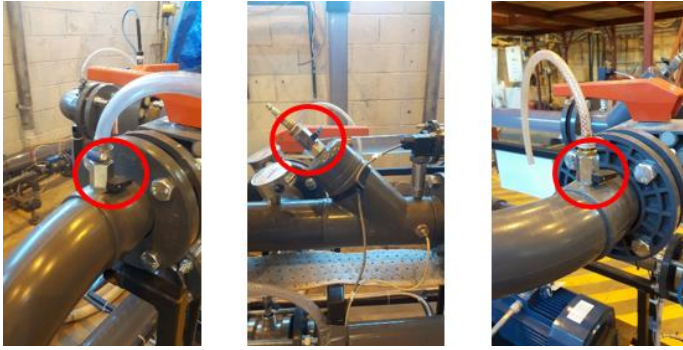
1. Make sure oil and water valves at separator are closed.
2. Place the drainage hose in a container/bucket.
3. Open oil and water section valves.



4. Open drainage valves.



5. When water and oil level are below top of the upper pipes, open venting valves to increase draining.



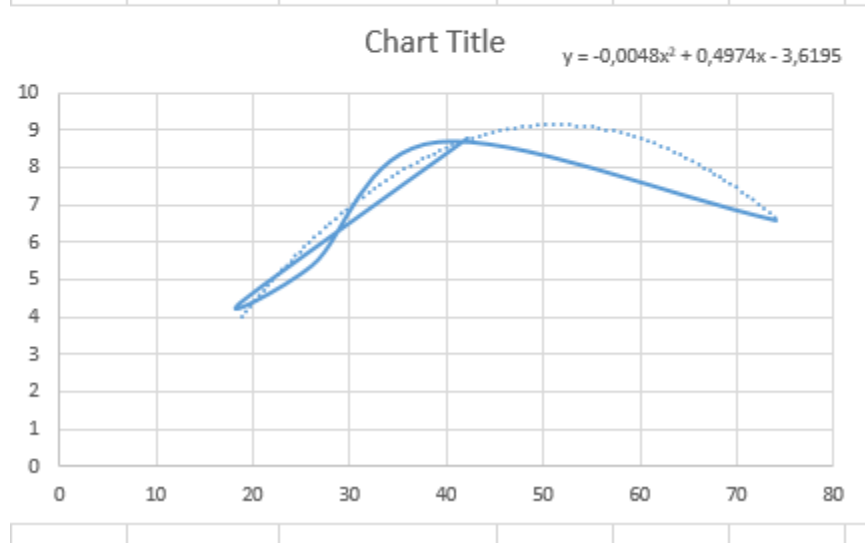
6. Make sure the container/bucket does not overflow.
7. Close drainage valves and make sure drainage hose is empty.
8. Empty container/bucket by using the downhole pump and pump the fluids to the separator, or by manually pouring the liquids into the separator.

Appendix C Calibration Sheet

Existing K-faktor	15200		Small pump	Measured (liters)	Tank (liters)	%error	K-factor
			Test 1	475	480	1,04	15041,66667
			Test 2	733	734,4	0,19	15171,02397
			Test 3	513	516,6	0,70	15094,07666
				Average		0,64	15102,25576
				497	497,8	-0,160707111	
Existing K-faktor	15200		Large pump	Measured (liters)	Tank (liters)	%error	K-factor
			Test 1	857	890,55	3,77	14627,36511
			Test 2	861	893,3	3,62	14650,3974
			Test 3	886	917,8	3,46	14673,34931
				Average		3,62	14650,37061
				891	886,7	0,484944175	

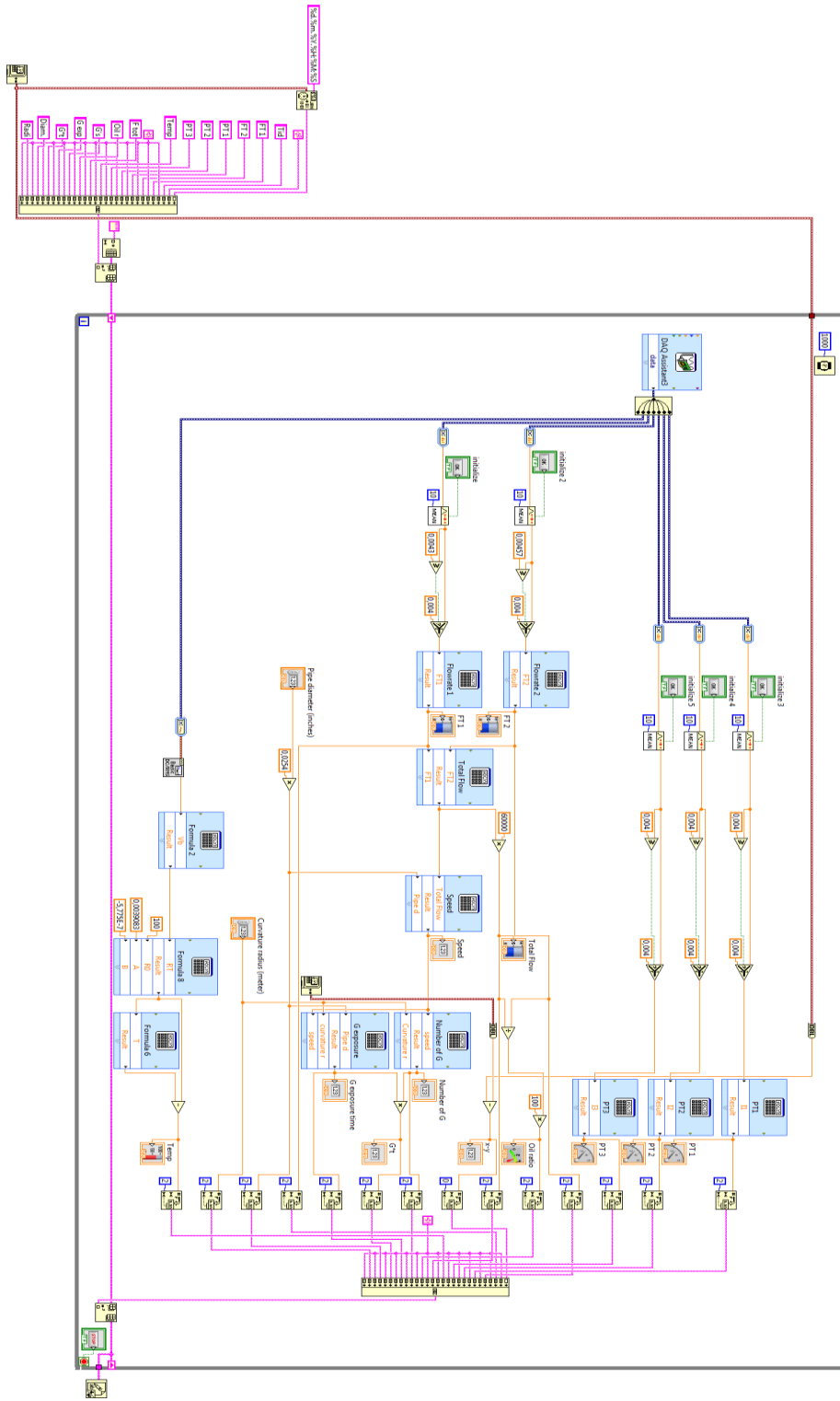
Calibration sheet for flow meters. New K-factor was calculated based on average error from the tests.

Temptest	Labview (°C)	Thermometer (°C)	Error
1	74	67,4	6,6
2	39,2	30,5	8,7
3	26,2	20,8	5,4
4	18,8	14,4	4,4
5	42,2	33,4	8,8



Calibration sheet for PT100 element. A correction formula was created based on the errors.

Appendix D LabVIEW Block Diagram



Appendix E Experimental Matrix

		Bend radius		0,31 m								
		Pipe Areal		0,00202683 m ²								
Wanted ratio		0,9										
ID	Oil flow [l/min]	Water flow [l/min]	Total flow [l/min]	Velocity [m/s]	g	Measured Conditions						
0,9_10	604	67	671	5,5	10,0	Total volume [ml]	Water volume [ml]	Ratio Sample	Ratio LabVIEW	Total Flow [l/min]	Oil flow [l/min]	Water flow [l/min]
0,9_20	854	95	948	7,8	20,0	480,0	55,0	0,89	0,89	695,0	615,4	79,6
0,9_30	1045	116	1162	9,6	30,0	500,0	50,0	0,90	0,89	948,0	853,2	94,8
0,9_40	1207	134	1341	11,0	40,0	485,0	55,0	0,89	0,90	1166,0	1033,8	132,2
0,9_50	1350	150	1500	12,3	50,0	510,0	50,0	0,90	0,90	1337,0	1205,9	131,1
						485,0	45,0	0,91	0,89	1555,0	1410,7	144,3
Wanted ratio		0,8										
ID	Oil flow [l/min]	Water flow [l/min]	Total flow [l/min]	Velocity [m/s]	g	Measured Conditions						
0,8_10	537	134	671	5,5	10,0	Total volume [ml]	Water volume [ml]	Ratio Sample	Ratio LabVIEW	Total Flow [l/min]	Oil flow [l/min]	Water flow [l/min]
0,8_20	759	190	948	7,8	20,0	485,0	85,0	0,82	0,83	692,0	573,2	121,8
0,8_30	929	232	1162	9,6	30,0	480,0	85,0	0,82	0,80	948,0	780,1	167,9
0,8_40	1073	268	1341	11,0	40,0	497,0	85,0	0,83	0,80	1166,0	966,6	199,4
0,8_50	1200	300	1500	12,3	50,0	512,0	90,0	0,82	0,81	1337,0	1102,0	235,0
0,8_60	1314	329	1643	13,5	60,0	475,0	90,0	0,81	0,80	1555,0	1260,4	294,6
						512,0	95,0	0,81	0,80	1772,9	1443,9	329,0
Wanted ratio		0,7										
ID	Oil flow [l/min]	Water flow [l/min]	Total flow [l/min]	Velocity [m/s]	g	Measured Conditions						
0,7_10	469	201	671	5,5	10,0	Total volume [ml]	Water volume [ml]	Ratio Sample	Ratio LabVIEW	Total Flow [l/min]	Oil flow [l/min]	Water flow [l/min]
0,7_20	664	285	948	7,8	20,0	460,0	145,0	0,68	0,69	672,0	460,2	211,8
0,7_30	813	348	1162	9,6	30,0	448,0	110,0	0,75	0,70	961,0	725,0	236,0
0,7_40	939	402	1341	11,0	40,0	465,0	115,0	0,75	0,70	1170,0	880,6	289,4
0,7_50	1050	450	1500	12,3	50,0	455,0	105,0	0,77	0,70	1331,0	1023,8	307,2
0,7_60	1150	493	1643	13,5	60,0	447,0	105,0	0,77	0,70	1515,0	1159,1	355,9
0,7_70	1242	532	1774	14,6	70,0	470,0	110,0	0,77	0,70	1662,0	1273,0	389,0
						430,0	100,0	0,77	0,69	1758,0	1349,2	408,8
Wanted ratio		0,6										
ID	Oil flow [l/min]	Water flow [l/min]	Total flow [l/min]	Velocity [m/s]	g	Measured Conditions						
0,6_10	402	268	671	5,5	10,0	Total volume [ml]	Water volume [ml]	Ratio Sample	Ratio LabVIEW	Total Flow [l/min]	Oil flow [l/min]	Water flow [l/min]
0,6_20	569	379	948	7,8	20,0	460,0	340,0	0,26	0,60	685,0	178,7	506,3
0,6_30	697	465	1162	9,6	30,0	422,0	226,0	0,46	0,60	948,0	440,3	507,7
0,6_40	805	537	1341	11,0	40,0	410,0	152,0	0,63	0,61	1178,0	741,3	436,7
0,6_50	900	600	1500	12,3	50,0	442,0	140,0	0,68	0,60	1318,0	900,5	417,5
0,6_60	986	657	1643	13,5	60,0	430,0	125,0	0,71	0,60	1504,0	1066,8	437,2
0,6_70	1065	710	1774	14,6	70,0	520,0	155,0	0,70	0,61	1627,0	1142,0	485,0
						505,0	150,0	0,70	0,60	1781,0	1252,0	529,0
Wanted ratio		0,1										
ID	Oil flow [l/min]	Water flow [l/min]	Total flow [l/min]	Velocity [m/s]	g	Measured Conditions						
0,1_10	67	604	671	5,5	10,0	Total volume [ml]	Water volume [ml]	Ratio Sample	Ratio LabVIEW	Total Flow [l/min]	Oil flow [l/min]	Water flow [l/min]
0,1_20	95	854	948	7,8	20,0	510,0	432,0	0,15	0,12	696,0	106,4	589,6
0,1_30	116	1045	1162	9,6	30,0	505,0	360,0	0,29	0,12	933,0	267,9	665,1
0,1_40	134	1207	1341	11,0	40,0	477,0	318,0	0,33	0,11	1135,0	378,3	756,7
0,1_50	150	1350	1500	12,3	50,0	507,0	335,0	0,34	0,10	1322,0	448,5	873,5
0,1_60	164	1478	1643	13,5	60,0	508,0	337,0	0,34	0,09	1505,0	506,6	998,4
0,1_70	177	1597	1774	14,6	70,0	402,0	260,0	0,35	0,11	1638,0	578,6	1059,4
						390,0	250,0	0,36	0,12	1777,0	637,9	1139,1
Wanted ratio		0,2										
ID	Oil flow [l/min]	Water flow [l/min]	Total flow [l/min]	Velocity [m/s]	g	Measured Conditions						
0,2_10	134	537	671	5,5	10,0	Total volume [ml]	Water volume [ml]	Ratio Sample	Ratio LabVIEW	Total Flow [l/min]	Oil flow [l/min]	Water flow [l/min]
0,2_20	190	759	948	7,8	20,0	455,0	400,0	0,12	0,20	696,0	84,1	611,9
0,2_30	232	929	1162	9,6	30,0	475,0	335,0	0,29	0,22	933,0	275,0	658,0
0,2_40	268	1073	1341	11,0	40,0	485,0	290,0	0,40	0,23	1135,0	456,3	678,7
0,2_50	300	1200	1500	12,3	50,0	495,0	315,0	0,36	0,22	1322,0	480,7	841,3
0,2_60	329	1314	1643	13,5	60,0	445,0	285,0	0,36	0,21	1505,0	541,1	963,9
0,2_70	355	1419	1774	14,6	70,0	402,0	260,0	0,35	0,18	1638,0	578,6	1059,4
						460,0	285,0	0,38	0,18	1777,0	676,0	1101,0

Appendix F CFX Settings

State file created: 2016/06/01 12:26:30

Build 16.2 2015.06.30-00.06-134402

LIBRARY:

CEL:

EXPRESSIONS:

G = 10

Hastighet = sqrt(G * 0.31 * 9.81) [m/s]

OilRatio = 0.9

WaterRatio = 0.1

END

END

MATERIAL GROUP: Air Data

Group Description = Ideal gas and constant property air. Constant \ properties are for dry air at STP (0 C, 1 atm) and 25 C, 1 atm.

END

MATERIAL GROUP: CHT Solids

Group Description = Pure solid substances that can be used for conjugate \ heat transfer.

END

MATERIAL GROUP: Calorically Perfect Ideal Gases

Group Description = Ideal gases with constant specific heat capacity. \ Specific heat is evaluated at STP.

END

MATERIAL GROUP: Constant Property Gases

Group Description = Gaseous substances with constant properties. \ Properties are calculated at STP (0C and 1 atm). Can be combined with \ NASA SP-273 materials for combustion modelling.

END

MATERIAL GROUP: Constant Property Liquids

Group Description = Liquid substances with constant properties.

END

MATERIAL GROUP: Dry Peng Robinson

Group Description = Materials with properties specified using the built \ in Peng Robinson equation of state. Suitable for dry real gas modelling.

END

MATERIAL GROUP: Dry Redlich Kwong

Group Description = Materials with properties specified using the built \ in Redlich Kwong equation of state. Suitable for dry real gas modelling.

END

MATERIAL GROUP: Dry Soave Redlich Kwong

Group Description = Materials with properties specified using the built \ in Soave Redlich Kwong equation of state. Suitable for dry real gas \ modelling.

END

MATERIAL GROUP: Dry Steam

Group Description = Materials with properties specified using the IAPWS \

equation of state. Suitable for dry steam modelling.

END

MATERIAL GROUP: Gas Phase Combustion

Group Description = Ideal gas materials which can be use for gas phase \ combustion. Ideal gas specific heat coefficients are specified using \ the NASA SP-273 format.

END

MATERIAL GROUP: IAPWS IF97

Group Description = Liquid, vapour and binary mixture materials which use \ the IAPWS IF-97 equation of state. Materials are suitable for \ compressible liquids, phase change calculations and dry steam flows.

END

MATERIAL GROUP: Interphase Mass Transfer

Group Description = Materials with reference properties suitable for \ performing either Eulerian or Lagrangian multiphase mass transfer \ problems. Examples include cavitation, evaporation or condensation.

END

MATERIAL GROUP: Liquid Phase Combustion

Group Description = Liquid and homogenous binary mixture materials which \ can be included with Gas Phase Combustion materials if combustion \ modelling also requires phase change (eg: evaporation) for certain \ components.

END

MATERIAL GROUP: Particle Solids

Group Description = Pure solid substances that can be used for particle \ tracking

END

MATERIAL GROUP: Peng Robinson Dry Hydrocarbons

Group Description = Common hydrocarbons which use the Peng Robinson \ equation of state. Suitable for dry real gas models.

END

MATERIAL GROUP: Peng Robinson Dry Refrigerants

Group Description = Common refrigerants which use the Peng Robinson \ equation of state. Suitable for dry real gas models.

END

MATERIAL GROUP: Peng Robinson Dry Steam

Group Description = Water materials which use the Peng Robinson equation \ of state. Suitable for dry steam modelling.

END

MATERIAL GROUP: Peng Robinson Wet Hydrocarbons

Group Description = Common hydrocarbons which use the Peng Robinson \ equation of state. Suitable for condensing real gas models.

END

MATERIAL GROUP: Peng Robinson Wet Refrigerants

Group Description = Common refrigerants which use the Peng Robinson \ equation of state. Suitable for condensing real gas models.

END

MATERIAL GROUP: Peng Robinson Wet Steam

Group Description = Water materials which use the Peng Robinson equation \ of state. Suitable for condensing steam modelling.

END

MATERIAL GROUP: Real Gas Combustion

Group Description = Real gas materials which can be use for gas phase \ combustion. Ideal gas specific heat coefficients are specified using \ the NASA SP-273 format.

END

MATERIAL GROUP: Redlich Kwong Dry Hydrocarbons

Group Description = Common hydrocarbons which use the Redlich Kwong \ equation of state. Suitable for dry real gas models.

END

MATERIAL GROUP: Redlich Kwong Dry Refrigerants

Group Description = Common refrigerants which use the Redlich Kwong \ equation of state. Suitable for dry real gas models.

END

MATERIAL GROUP: Redlich Kwong Dry Steam

Group Description = Water materials which use the Redlich Kwong equation \ of state. Suitable for dry steam modelling.

END

MATERIAL GROUP: Redlich Kwong Wet Hydrocarbons

Group Description = Common hydrocarbons which use the Redlich Kwong \ equation of state. Suitable for condensing real gas models.

END

MATERIAL GROUP: Redlich Kwong Wet Refrigerants

Group Description = Common refrigerants which use the Redlich Kwong \ equation of state. Suitable for condensing real gas models.

END

MATERIAL GROUP: Redlich Kwong Wet Steam

Group Description = Water materials which use the Redlich Kwong equation \ of state. Suitable for condensing steam modelling.

END

MATERIAL GROUP: Soave Redlich Kwong Dry Hydrocarbons

Group Description = Common hydrocarbons which use the Soave Redlich Kwong \ equation of state. Suitable for dry real gas models.

END

MATERIAL GROUP: Soave Redlich Kwong Dry Refrigerants

Group Description = Common refrigerants which use the Soave Redlich Kwong \ equation of state. Suitable for dry real gas models.

END

MATERIAL GROUP: Soave Redlich Kwong Dry Steam

Group Description = Water materials which use the Soave Redlich Kwong \ equation of state. Suitable for dry steam modelling.

END

MATERIAL GROUP: Soave Redlich Kwong Wet Hydrocarbons

Group Description = Common hydrocarbons which use the Soave Redlich Kwong \ equation of state. Suitable for condensing real gas models.

END

MATERIAL GROUP: Soave Redlich Kwong Wet Refrigerants

Group Description = Common refrigerants which use the Soave Redlich Kwong \ equation of state. Suitable for condensing real gas models.

END

MATERIAL GROUP: Soave Redlich Kwong Wet Steam
 Group Description = Water materials which use the Soave Redlich Kwong \
 equation of state. Suitable for condensing steam modelling.
 END

MATERIAL GROUP: Soot
 Group Description = Solid substances that can be used when performing \
 soot modelling
 END

MATERIAL GROUP: User
 Group Description = Materials that are defined by the user
 END

MATERIAL GROUP: Water Data
 Group Description = Liquid and vapour water materials with constant \
 properties. Can be combined with NASA SP-273 materials for combustion \
 modelling.
 END

MATERIAL GROUP: Wet Peng Robinson
 Group Description = Materials with properties specified using the built \
 in Peng Robinson equation of state. Suitable for wet real gas modelling.
 END

MATERIAL GROUP: Wet Redlich Kwong
 Group Description = Materials with properties specified using the built \
 in Redlich Kwong equation of state. Suitable for wet real gas modelling.
 END

MATERIAL GROUP: Wet Soave Redlich Kwong
 Group Description = Materials with properties specified using the built \
 in Soave Redlich Kwong equation of state. Suitable for wet real gas \
 modelling.
 END

MATERIAL GROUP: Wet Steam
 Group Description = Materials with properties specified using the IAPWS \
 equation of state. Suitable for wet steam modelling.
 END

MATERIAL: Air Ideal Gas
 Material Description = Air Ideal Gas (constant Cp)
 Material Group = Air Data, Calorically Perfect Ideal Gases
 Option = Pure Substance
 Thermodynamic State = Gas
 PROPERTIES:
 Option = General Material
 EQUATION OF STATE:
 Molar Mass = 28.96 [kg kmol⁻¹]
 Option = Ideal Gas
 END

SPECIFIC HEAT CAPACITY:
 Option = Value
 Specific Heat Capacity = 1.0044E+03 [J kg⁻¹ K⁻¹]
 Specific Heat Type = Constant Pressure
 END

REFERENCE STATE:

Option = Specified Point
 Reference Pressure = 1 [atm]
 Reference Specific Enthalpy = 0. [J/kg]
 Reference Specific Entropy = 0. [J/kg/K]
 Reference Temperature = 25 [C]
 END
 DYNAMIC VISCOSITY:
 Dynamic Viscosity = 1.831E-05 [kg m⁻¹ s⁻¹]
 Option = Value
 END
 THERMAL CONDUCTIVITY:
 Option = Value
 Thermal Conductivity = 2.61E-2 [W m⁻¹ K⁻¹]
 END
 ABSORPTION COEFFICIENT:
 Absorption Coefficient = 0.01 [m⁻¹]
 Option = Value
 END
 SCATTERING COEFFICIENT:
 Option = Value
 Scattering Coefficient = 0.0 [m⁻¹]
 END
 REFRACTIVE INDEX:
 Option = Value
 Refractive Index = 1.0 [m m⁻¹]
 END
 END
 END
 MATERIAL: Air at 25 C
 Material Description = Air at 25 C and 1 atm (dry)
 Material Group = Air Data, Constant Property Gases
 Option = Pure Substance
 Thermodynamic State = Gas
 PROPERTIES:
 Option = General Material
 EQUATION OF STATE:
 Density = 1.185 [kg m⁻³]
 Molar Mass = 28.96 [kg kmol⁻¹]
 Option = Value
 END
 SPECIFIC HEAT CAPACITY:
 Option = Value
 Specific Heat Capacity = 1.0044E+03 [J kg⁻¹ K⁻¹]
 Specific Heat Type = Constant Pressure
 END
 REFERENCE STATE:
 Option = Specified Point
 Reference Pressure = 1 [atm]
 Reference Specific Enthalpy = 0. [J/kg]
 Reference Specific Entropy = 0. [J/kg/K]

Reference Temperature = 25 [C]
 END
 DYNAMIC VISCOSITY:
 Dynamic Viscosity = 1.831E-05 [kg m⁻¹ s⁻¹]
 Option = Value
 END
 THERMAL CONDUCTIVITY:
 Option = Value
 Thermal Conductivity = 2.61E-02 [W m⁻¹ K⁻¹]
 END
 ABSORPTION COEFFICIENT:
 Absorption Coefficient = 0.01 [m⁻¹]
 Option = Value
 END
 SCATTERING COEFFICIENT:
 Option = Value
 Scattering Coefficient = 0.0 [m⁻¹]
 END
 REFRACTIVE INDEX:
 Option = Value
 Refractive Index = 1.0 [m m⁻¹]
 END
 THERMAL EXPANSIVITY:
 Option = Value
 Thermal Expansivity = 0.003356 [K⁻¹]
 END
 END
 END
 MATERIAL: Aluminium
 Material Group = CHT Solids, Particle Solids
 Option = Pure Substance
 Thermodynamic State = Solid
 PROPERTIES:
 Option = General Material
 EQUATION OF STATE:
 Density = 2702 [kg m⁻³]
 Molar Mass = 26.98 [kg kmol⁻¹]
 Option = Value
 END
 SPECIFIC HEAT CAPACITY:
 Option = Value
 Specific Heat Capacity = 9.03E+02 [J kg⁻¹ K⁻¹]
 END
 REFERENCE STATE:
 Option = Specified Point
 Reference Specific Enthalpy = 0 [J/kg]
 Reference Specific Entropy = 0 [J/kg/K]
 Reference Temperature = 25 [C]
 END
 THERMAL CONDUCTIVITY:

Option = Value
 Thermal Conductivity = 237 [W m⁻¹ K⁻¹]
 END
 END
 END
 MATERIAL: Copper
 Material Group = CHT Solids, Particle Solids
 Option = Pure Substance
 Thermodynamic State = Solid
 PROPERTIES:
 Option = General Material
 EQUATION OF STATE:
 Density = 8933 [kg m⁻³]
 Molar Mass = 63.55 [kg kmol⁻¹]
 Option = Value
 END
 SPECIFIC HEAT CAPACITY:
 Option = Value
 Specific Heat Capacity = 3.85E+02 [J kg⁻¹ K⁻¹]
 END
 REFERENCE STATE:
 Option = Specified Point
 Reference Specific Enthalpy = 0 [J/kg]
 Reference Specific Entropy = 0 [J/kg/K]
 Reference Temperature = 25 [C]
 END
 THERMAL CONDUCTIVITY:
 Option = Value
 Thermal Conductivity = 401.0 [W m⁻¹ K⁻¹]
 END
 END
 END
 MATERIAL: Soot
 Material Group = Soot
 Option = Pure Substance
 Thermodynamic State = Solid
 PROPERTIES:
 Option = General Material
 EQUATION OF STATE:
 Density = 2000 [kg m⁻³]
 Molar Mass = 12 [kg kmol⁻¹]
 Option = Value
 END
 REFERENCE STATE:
 Option = Automatic
 END
 ABSORPTION COEFFICIENT:
 Absorption Coefficient = 0 [m⁻¹]
 Option = Value
 END

END
 END
 MATERIAL: Steel
 Material Group = CHT Solids, Particle Solids
 Option = Pure Substance
 Thermodynamic State = Solid
 PROPERTIES:
 Option = General Material
 EQUATION OF STATE:
 Density = 7854 [kg m⁻³]
 Molar Mass = 55.85 [kg kmol⁻¹]
 Option = Value
 END
 SPECIFIC HEAT CAPACITY:
 Option = Value
 Specific Heat Capacity = 4.34E+02 [J kg⁻¹ K⁻¹]
 END
 REFERENCE STATE:
 Option = Specified Point
 Reference Specific Enthalpy = 0 [J/kg]
 Reference Specific Entropy = 0 [J/kg/K]
 Reference Temperature = 25 [C]
 END
 THERMAL CONDUCTIVITY:
 Option = Value
 Thermal Conductivity = 60.5 [W m⁻¹ K⁻¹]
 END
 END
 END
 MATERIAL: Turpentine
 Material Group = Constant Property Liquids
 Option = Pure Substance
 Thermodynamic State = Liquid
 PROPERTIES:
 Option = General Material
 EQUATION OF STATE:
 Density = 790 [kg m⁻³]
 Molar Mass = 1 [kg kmol⁻¹]
 Option = Value
 END
 SPECIFIC HEAT CAPACITY:
 Option = Value
 Specific Heat Capacity = 1760 [J kg⁻¹ K⁻¹]
 Specific Heat Type = Constant Pressure
 END
 REFERENCE STATE:
 Option = Specified Point
 Reference Pressure = 1 [atm]
 Reference Specific Enthalpy = 0 [J/kg]
 Reference Specific Entropy = 0 [J/kg/K]

Reference Temperature = 25 [C]
 END
 DYNAMIC VISCOSITY:
 Dynamic Viscosity = 1.49E-03 [kg m⁻¹ s⁻¹]
 Option = Value
 END
 THERMAL CONDUCTIVITY:
 Option = Value
 Thermal Conductivity = 0.136 [W m⁻¹ K⁻¹]
 END
 ABSORPTION COEFFICIENT:
 Absorption Coefficient = 1.0 [m⁻¹]
 Option = Value
 END
 SCATTERING COEFFICIENT:
 Option = Value
 Scattering Coefficient = 0.0 [m⁻¹]
 END
 REFRACTIVE INDEX:
 Option = Value
 Refractive Index = 1.0 [m m⁻¹]
 END
 THERMAL EXPANSIVITY:
 Option = Value
 Thermal Expansivity = 9.7E-04 [K⁻¹]
 END
 END
 END
 MATERIAL: Water
 Material Description = Water (liquid)
 Material Group = Water Data, Constant Property Liquids
 Option = Pure Substance
 Thermodynamic State = Liquid
 PROPERTIES:
 Option = General Material
 EQUATION OF STATE:
 Density = 997.0 [kg m⁻³]
 Molar Mass = 18.02 [kg kmol⁻¹]
 Option = Value
 END
 SPECIFIC HEAT CAPACITY:
 Option = Value
 Specific Heat Capacity = 4181.7 [J kg⁻¹ K⁻¹]
 Specific Heat Type = Constant Pressure
 END
 REFERENCE STATE:
 Option = Specified Point
 Reference Pressure = 1 [atm]
 Reference Specific Enthalpy = 0.0 [J/kg]
 Reference Specific Entropy = 0.0 [J/kg/K]

Reference Temperature = 25 [C]
 END
 DYNAMIC VISCOSITY:
 Dynamic Viscosity = 8.899E-4 [kg m⁻¹ s⁻¹]
 Option = Value
 END
 THERMAL CONDUCTIVITY:
 Option = Value
 Thermal Conductivity = 0.6069 [W m⁻¹ K⁻¹]
 END
 ABSORPTION COEFFICIENT:
 Absorption Coefficient = 1.0 [m⁻¹]
 Option = Value
 END
 SCATTERING COEFFICIENT:
 Option = Value
 Scattering Coefficient = 0.0 [m⁻¹]
 END
 REFRACTIVE INDEX:
 Option = Value
 Refractive Index = 1.0 [m m⁻¹]
 END
 THERMAL EXPANSIVITY:
 Option = Value
 Thermal Expansivity = 2.57E-04 [K⁻¹]
 END
 END
 END
 MATERIAL: Water Ideal Gas
 Material Description = Water Vapour Ideal Gas (100 C and 1 atm)
 Material Group = Calorically Perfect Ideal Gases, Water Data
 Option = Pure Substance
 Thermodynamic State = Gas
 PROPERTIES:
 Option = General Material
 EQUATION OF STATE:
 Molar Mass = 18.02 [kg kmol⁻¹]
 Option = Ideal Gas
 END
 SPECIFIC HEAT CAPACITY:
 Option = Value
 Specific Heat Capacity = 2080.1 [J kg⁻¹ K⁻¹]
 Specific Heat Type = Constant Pressure
 END
 REFERENCE STATE:
 Option = Specified Point
 Reference Pressure = 1.014 [bar]
 Reference Specific Enthalpy = 0. [J/kg]
 Reference Specific Entropy = 0. [J/kg/K]
 Reference Temperature = 100 [C]

```

END
DYNAMIC VISCOSITY:
  Dynamic Viscosity = 9.4E-06 [kg m^-1 s^-1]
  Option = Value
END
THERMAL CONDUCTIVITY:
  Option = Value
  Thermal Conductivity = 193E-04 [W m^-1 K^-1]
END
ABSORPTION COEFFICIENT:
  Absorption Coefficient = 1.0 [m^-1]
  Option = Value
END
SCATTERING COEFFICIENT:
  Option = Value
  Scattering Coefficient = 0.0 [m^-1]
END
REFRACTIVE INDEX:
  Option = Value
  Refractive Index = 1.0 [m m^-1]
END
END
END
END
FLOW: Flow Analysis 1
SOLUTION UNITS:
  Angle Units = [rad]
  Length Units = [m]
  Mass Units = [kg]
  Solid Angle Units = [sr]
  Temperature Units = [K]
  Time Units = [s]
END
ANALYSIS TYPE:
  Option = Steady State
EXTERNAL SOLVER COUPLING:
  Option = None
END
END
DOMAIN: Default Domain Modified
  Coord Frame = Coord 0
  Domain Type = Fluid
  Location = B8
BOUNDARY: inlet
  Boundary Type = INLET
  Location = Inlet
BOUNDARY CONDITIONS:
FLOW REGIME:
  Option = Subsonic
END

```

```

MASS AND MOMENTUM:
  Normal Speed = Hastighet
  Option = Normal Speed
END
TURBULENCE:
  Option = Medium Intensity and Eddy Viscosity Ratio
END
END
FLUID: oil
BOUNDARY CONDITIONS:
  VOLUME FRACTION:
    Option = Value
    Volume Fraction = OilRatio
  END
  END
END
FLUID: water
BOUNDARY CONDITIONS:
  VOLUME FRACTION:
    Option = Value
    Volume Fraction = WaterRatio
  END
  END
END
BOUNDARY: outlet
Boundary Type = OUTLET
Location = Outlet
BOUNDARY CONDITIONS:
  FLOW REGIME:
    Option = Subsonic
  END
  MASS AND MOMENTUM:
    Option = Average Static Pressure
    Pressure Profile Blend = 0.05
    Relative Pressure = 1 [atm]
  END
  PRESSURE AVERAGING:
    Option = Average Over Whole Outlet
  END
  END
END
BOUNDARY: wall
Boundary Type = WALL
Location = Wall
BOUNDARY CONDITIONS:
  MASS AND MOMENTUM:
    Option = Fluid Dependent
  END
  WALL CONTACT MODEL:

```

```

    Option = Use Volume Fraction
END
WALL ROUGHNESS:
    Option = Smooth Wall
END
END
FLUID: oil
BOUNDARY CONDITIONS:
    MASS AND MOMENTUM:
        Option = No Slip Wall
    END
END
END
FLUID: water
BOUNDARY CONDITIONS:
    MASS AND MOMENTUM:
        Option = No Slip Wall
    END
END
END
DOMAIN MODELS:
    BUOYANCY MODEL:
        Buoyancy Reference Density = 790 [kg m-3]
        Gravity X Component = 0 [m s-2]
        Gravity Y Component = 0 [m s-2]
        Gravity Z Component = -9.81 [m s-2]
        Option = Buoyant
    BUOYANCY REFERENCE LOCATION:
        Option = Automatic
    END
END
DOMAIN MOTION:
    Option = Stationary
END
MESH DEFORMATION:
    Option = None
END
REFERENCE PRESSURE:
    Reference Pressure = 1 [atm]
END
END
FLUID DEFINITION: oil
    Material = Turpentine
    Option = Material Library
MORPHOLOGY:
    Option = Continuous Fluid
END
END
FLUID DEFINITION: water

```

```
Material = Water
Option = Material Library
MORPHOLOGY:
  Option = Continuous Fluid
END
END
FLUID MODELS:
COMBUSTION MODEL:
  Option = None
END
FLUID: oil
FLUID BUOYANCY MODEL:
  Option = Density Difference
END
TURBULENCE MODEL:
  Option = k epsilon
  BUOYANCY TURBULENCE:
    Option = None
  END
END
TURBULENT WALL FUNCTIONS:
  Option = Scalable
END
END
FLUID: water
FLUID BUOYANCY MODEL:
  Option = Density Difference
END
TURBULENCE MODEL:
  Option = k epsilon
  BUOYANCY TURBULENCE:
    Option = None
  END
END
TURBULENT WALL FUNCTIONS:
  Option = Scalable
END
END
HEAT TRANSFER MODEL:
  Fluid Temperature = 25 [C]
  Homogeneous Model = False
  Option = Isothermal
END
THERMAL RADIATION MODEL:
  Option = None
END
TURBULENCE MODEL:
  Homogeneous Model = False
  Option = Fluid Dependent
END
```

```

END
FLUID PAIR: oil | water
INTERPHASE TRANSFER MODEL:
  Interface Length Scale = 1. [mm]
  Option = Mixture Model
END
MASS TRANSFER:
  Option = None
END
MOMENTUM TRANSFER:
  DRAG FORCE:
    Drag Coefficient = 0.44
    Option = Drag Coefficient
  END
END
END
INITIALISATION:
  Option = Automatic
  FLUID: oil
  INITIAL CONDITIONS:
    Velocity Type = Cartesian
    CARTESIAN VELOCITY COMPONENTS:
      Option = Automatic with Value
      U = 0 [m s-1]
      V = 0 [m s-1]
      W = 0 [m s-1]
    END
    TURBULENCE INITIAL CONDITIONS:
      Option = Medium Intensity and Eddy Viscosity Ratio
    END
    VOLUME FRACTION:
      Option = Automatic with Value
      Volume Fraction = 0.9
    END
  END
END
FLUID: water
  INITIAL CONDITIONS:
    Velocity Type = Cartesian
    CARTESIAN VELOCITY COMPONENTS:
      Option = Automatic with Value
      U = 0 [m s-1]
      V = 0 [m s-1]
      W = 0 [m s-1]
    END
    TURBULENCE INITIAL CONDITIONS:
      Option = Medium Intensity and Eddy Viscosity Ratio
    END
    VOLUME FRACTION:
      Option = Automatic with Value

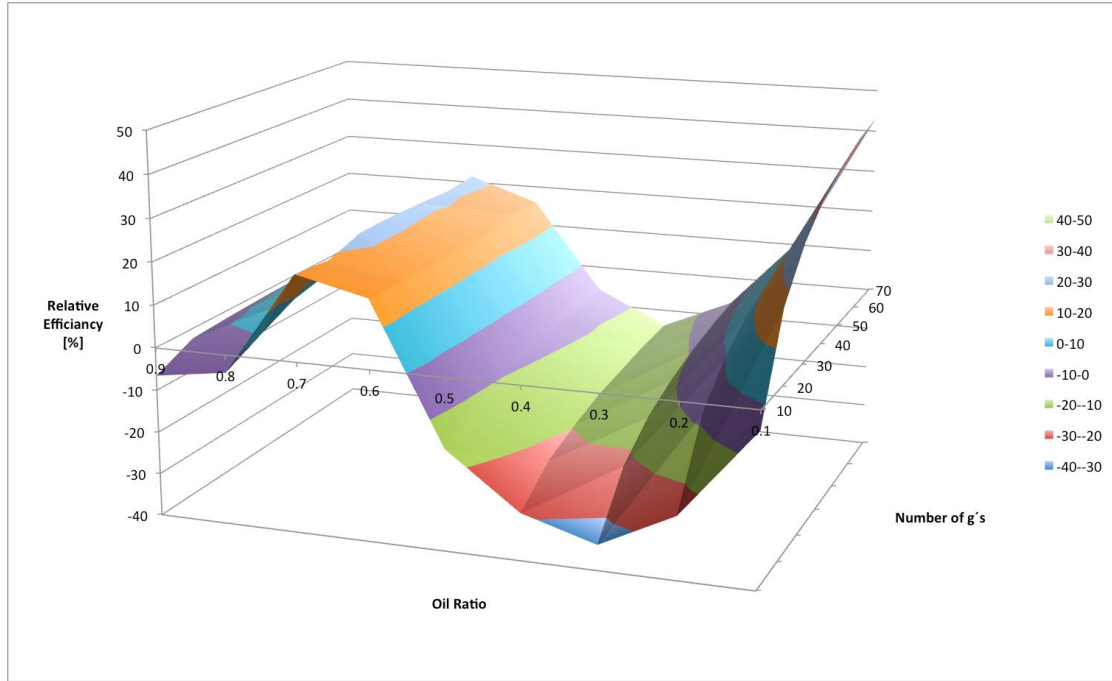
```

```
    Volume Fraction = 0.1
  END
END
END
INITIAL CONDITIONS:
  STATIC PRESSURE:
    Option = Automatic with Value
    Relative Pressure = 1 [atm]
  END
END
END
MULTIPHASE MODELS:
  Homogeneous Model = False
FREE SURFACE MODEL:
  Option = None
END
END
END
OUTPUT CONTROL:
  RESULTS:
    File Compression Level = Default
    Option = Standard
  END
END
SOLVER CONTROL:
  Turbulence Numerics = First Order
ADVECTION SCHEME:
  Option = High Resolution
END
CONVERGENCE CONTROL:
  Length Scale Option = Conservative
  Maximum Number of Iterations = 100
  Minimum Number of Iterations = 1
  Timescale Control = Auto Timescale
  Timescale Factor = 1.0
END
CONVERGENCE CRITERIA:
  Residual Target = 1.E-4
  Residual Type = RMS
END
DYNAMIC MODEL CONTROL:
  Global Dynamic Model Control = Yes
END
END
COMMAND FILE:
  Version = 16.2
END
```

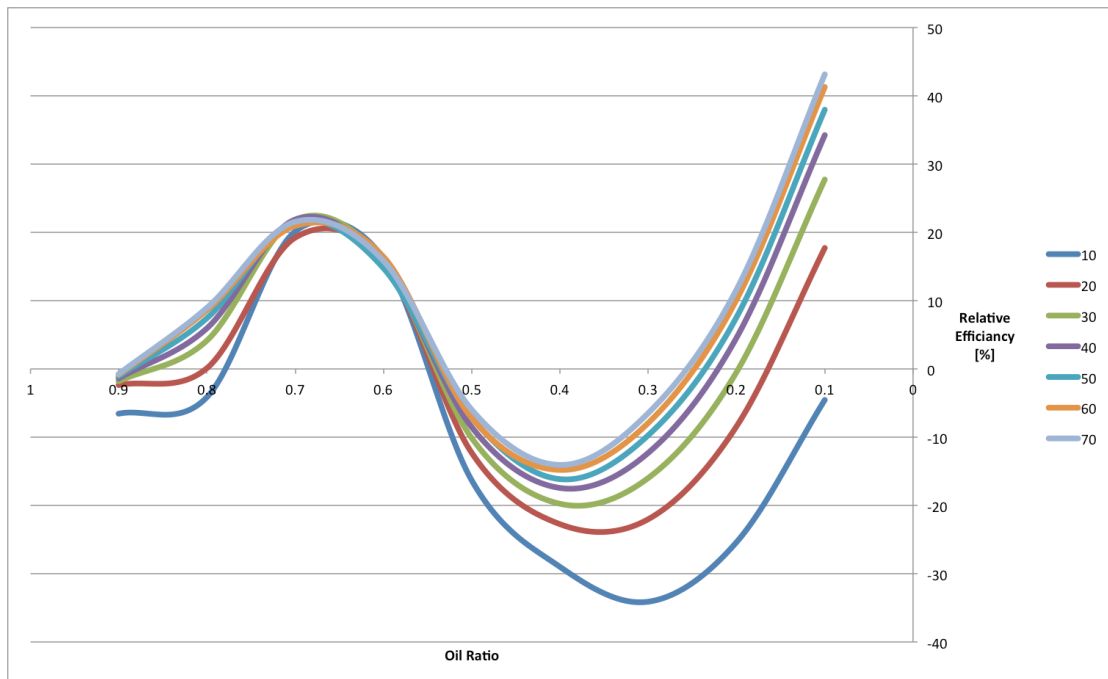

Appendix H Raw data from particle model simulations

Name	G	Oil ratio	Secondary	Water Kinetic Inlet	Water Kinetic Outlet	Oil Fraction Inlet	Oil Inlet Nedre	Oil Inlet Ovre	Oil fraction Outlet	Oil Outlet Nedre	Oil Outlet Ovre
DP0	10	0.9	0.147015	0.106078	0.035189	0.89502	0.871304	0.920746	0.854642	0.847329	0.861966
DP1	20	0.9	0.21	0.153399	0.0634912	0.896331	0.915794	0.915794	0.890363	0.886233	0.894504
DP2	30	0.9	0.255501	0.211277	0.0889824	0.896427	0.88071	0.912152	0.891894	0.887698	0.896104
DP3	40	0.9	0.293487	0.272818	0.11269	0.896538	0.883491	0.909592	0.892621	0.889797	0.897276
DP4	50	0.9	0.327216	0.331464	0.135427	0.896648	0.885309	0.907992	0.893018	0.888055	0.897994
DP5	60	0.9	0.357808	0.391279	0.157241	0.896828	0.888883	0.906778	0.89338	0.888071	0.898704
DP6	70	0.9	0.386095	0.451199	0.178337	0.897011	0.888296	0.905851	0.893699	0.888048	0.899365
DP7	10	0.8	0.148464	0.106038	0.036718	0.895772	0.870917	0.920637	0.881549	0.875	0.887612
DP8	20	0.8	0.209832	0.159848	0.065617	0.874283	0.854419	0.894154	0.890917	0.886786	0.895061
DP9	30	0.8	0.255163	0.223961	0.0888795	0.866333	0.829432	0.86328	0.892191	0.887813	0.896582
DP10	40	0.8	0.293487	0.281254	0.11269	0.864698	0.819805	0.849697	0.892619	0.889797	0.897272
DP11	50	0.8	0.327215	0.33803	0.135427	0.82511	0.811768	0.838458	0.895011	0.88805	0.897986
DP12	60	0.8	0.357805	0.393615	0.157242	0.817634	0.805561	0.829712	0.893361	0.888052	0.898683
DP13	70	0.8	0.386022	0.445184	0.179353	0.815981	0.804788	0.827179	0.893479	0.888092	0.898879
DP14	10	0.7	0.14918	0.0905098	0.0378916	0.698899	0.641352	0.75647	0.892564	0.887645	0.897499
DP15	20	0.7	0.20902	0.166836	0.0631861	0.736379	0.709404	0.763365	0.892928	0.887884	0.897985
DP16	30	0.7	0.254898	0.219183	0.0870123	0.723093	0.700434	0.745762	0.893274	0.887812	0.898751
DP17	40	0.7	0.293306	0.27705	0.10659	0.726784	0.708052	0.745705	0.893361	0.887842	0.898894
DP18	50	0.7	0.327155	0.332771	0.134032	0.731558	0.715156	0.747965	0.893378	0.887926	0.898845
DP19	60	0.7	0.357803	0.385336	0.157242	0.737183	0.722461	0.751911	0.89334	0.888033	0.898866
DP20	70	0.7	0.386026	0.434739	0.179361	0.74261	0.720606	0.74792	0.893445	0.888054	0.89885
DP21	10	0.6	0.143013	0.0877205	0.0350873	0.592001	0.50684	0.677207	0.757816	0.741424	0.774234
DP22	20	0.6	0.198244	0.145315	0.0583274	0.593893	0.539073	0.648734	0.728828	0.711167	0.742511
DP23	30	0.6	0.24062	0.198634	0.0802975	0.595116	0.553676	0.636572	0.715404	0.7020297	0.730352
DP24	40	0.6	0.276117	0.250003	0.101332	0.595902	0.562338	0.629477	0.706475	0.721169	0.730352
DP25	50	0.6	0.307229	0.300021	0.121583	0.596449	0.56812	0.624078	0.698743	0.684627	0.713338
DP26	60	0.6	0.337326	0.349075	0.142314	0.596853	0.572277	0.62437	0.705981	0.691951	0.720031
DP27	70	0.6	0.363106	0.397206	0.161547	0.597183	0.57544	0.618932	0.700111	0.686306	0.713937
DP28	10	0.5	0.124723	0.0835778	0.0276981	0.493943	0.396886	0.591054	0.496455	0.484497	0.509424
DP29	20	0.5	0.176823	0.13918	0.0498714	0.494635	0.431752	0.557546	0.493959	0.49187	0.496056
DP30	30	0.5	0.216494	0.1912	0.0704967	0.495421	0.447804	0.543057	0.493983	0.495574	0.4924
DP31	40	0.5	0.250133	0.241468	0.0901427	0.495999	0.457398	0.534615	0.495091	0.498232	0.491956
DP32	50	0.5	0.279902	0.290446	0.109093	0.496431	0.46384	0.529032	0.497012	0.500671	0.49336
DP33	60	0.5	0.306187	0.338408	0.127453	0.496773	0.46847	0.529085	0.494607	0.500021	0.489198
DP34	70	0.5	0.331073	0.385531	0.147458	0.497053	0.471998	0.522116	0.497268	0.492312	0.489232
DP35	10	0.4	0.11406	0.0799346	0.025906	0.396946	0.296351	0.469742	0.383682	0.385929	0.38144
DP36	20	0.4	0.163781	0.133707	0.0467481	0.396187	0.333004	0.4614	0.381776	0.398122	0.370432
DP37	30	0.4	0.200658	0.184513	0.0659578	0.396333	0.346974	0.445753	0.380487	0.394238	0.366736
DP38	40	0.4	0.231524	0.233726	0.0843151	0.396607	0.356532	0.436697	0.380758	0.394564	0.366952
DP39	50	0.4	0.257985	0.28172	0.101851	0.396857	0.362987	0.430739	0.380099	0.394025	0.366171
DP40	60	0.4	0.282188	0.328727	0.118073	0.397072	0.367643	0.426512	0.380618	0.393897	0.367337
DP41	70	0.4	0.303743	0.374896	0.135642	0.397261	0.371185	0.423345	0.380138	0.393171	0.367101
DP42	10	0.3	0.0964733	0.0764941	0.0245474	0.300215	0.20642	0.394069	0.285566	0.279354	0.291781
DP43	20	0.3	0.138725	0.128691	0.0442492	0.298129	0.237162	0.359127	0.28583	0.278557	0.293101
DP44	30	0.3	0.170001	0.178425	0.0624184	0.2977	0.251542	0.343877	0.286046	0.276144	0.295946
DP45	40	0.3	0.19626	0.22669	0.0798281	0.297625	0.260148	0.335116	0.285549	0.274862	0.298232
DP46	50	0.3	0.218972	0.273774	0.096422	0.29765	0.265973	0.329339	0.286567	0.272938	0.300192
DP47	60	0.3	0.239683	0.319889	0.112745	0.297718	0.270196	0.325249	0.286914	0.272303	0.301521
DP48	70	0.3	0.2584	0.365195	0.128451	0.297798	0.273409	0.322195	0.286896	0.270993	0.302795
DP49	10	0.2	0.0857049	0.0729327	0.0239082	0.202972	0.126951	0.279045	0.194357	0.160437	0.228286
DP50	20	0.2	0.124004	0.123926	0.0430888	0.199997	0.150651	0.249599	0.19575	0.15797	0.232542
DP51	30	0.2	0.152547	0.172803	0.0608888	0.199114	0.161807	0.236438	0.195783	0.156074	0.235504
DP52	40	0.2	0.176105	0.220247	0.0776949	0.198772	0.168516	0.22419	0.196831	0.153502	0.238172
DP53	50	0.2	0.196847	0.266522	0.0939974	0.198626	0.173071	0.22419	0.196095	0.152871	0.239332
DP54	60	0.2	0.215377	0.311845	0.109666	0.19856	0.176374	0.220777	0.196047	0.15105	0.241057
DP55	70	0.2	0.232556	0.356372	0.125108	0.19856	0.178892	0.218234	0.196241	0.151021	0.241475
DP56	10	0.1	0.080256	0.0687338	0.0238065	0.103858	0.058407	0.14394	0.100714	0.056502	0.1448
DP57	20	0.1	0.114127	0.119192	0.0428743	0.101062	0.0716912	0.130049	0.10102	0.0538849	0.148175
DP58	30	0.1	0.139729	0.167533	0.0656827	0.100135	0.0779922	0.122288	0.101394	0.0527711	0.150037
DP59	40	0.1	0.160815	0.214333	0.0775649	0.0997396	0.0818273	0.117659	0.101396	0.0508988	0.151912
DP60	50	0.1	0.179602	0.259935	0.0935198	0.0995429	0.0844453	0.114646	0.101634	0.0506631	0.152623
DP61	60	0.1	0.196168	0.304566	0.109197	0.0994378	0.0863415	0.112538	0.101588	0.0493566	0.153838
DP62	70	0.1	0.211792	0.348379	0.124446	0.0999774	0.0877897	0.11097	0.10179	0.0494711	0.154128

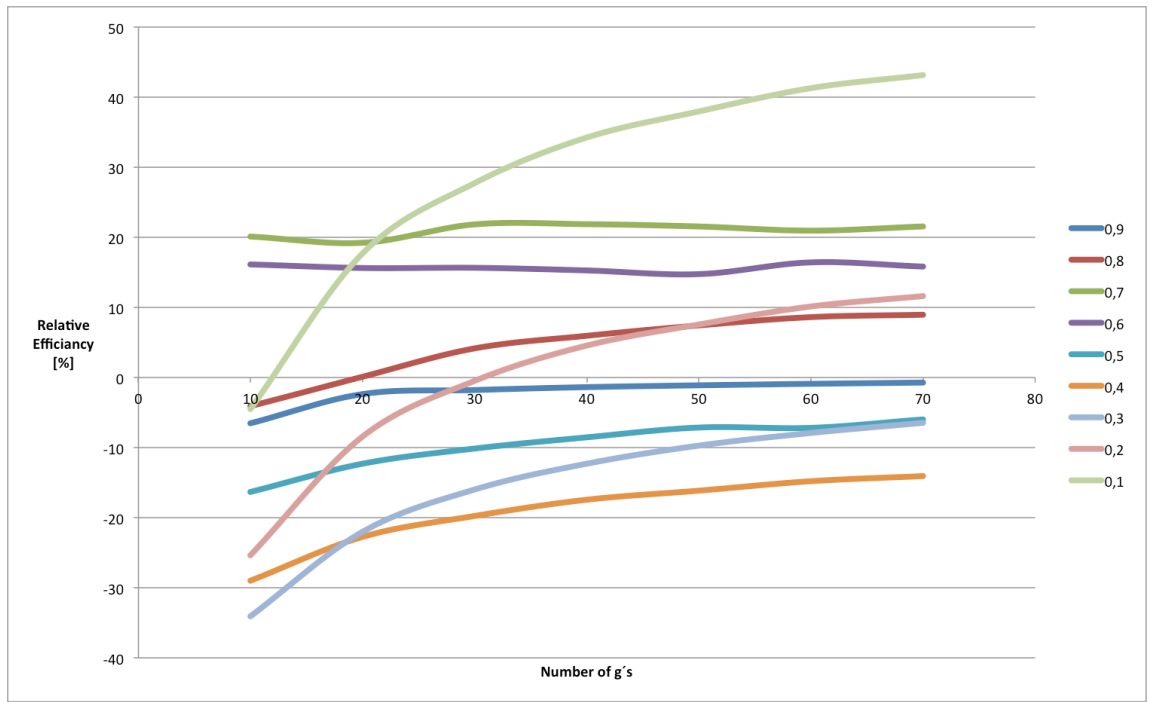
Appendix I Graphs from Particle Model



Relative efficiency given oil ratio and number of g's upper section, particle model



Relative efficiency given oil ratio, upper section, particle model



Relative efficiency given number of g's, upper section, particle model.

Appendix J Risk Assessment

ID	3845	Status	Dato
Risikoområde	Risikovurdering: Helse, miljø og sikkerhet (HMS)	Opprettet	27.01.2016
Opprettet av	Henrik Nikolai Gussiås Kulseth	Vurdering startet	28.01.2016
Ansvarlig	Henrik Nikolai Gussiås Kulseth	Tiltak besluttet	28.01.2016
		Avsluttet	02.06.2016

Forsøk i verkstedshallen med Exxsol D-60

Gyldig i perioden:

1/27/2016 - 6/27/2016

Sted:

Forsøkshall PTS1

Mål / hensikt

Redusere risiko ved forsøk hvor større mengder Exxsol D-60 vil bli brukt.

Bakgrunn

Krav fra NTNU sier at en risikovurdering skal gjennomføres ved forsøk som kan innebære en risiko for helse, miljø og sikkerhet.

Beskrivelse og avgrensninger

Exxsol D-60 er et brannfarlig stoff og kan være giftig ved inntak. Før forsøk med dette stoffet begynner, er det derfor viktig å vurdere farer og planlegge sikkerhetstiltak ved bruk og ved uønskede hendelser. Denne risikovurderingen er avgrenset til risiko rundt forsøket og bruk av Exxsol D-60.

Forutsetninger, antakelser og forenklinger

Risikovurderingen er basert på tiltak og farer beskrevet i sikkerhetsdatabladet til Exxsol D-60, samt tenkte scenarioer og tiltak spesifikt for vårt forsøk.

Vedlegg

Datablad EXXSOL D-60.rtf
P&ID.png

Referanser









[Ingen registreringer]

Oppsummering, resultat og endelig vurdering

I oppsummeringen presenteres en oversikt over farer og uønskede hendelser, samt resultat for det enkelte konsekvensområdet.

Farekilde: **Tennkilde**









Uønsket hendelse: Antennelse av olje

Konsekvensområde: Helse	Risiko før tiltak:		Risiko etter tiltak:	
Ytre miljø	Risiko før tiltak:		Risiko etter tiltak:	
Materielle verdier	Risiko før tiltak:		Risiko etter tiltak:	
Omdømme	Risiko før tiltak:		Risiko etter tiltak:	

Risikoreducerende tiltak	Ansvarlig	Registrert	Frist	Status
Skilting	Henrik Nikolai Gussiås Kulseth	04.02.2016	29.02.2016	Til behandling

Farekilde: **Lekkasje**

Uønsket hendelse: Lekkasje av Exxsol D-60

Konsekvensområde: Helse	Risiko før tiltak:		Risiko etter tiltak:	
Ytre miljø	Risiko før tiltak:		Risiko etter tiltak:	
Materielle verdier	Risiko før tiltak:		Risiko etter tiltak:	
Omdømme	Risiko før tiltak:		Risiko etter tiltak:	

Risikoreducerende tiltak	Ansvarlig	Registrert	Frist	Status
Skilting	Henrik Nikolai Gussiås Kulseth	04.02.2016	29.02.2016	Til behandling

Farekilde: **Tildekket brannslange og brannslukningsapparat**

Uønsket hendelse: **Vanskelig framkomst til brannslange og brannslukningsapparat**

Konsekvensområde: Helse

Risiko før
tiltak:



Risiko etter
tiltak:



Materielle verdier

Risiko før
tiltak:



Risiko etter
tiltak:



Risikoreduserende tiltak	Ansvarlig	Registrert	Frist	Status
Sette fram brannslukningsapparat når forsøk pågår	Henrik Nikolai Gussiås Kulseth	14.04.2016	14.04.2016	Til behandling
Klaring til brannslange	Henrik Nikolai Gussiås Kulseth	14.04.2016		Til behandling

Endelig vurdering

Basert på den totale risikovurdering vil bruk av exxsol D60 i forsøkshallen være akseptabelt, dersom de retningslinjene som er angitt i rapporten følges.

Oversikt involverte enheter og personell

En risikovurdering kan gjelde for en, eller flere enheter i organisasjonen. Denne oversikten presenterer involverte enheter og personell for gjeldende risikovurdering.

Enhet /-er risikovurderingen omfatter

- Institutt for petroleumsteknologi og anvendt geofysikk

Deltakere

Roger Overå

Jon Arne Karstad Opstvedt

Erik Hjertholm

Lesere

Kari Karlsen

Milan Stankovic

Andre involverte/interessenter

[Ingen registreringer]

Følgende akseptkriterier er besluttet for risikoområdet Risikovurdering: Helse, miljø og sikkerhet (HMS):

Helse



Materielle verdier



Omdømme



Ytre miljø



Oversikt over eksisterende, relevante tiltak som er hensyntatt i risikovurderingen

I tabellen under presenteres eksisterende tiltak som er hensyntatt ved vurdering av sannsynlighet og konsekvens for aktuelle uønskede hendelser.

Farekilde	Uønsket hendelse	Tiltak hensyntatt ved vurdering
Tennkilde	Antennelse av olje	Personlig verneutstyr
	Antennelse av olje	Brannslange
	Antennelse av olje	Brannalarm
	Antennelse av olje	Brannslukningsapparat
	Antennelse av olje	Nødprosedyrer og automatisk brannvarslingssystem
	Antennelse av olje	Grav
Lekkasje	Lekkasje av Exxsol D-60	Personlig verneutstyr
	Lekkasje av Exxsol D-60	Brannslange
	Lekkasje av Exxsol D-60	Øyeskyllemiddel
	Lekkasje av Exxsol D-60	Sluk
	Lekkasje av Exxsol D-60	Avtrekk fra separator/tank
	Lekkasje av Exxsol D-60	Vask
	Lekkasje av Exxsol D-60	Grav
Tildekket brannslange og brannslukningsapparat	Vanskelig framkomst til brannslange og brannslukningsapparat	

Eksisterende og relevante tiltak med beskrivelse:

Personlig verneutstyr

Hansker, vernebriller, kjeledress, vernesko, hjelm, hørselsvern

Brannslange

Nærliggende brannslange med justerbar stråle

Brannalarm

Brannalarm i verkstedshallen

Brannslukningsapparat

Nærliggende brannslukningsapparat

Øyeskyllemiddel

Nærliggende øyeskyllemiddel hvis man skulle få utsatt øynene sine for støv, kjemikalier og andre stoffer som skaper irritasjon/skade.

Sluk

Nærliggende sluk hvis lekkasje skulle inntre.

Avtrekk fra separator/tank

Et avtrekk skal være montert på lokket til separatorens/tanken som vil ventilere avgasser til utsiden av verkstedshallen

Nødprosedyrer og automatisk brannvarslingssystem

Skolen har rutiner for evakuering dersom brannalarmen skulle gå, samt et automatisk varslingssystem som varsler brannvesenet.

Vask

Dersom man skulle få huden sin eksponert for Exxsol D-60, kan man vaske eksponert område i en nærliggende vask.

Grav

En nærliggende grav vil føre til at mesteparten av en eventuell lekkasje vil renne ned i den, og derfor begrense lekkasjeområdet og en eventuell brann.

Risikoanalyse med vurdering av sannsynlighet og konsekvens

I denne delen av rapporten presenteres detaljer dokumentasjon av de farer, uønskede hendelser og årsaker som er vurdert. Innledningsvis oppsummeres farer med tilhørende uønskede hendelser som er tatt med i vurderingen.

Følgende farer og uønskede hendelser er vurdert i denne risikovurderingen:

- **Tennkilde**
 - Antennelse av olje
- **Lekkasje**
 - Lekkasje av Exxsol D-60
- **Tildekket brannslange og brannslukningsapparat**
 - Vanskelig framkomst til brannslange og brannslukningsapparat

Oversikt over besluttede risikoreducerende tiltak med beskrivelse:

Skilting

Skilting som informerer om at brannfarlig væske brukes. I tillegg til skilt som viser hvem som er ansvarlig for riggen med kontaktinformasjon.

Sette fram brannslukningsapparat når forsøk pågår

Løsne brannslukningsapparat fra veggfestet og sette det i nærheten når forsøk utføres.

Klaring til brannslange

Siden forsøksriggen er bevegelig kan denne posisjoneres slik at det er minimum én meters klaring til brannslange.

Tennkilde (farekilde)

Nærliggende tennkilde. F.eks åpen ild, gnist fra elektrisk anlegg eller glødende materialer. Verkstedshallen er registrert som en egen branncelle og vil derfor forhindre spredning av brann

og røyk til andre deler av bygningen.

Tennkilde/Antennelse av olje (uønsket hendelse)

Oljen som benyttes er brannfarlig. Hvis den kommer i kontakt med en potensiell tennkilde kan det føre til brann.

Årsak: Feil i elektrisk anlegg

Beskrivelse:

Systemet som inneholder Exxsol D-60 er lukket. Men hvis en lekkasje skulle oppstå, kan en feil i elektrisk anlegg kan skape en potensiell tennkilde i form av gnister.

Årsak: Nærliggende parallelt arbeid

Beskrivelse:

Arbeid som utføres i nærheten av installasjonen kan bestå av varmt arbeid som kan forårsake åpen ild eller glød.

Årsak: Temperatur i systemet når et farlig nivå

Beskrivelse:

Effekten til pumpene som brukes er relativt høye, noe som kan føre til temperaturøkning av væsken i systemet hvis forsøket kjører over lengre tid. Blir det høyt nok kan oljen avgi damp i en antennelig konsentrasjon. Flammepunkt til Exxsol D-60 er >61 C, mens selvantennelsestemperatur er >200 C.

Samlet sannsynlighet vurdert for hendelsen: Svært lite sannsynlig (1)

Kommentar til vurdering av sannsynlighet:

Systemet er i utgangspunktet et lukket system, så en lekkasje må skje for at potensielle nærliggende tennkilder skal antenne oljen. I tillegg er det elektriske anlegget i verkstedshallen kontrollert av sertifisert elektriker. Det vil bli satt opp skilting/sperring rundt forsøksområdet som vil opplyse om brannfarlig væske. Det vil bli montert temperatursensorer i systemet som er koblet til et styringssystem som vil stanse pumpene dersom temperaturen nærmer

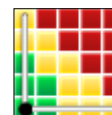
Vurdering av risiko for følgende konsekvensområde: Helse

Vurdert sannsynlighet (felles for hendelsen): Svært lite sannsynlig (1)

Vurdert konsekvens: Liten (1)

Kommentar til vurdering av konsekvens:

Med eksisterende tiltak som brannslange, brannslukningsapparat, evakueringsprosedyrer, luftemuligheter og automatisk brannvarslingssystem vil den mest sannsynlige konsekvensen for helse på personell være liten.



Lekkasje (farekilde)

Lekkasje på forsøksriggen

Lekkasje/Lekkasje av Exxsol D-60 (uønsket hendelse)

Selv om Exxsol D-60 er gradert som minimalt giftig, kan en lekkasje av Exxsol D-60 føre til ubehag og irritasjon i kontakt med øyne og hud. Ved inhalering kan oljen føre til svimmelhet og hodepine.

Årsak: Sprekk i slange eller rør

Beskrivelse:

En sprekk i en slange eller rør vil føre til en mindre lekkasje av Exxsol D-60. En sprekk i rør eller slange kan oppstå pga. svakheter i materialet eller kan oppstå pga. av personfeil, som påkjøring med gaffeltruck, fallende objekt fra traverskran eller uforsiktig bruk av tunge verktøy/utstyr i nærheten.

Årsak: Feil ved utstyr eller montering

Beskrivelse:

Ved en feil på utstyr/tilkobling eller ved montering kan det føre til en lekkasje av Exxsol D-60. Dette kan være en dårlig festet flens, slangeklemme eller feil ved liming av rør. Eksisterende skader på utstyr som tetninger, bolter og rør kan også avsløre seg.

Årsak: Sprekk i separator/tank

Beskrivelse:

Hvis det oppstår en sprekk i separatorens/tanken kan det føre til en lekkasje av Exxsol D-60, som kan være vanskelig å stoppe før innholdet over sprekken er lekket ut. En sprekk kan oppstå pga. svakheter i materialet eller kan oppstå pga. av personfeil, som påkjøring med gaffeltruck, fallende objekt fra traverskran eller uforsiktig bruk av tunge verktøy/utstyr i nærheten.

Årsak: Glipp mellom lokk og separator/tank.

Beskrivelse:

Hvis lokket med avtrekk ikke er tett mot separatorens/tanken, kan Exxsol D-60 damp/gass lekke ut i verkstedshallen og ved høye nok konsentrasjoner forårsake ubehag for folk som befinner seg i nærheten.

Samlet sannsynlighet vurdert for hendelsen: Lite sannsynlig (2)

Kommentar til vurdering av sannsynlighet:

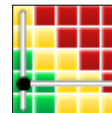
Alt utstyr vil først trykktestes ved lave rater ved bruk av vann. Så eksisterende sprekker/lekkasjer vil oppdages før Exxsol D-60 tas i bruk. Alt utstyr er gradert for trykket som skal benyttes. Gaffeltruck og traverskran brukes sjeldent og av få ansatte som er godt informert om prosjektet og systemet som skal brukes. Det vil bli satt opp skilting/avgrensning rundt forsøksområdet.

Vurdering av risiko for følgende konsekvensområde: Helse

Vurdert sannsynlighet (felles for hendelsen): Lite sannsynlig (2)

Vurdert konsekvens: Liten (1)

Kommentar til vurdering av konsekvens:



Ved en lekkasje ved rør/slanger vil volumet være begrenset da det er montert isolasjonsventiler ved hvert endepunkt og pumpene kan stanses. Hvis det skulle oppstå en større lekkasje fra separator er verkstedshallen godt ventilert og to store porter kan åpnes til utsiden. Hvis gassen fra den lekkede oljen fortsatt skulle føre til ubehag kan verkstedshallen lett evakueres. Oljen er kategorisert som minimal giftig ved inhalering og ved kontakt med hud.

Tildekket brannslange og brannslukningsapparat (farekilde)

Forsøksriggen står delvis foran brannslange og brannslukningsapparat.

Tildekket brannslange og brannslukningsapparat/Vanskelig framkomst til brannslange og brannslukningsapparat (uønsket hendelse)

Hvis det skulle bryte ut brann kan forsøksriggen gjøre framkomst til brannslange og brannslukningsapparat vanskeligere.

Årsak: Forsøksrigg gir liten klaring til brannslange

Beskrivelse:

Forsøksriggen skal stå i nærheten av brannslangen og kan gi liten klaring hvis den er posisjonert for tett innpå.

Årsak: Separator gir liten klaring til brannslukningsapparat på veggen

Beskrivelse:

Separatoren står i en låst posisjon og kan ikke beveges. Dette kan føre til redusert fremkommelighet.

Samlet sannsynlighet vurdert for hendelsen: Sannsynlig (3)

Kommentar til vurdering av sannsynlighet:

[Ingen registreringer]

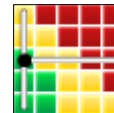
Vurdering av risiko for følgende konsekvensområde: Helse

Vurdert sannsynlighet (felles for hendelsen): Sannsynlig (3)

Vurdert konsekvens: Liten (1)

Kommentar til vurdering av konsekvens:

Selv om det er redusert fremkommelighet har det mest sannsynlig ikke særlig stor innvirkning på tiden det tar for å gjøre klar brannslange og brannslukningsapparat



Oversikt over besluttede risikoreducerende tiltak:

Under presenteres en oversikt over risikoreducerende tiltak som skal bidra til å redusere sannsynlighet og/eller konsekvens for uønskede hendelser.

- Skilting
- Sette fram brannslukningsapparat når forsøk pågår
- Klaring til brannslange

Oversikt over besluttede risikoreducerende tiltak med beskrivelse:

Skilting

Skilting som informerer om at brannfarlig væske brukes. I tillegg til skilt som viser hvem som er ansvarlig for riggen med kontaktinformasjon.

Tiltak besluttet av: Henrik Nikolai Gussiås Kulseth

Ansvarlig for gjennomføring: Henrik Nikolai Gussiås Kulseth

Frist for gjennomføring: 2/29/2016

Sette fram brannslukningsapparat når forsøk pågår

Løsne brannslukningsapparat fra veggfestet og sette det i nærheten når forsøk utføres.

Tiltak besluttet av: Henrik Nikolai Gussiås Kulseth

Ansvarlig for gjennomføring: Henrik Nikolai Gussiås Kulseth

Frist for gjennomføring: 4/14/2016

Klaring til brannslange

Siden forsøksriggen er bevegelig kan denne posisjoneres slik at det er minimum én meters klaring til brannslange.

Tiltak besluttet av: Henrik Nikolai Gussiås Kulseth

Ansvarlig for gjennomføring: Henrik Nikolai Gussiås Kulseth

Frist for gjennomføring:

Appendix K Exxsol D60 datasheet

Product Datasheet



Exxsol™ D60 Dearomatized Fluid

General			
Availability ¹	<ul style="list-style-type: none">Africa & Middle EastAsia Pacific	<ul style="list-style-type: none">EuropeLatin America	<ul style="list-style-type: none">North America
Appearance	<ul style="list-style-type: none">Clear/Transparent		
Form(s)	<ul style="list-style-type: none">Liquid		
Revision Date	<ul style="list-style-type: none">03/01/2014		

Properties	Typical Value (English)	Typical Value (SI)	Test Method
Distillation Range			ASTM D86
Initial Boiling Point (IBP)	365 °F	185 °C	
Dry Point (DP)	419 °F	215 °C	
Flash Point (Method A)	149 °F	65 °C	ASTM D93
Aromatic Content (UV)	< 1E-3 wt%	< 1E-3 wt%	ExxonMobil Method
Density (59.0°F (15.0°C))	6.62 lb/gal	0.793 g/ml	ISO 12185
Vapor Pressure (68.0°F (20.0°C))	0.4 mm Hg	5E-2 kPa	ExxonMobil Method
Aniline Point (Method E)	158 °F	70 °C	ASTM D611
Kinematic Viscosity (77.0°F (25.0°C))	1.64 cSt	1.64 mm ² /s	ASTM D7042

Additional Information

Typical values listed represent product from a primary source location. Actual values may vary slightly for product from alternate source locations.

Legal Statement

This product, including the product name, shall not be used or tested in any medical application without the prior written acknowledgement of ExxonMobil Chemical as to the intended use.

Notes

Typical properties: these are not to be construed as specifications.

The values indicated in this document may deviate from the test method requirements by the number of significant figures shown.

¹ Product may not be available in one or more countries in the identified Availability regions. Please contact your Sales Representative for complete Country Availability.

For additional technical, sales and order assistance: www.exxonmobilchemical.com/ContactUs

©2016 ExxonMobil. ExxonMobil, the ExxonMobil logo, the interlocking "X" device and other product or service names used herein are trademarks of ExxonMobil, unless indicated otherwise. This document may not be distributed, displayed, copied or altered without ExxonMobil's prior written authorization. To the extent ExxonMobil authorizes distributing, displaying and/or copying of this document, the user may do so only if the document is unaltered and complete, including all of its headers, footers, disclaimers and other information. You may not copy this document to or reproduce it in whole or in part on a website. ExxonMobil does not guarantee the typical (or other) values. Any data included herein is based upon analysis of representative samples and not the actual product shipped. The information in this document relates only to the named product or materials when not in combination with any other product or materials. We based the information on data believed to be reliable on the date compiled, but we do not represent, warrant, or otherwise guarantee, expressly or impliedly, the merchantability, fitness for a particular purpose, freedom from patent infringement, suitability, accuracy, reliability, or completeness of this information or the products, materials or processes described. The user is solely responsible for all determinations regarding any use of material or product and any process in its territories of interest. We expressly disclaim liability for any loss, damage or injury directly or indirectly suffered or incurred as a result of or related to anyone using or relying on any of the information in this document. This document is not an endorsement of any non-ExxonMobil product or process, and we expressly disclaim any contrary implication. The terms "we," "our," "ExxonMobil Chemical" and "ExxonMobil" are each used for convenience, and may include any one or more of ExxonMobil Chemical Company, Exxon Mobil Corporation, or any affiliate either directly or indirectly stewarded.

exxonmobilchemical.com

Effective Date: 03/01/2014

ExxonMobil

Page: 1 of 1